AB INITIO QUANTUM MECHANICAL APPLICATIONS TO MOLECULAR SYSTEMS FROM TRIATOMICS TO NUCLEIC ACID BASES

by

SUYUN WANG

(Under the Direction of Henry F. Schaefer)

ABSTRACT

Ab initio quantum mechanical computational techniques have been applied to questions in various molecular systems from triatomics to nucleic acid (NA) bases. For triatomic copper hydroxide (CuOH), a range of *ab initio* methods have been employed to investigate the ground and two lowest-lying singlet excited electronic states. The optimized geometrical parameters for the $\tilde{X}$ ^{1}A' and 1 ^{1}A" states agree fairly well with available experimental values. However, the 2 ^{1}A' structure is in poor agreement with experiment. The predicted adiabatic excitation energies are also inconsistent with experiment for the 2 ^{1}A' and 1 ^{1}A" states. All theoretical methods show lower adiabatic excitation energies for the 1 ^{1}A" state (53.1 kcal mol^{-1}) than those for the corresponding 2 ^{1}A' state (57.6 kcal mol^{-1}), suggesting that the 1 ^{1}A" state might be the first singlet excited state while the 2 ^{1}A' state might be the second singlet excited state.

Extensive *ab initio* methods have been used to study the triatomic PCN / PNC species and the transition state of the exothermic PNC → PCN reaction. Both PCN and PNC are linear with $^3\Sigma^-$ ground states, and linear PNC ($\tilde{X}$ $^3\Sigma^-$) is predicted to lie 13.5 kcal mol^{-1} [with zero-point vibrational energy (ZPVE) correction] above linear PCN

($\tilde{X}\ ^3\Sigma^-$). The isomerization transition state is found to be cyclic PCN ($\tilde{X}\ ^3A''$) with angles θ_e (PCN) = 82.2°, θ_e (CNP) = 63.1°, and θ_e (NPC) = 34.7°. The isomerization barrier is predicted to be 35.7 kcal mol^{-1} relative to linear PCN ($\tilde{X}\ ^3\Sigma^-$).

With respect to the NA bases, the *ab initio* Hartree-Fock (HF) and second-order Møller-Plesset perturbation (MP2) methods have been applied to analyze the nonplanarity of the NA base amino group. New benchmark predictions have been obtained at the cc-pCVQZ and aug-cc-pVQZ MP2 levels of theory for adenine, guanine, cytosine, thymine, and uracil. Three out of the five NA bases, namely adenine, guanine, and cytosine, are intrinsically nonplanar due to the existence of pyramidal amino groups. Guanine is much more nonplanar than adenine and cytosine. The predicted classical barriers to planarization are 0.020 (adenine), 0.742 (guanine), and 0.032 (cytosine) kcal mol^{-1}.

INDEX WORDS: Ab Initio Method, Coupled-Cluster Theory, Equation-of-Motion Coupled-Cluster Method, Second-Order Møller-Plesset Perturbation Method, CuOH, Singlet Excited State, Adiabatic Excitation Energy, PCN, PNC, Transition State, Isomerization Barrier, Nucleic Acid Base, Amino Group, Planarization Barrier.

AB INITIO QUANTUM MECHANICAL APPLICATIONS TO MOLECULAR SYSTEMS FROM TRIATOMICS TO NECLEIC ACID BASES

by

SUYUN WANG

M.E., University of Petroleum, China, 1998

M.S., Ohio University, USA, 2002

A Dissertation Submitted to the Graduate Faculty of The University of Georgia in Partial Fulfillment of the Requirements for the Degree

DOCTOR OF PHILOSOPHY

ATHENS, GEORGIA

2006

AB INITIO QUANTUM MECHANICAL APPLICATIONS TO MOLECULAR SYSTEMS FROM TRIATOMICS TO NUCLEIC ACID BASES

by

SUYUN WANG

Major Professor:	Henry F. Schaefer
Committee:	Nigel G. Adams Geoffrey D. Smith

Electronic Version Approved:

Maureen Grasso
Dean of the Graduate School
The University of Georgia
May 2006

To my beloved husband, daughter, and parents

ACKNOWLEDGEMENTS

I am grateful to many people who have helped me during my study at the University of Georgia (UGA) and supported me to complete my Ph.D. degree. I first and foremost thank my husband, Hongbin (Victor) Wang. Although Victor has a lot of work to do in places far away from Athens, Georgia, he continues to encourage my academic pursuits, provide me strong support in all aspects, and help me through every event in my life. His love and consideration is consistently reflected in every accomplishment of mine. I thank another member of my family, Louise, my five year old daughter. She is cute and happy. Her smile always clears my mind and brings me joy and hope.

I would like to deeply thank my parents, Yonghong Wang and Nilian Wang, who gave me a warm home and provided me education. They taught me to be kind, honest, and strong. I thank my parents-in-law, Biao Wang and Yuying Jiang, and their families together with my own parents for taking care of my daughter, so that I can finish my study successfully. I thank my younger brother, Jiangyun, for accompanying my parents in China and helping them look after Louise.

I am cordially grateful to my advisor, Prof. Henry F. Schaefer for providing me an opportunity to study at the Center for Computational Chemistry (CCC) and leading me into the world of quantum mechanics. He creates a wonderful academic research environment at CCC for graduate students and visiting scholars. He has a pleasure personality; he is generous, trustworthy, and helpful.

I would like to sincerely thank Prof. Nigel Adams and Prof. Geoffrey Smith for being my committee members. They are very nice and respectful. I would like to thank Dr. Yukio Yamaguchi for being a great mentor and a patient teacher in my research. I learned a lot from him. I thank Dr. Yaoming Xie, Prof. Schleyer, and Dr. Zhongfang Chen for very helpful discussion on my research projects. I thank Dr. Wesley Allen for challenging questions in lectures and group meeting presentations. I also thank all the professors of the courses that I took during my Ph.D. study.

I am very thankful to the support staff in the research group at CCC. I thank Linda Rowe, Amy Peterson, and Karen Branch for taking care of so many details. I thank Richard Remington for introducing me into the CCC network.

Finally, I want to thank all my fellow graduate students at CCC for their professional help. In particular, Ankan and Nathan helped me on my first big project, Justin on software issues, Eric on research, and Brian on difficult problems in homework. I want to thank my former and current officemates, Nancy, Veronica, and Maria, for making our office the most beautiful one at CCC with a lot of plants and, yes, Maria's fish, Peter. I also want to thank my friends, Lisa and Furong, for their help in my life and the good times we enjoyed together at UGA.

TABLE OF CONTENTS

LIST OF TABLES

Page

LIST OF FIGURES

Page

CHAPTER 1

INTRODUCTION AND BACKGROUND MATERIAL

The Schrödinger equation, $\hat{H}|\Psi\rangle = E|\Psi\rangle$, has been applied to describe the behavior of atomic or molecular systems in modern computational quantum chemistry. The solutions to the Schrödinger equation give the quantized energies of the system and the form of the wavefunction so that other properties, such as optimal geometries and vibrational frequencies, may be computed. The theoretical predictions from the Schrödinger equation either confirm or challenge experimental results, and even provide useful information that can not be easily determined by experiments. However, it is impossible to solve the Schrödinger equation exactly for most practical chemical systems with current computing power. Therefore, various *ab initio* methods using different levels of approximations have made it possible to carry out practical computations with balance between accuracy and computing cost.

Most commonly used *ab initio* quantum mechanical techniques in computational chemistry include self-consistent field (SCF),[1-4] Møller-Plesset perturbation theory,[5, 6] configuration interaction (CI),[4, 7, 8] and coupled-cluster theory.[9-19] Complete-active-space SCF[20, 21] and multi-reference CI[22] are also widely employed *ab initio* methods. A combination of large basis sets and high-level *ab initio* theories can usually yield results that achieve chemical or even subchemical accuracies. In this dissertation, the *ab initio* computations were carried out with MOLPRO,[23] NWCHEM,[24] GAUSSIAN 94,[25] ACES II,[26] and PSI II[27] computational chemistry software packages.

1.1 COUPLED-CLUSTER THEORY

Coupled-cluster (CC) theory was introduced into quantum chemistry in the late 1960s by Čížek and Paldus,[28-30] and computer implementations of the CC theory began to appear for realistic systems at the end of the 1970s.[31, 32] Nowadays, the CC approach has been regarded as perhaps the most reliable, yet computationally affordable method for small-size chemical systems.

The CC wavefunction, $|\Psi_{CC}\rangle = e^{\hat{T}}|\Phi_0\rangle$, is used to approximate the exact solution, $|\Psi\rangle$, to the Schrödinger equation, where $|\Phi_0\rangle$ is the reference determinant and $\hat{T}$ is the cluster operator. Truncation of the cluster operator at specific excitation levels leads to a hierarchy of CC techniques. For example, the CC method including single and double excitations (CCSD)[9, 33] only keeps the single and double excitation operators in the cluster operator; CCSD with triple excitations (CCSDT)[11, 34, 35] includes the excitation operators up to triple in the cluster operator. CCSD is the least expensive commonly used CC method, which computationally scales as N^6, where N corresponds to the number of basis functions and thereby the size of the system. The CCSDT method increases this scaling by a factor of N^2, i.e., CCSDT scales as N^8, thus it is not yet suitable for routine applications. Therefore, it is desirable for approximate treatments of triple excitations, and various such approaches have been suggested and implemented. The most popular of these is CCSD with perturbatively applied triple excitations [CCSD(T)].[12, 14] CCSD with iteratively applied partial triples [CCSDT-n (n = 1-3)[10] and CC3[18]] are also widely used for practical chemical systems.

1.2 EQUATION-OF-MOTION COUPLED-CLUSTER THEORY

The vast majority of states accessed by optically allowed transitions from a closed-shell molecule in the ground electronic state are open-shell singlets. These excited electronic states can not be qualitatively described correctly by single-determinant-based

CC methods, since two determinants having equal weights in the final wavefunction are needed to properly treat the spin symmetry. The equation-of-motion coupled-cluster (EOM-CC) theory[17, 36-38] offers an attractive approach to study these excited states of molecules.

In EOM-CC, the excited state wavefunction, $|\Psi_{EOM-CC}\rangle = \hat{R}|\Psi_{CC}\rangle = \hat{R}e^{\hat{T}}|\Phi_0\rangle$, is generated from some CC reference state $|\Psi_{CC}\rangle$, usually the CCSD wavefunction for the ground state, by applying a linear CI type excitation operator $\hat{R}$. Thus, the EOM-CC model constitutes a conceptually simple approach closely related to the CI model for the study of excited states, with the emphasis shifted away from excitations from determinants towards excitations from a more general state. In practical computations, the $\hat{R}$ and $\hat{T}$ operators are necessarily truncated to some tractable level of excitation to compromise the exactness of the method. Generally, singly and doubly substituted determinants are used in the excited state wavefunction, which defines the EOM-CCSD approximation.[17] Inclusion of partial triple excitation corrections in EOM-CCSD leads to the EOM-CCSDT-n[39] and EOM-CC3[18] methods. The EOM-CC techniques are computationally affordable. For instance, EOM-CCSD performance involves only a sixth-power dependence on the basis set size, the same as that associated with evaluation of the ground state CCSD energy.

1.3 MØLLER-PLESSET PERTURBATION THEORY

Møller-Plesset perturbation theory (MPPT)[5, 6] is a particular formulation of the more general many-body PT (MBPT) and it provides a systematic procedure for finding the correlation energy. In this approach, the Hartree-Fock (HF) wavefunction is used as a first approximation to the exact solution of the Schödinger equation. The total Hamiltonian operator, $\hat{H}$, of the system is divided or partitioned into two pieces: a zeroth-order part, $\hat{H}_0$, and a perturbation, $\hat{V}$. That is, $\hat{H} = \hat{H}_0 + \hat{V}$, where $\hat{H}_0$ is the HF Hamiltonian. The exact energy is then expressed as an infinite sum of contributions of increasing complexity, $E_{exact} = E^{(0)} + E^{(1)} + E^{(2)} + \cdots$, where $E^{(0)}$, $E^{(1)}$, and $E^{(2)}$ are the zeroth-, first-, and second-order energies, respectively. The expressions for these contributions contain the eigenvalues of $\hat{H}_0$ and matrix elements of the perturbation between the eigenfunctions of $\hat{H}_0$. Terms that involve products of *n* such matrix elements are grouped together and constitute the *n*th-order perturbation energy. Truncation of the infinite sum for the energy expression at *n*th order determines the specific MP*n* energy, thus defines the MP*n* method. For MP2 as an example, the zeroth-, first-, and second-order energies are included in the total MP2 energy expression. Note that the MP1 energy is actually the HF energy, which is the sum of the zeroth- and first-order energies.

The most commonly used MP method, MP2, recovers a large fraction of the correlation energy which represents a significant improvement from the SCF procedure. The MP2 step is computationally inexpensive, scaling as N^5, where N again is the number of basis functions. Compared to CCSD with the scaling property of N^6, MP2 can be applied to treat larger-size molecular systems.

1.4 OVERVIEW OF CHAPTERS

Both Chapter 2 and 3 are related to the applications of high-level *ab initio* methods to the triatomic molecular systems, while Chapter 4 is associated with the applications of less computationally expensive *ab initio* techniques to the nucleic acid (NA) bases. In Chapter 5, a brief conclusion is remarked for this dissertation.

Chapter 2 explores the physical properties of the ground and two lowest-lying singlet excited electronic states ($\tilde{X}$ ^{1}A′, 2 ^{1}A′, and 1 ^{1}A″) and the corresponding constrained linear stationary points ($\tilde{X}$ $^1\Sigma^+$ and 1 $^1\Pi$) of CuOH. The predicted properties consist of optimal geometries, dipole moments, harmonic vibrational frequencies, adiabatic excitation energies, and energy barriers to linearity. Because of the limited theoretical work reported for the excited states of CuOH, various *ab initio* methods, especially the more accurate advanced CC and EOM-CC approaches, have been used for the small triatomic molecule. Relativistic corrections have been considered due to the heavy Cu atom in CuOH. The purpose is to compare the theoretical predictions of physical properties for the electronic states of CuOH to the available experimental results, and resolve their inconsistency.

In Chapter 3, the PCN / PNC isomers and the isomerization transition state have been examined for the exothermic PNC → PCN reaction. Optimized geometries, harmonic vibrational frequencies, and isomerization energy barriers have been evaluated in the examination. PCN and PNC are possible interstellar species that have not been experimentally characterized. In addition, the high-level theoretical research is absent on the physical properties of the PCN – PNC system. Consequently, the advanced single-reference CC methods have been specially applied to the triatomic molecules to obtain the better predictions.

In Chapter 4, the molecular system of interests shifts from triatomics to the NA bases (adenine, guanine, cytosine, thymine, and uracil). The NA bases frequently interact with other bases or with other molecular systems through the amino group. Thus any nonplanarity of the amino group may affect the molecular recognition of nucleic acids. However, no direct experimental results are available on the nonplanarity of NA base amino group. In this chapter, the computationally inexpensive MP2 correlated level of theory has been used to study the amino group nonplanarity and its dependence on the basis set size. New benchmark predictions on NA bases have been obtained, including the optimal structures and the classical planarization energy barriers.

1.5 REFERENCES

1. Roothaan, C. C. J. *Rev. Mod. Phys.* **1951**, *23*, 69.
2. Roothaan, C. C. J. *Rev. Mod. Phys.* **1960**, *32*, 179.
3. Hurley, A. C. *Introduction to the Electron Theory of Small Molecules*. Academic Press: New York, 1976.
4. Szabo, A.; Ostlund, N. S. *Modern Quantum Chemistry*. McGraw-Hill: New York, 1989.
5. Møller, C.; Plesset, M. S. *Phys. Rev.* **1934**, *46*, 618.
6. Pople, J. A.; Binkley, J. S.; Seeger, R. *Int. J. Quantum Chem. Symp.* **1976**, *10*, 1.
7. Shavitt, I. In *Methods of Electronic Structure Theory*, Schaefer, H. F. Ed. Plenum: New York, 1977; pp 189-275.
8. Brooks, B. R.; Schaefer, H. F. *J. Chem. Phys.* **1979**, *70*, 5092.
9. Purvis, G. D.; Bartlett, R. J. *J. Chem. Phys.* **1982**, *76*, 1910.
10. Noga, J.; Bartlett, R. J.; Urban, M. *Chem. Phys. Lett.* **1987**, *134*, 126.
11. Scuseria, G. E.; Schaefer, H. F. *Chem. Phys. Lett.* **1988**, *152*, 382.

12. Raghavachari, K.; Trucks, G. W.; Pople, J. A.; Head-Gordon, M. *Chem. Phys. Lett.* **1989**, *157*, 479.

13. Bartlett, R. J. *J. Phys. Chem. A* **1989**, *93*, 1697.

14. Bartlett, R. J.; Watts, J. D.; Kucharski, S. A.; Noga, J. *Chem. Phys. Lett.* **1990**, *165*, 513.

15. Scuseria, G. E.; Lee, T. J. *J. Chem. Phys.* **1990**, *93*, 5851.

16. Scuseria, G. E. *Chem. Phys. Lett.* **1991**, *176*, 27.

17. Stanton, J. F.; Bartlett, R. J. *J. Chem. Phys.* **1993**, *98*, 7029.

18. Koch, H.; Christiansen, O.; Jørgensen, P.; Sanchez de Merás, A. M.; Helgaker, T. *J. Chem. Phys.* **1997**, *106*, 1808.

19. Crawford, T. D.; Schaefer, H. F. *Rev. Comput. Chem.* **2000**, *14*, 33.

20. Werner, H.-J.; Knowles, P. J. *J. Chem. Phys.* **1985**, *82*, 5053.

21. Knowles, P. J.; Werner, H.-J. *Chem. Phys. Lett.* **1985**, *115*, 259.

22. Werner, H.-J.; Knowles, P. J. *J. Chem. Phys.* **1988**, *89*, 5803.

23. MOLPRO, a package of *ab initio* programs designed by Werner, H.-J. and Knowles, P. J., version 2002.1. Amos, R. D.; Bernhardsson, A.; Berning, A.; Celani, P.; Cooper, D. L.; Deegan, M. J. O.; Dobbyn, A. J.; Eckert, F.; Hampel, C.; Hetzer, G.; Knowles, P. J.; Korona, T.; Lindh, R.; Lloyd, A. W.; McNicholas, S. J.; Manby, F. R.; Meyer, W.; Mura, M. E.; Nicklass, A.; Palmieri, P.; Pitzer, R. M.; Rauhut, G.; Schütz, M.; Schumann, U.; Stoll, H.; Stone, A. J.; Tarroni, R.; Thorsteinsson, T.; Werner, H.-J.

24. Aprà, E.; Windus, T. L.; Straatsma, T. P.; Bylaska, E. J.; de Jong, W.; Hirata, S.; Valiev, M.; Hackler, M.; Pollack, L.; Kowalski, K.; Harrison, R.; Dupuis, M.;

Smith, D. M. A.; Nieplocha, J.; Tipparaju, V.; Krishnan, M.; Auer, A. A.; Brown, E.; Cisneros, G.; Fann, G.; Früchtl, H.; Garza, J.; Hirao, K.; Kendall, R.; Nichols, J.; Tsemekhman, K.; Wolinski, K.; Anchell, J.; Bernholdt, D.; Borowski, P.; Clark, T.; Clerc, D.; Dachsel, H.; Deegan, M.; Dyall, K.; Elwood, D.; Glendening, E.; Gutowski, M.; Hess, A.; Jaffe, J.; Johnson, B.; Ju, J.; Kobayashi, R.; Kutteh, R.; Lin, Z.; Littlefield, R.; Long, X.; Meng, B.; Nakajima, T.; Niu, S.; Rosing, M.; Sandrone, G.; Stave, M.; Taylor, H.; Thomas, G.; van Lenthe, J.; Wong, A.; Zhang, Z. NWChem, A Computational Chemistry Package for Parallel Computers, Version 4.7; Pacific Northwest National Laboratory: Richland, Washington 99352-0999, USA, 2005.

25. Frisch, M. J.; Trucks, G. W.; Schlegel, H. B.; Gill, P. M. W.; Johnson, B. G.; Robb, M. A.; Cheeseman, J. R.; Keith, T.; Petersson, G. A.; Montgomery, J. A.; Raghavachari, K.; Al-Laham, M. A.; Zakrzewski, V. G.; Ortiz, J. V.; Foresman, J. B.; Cioslowski, J.; Stefanov, B. B.; Nanayakkara, A.; Challacombe, M.; Peng, C. Y.; Ayala, P. Y.; Chen, W.; Wong, M. W.; Andres, J. L.; Replogle, E. S.; Gomperts, R.; Martin, R. L.; Fox, D. J.; Binkley, J. S.; Defrees, D. J.; Baker, J.; Stewart, J. P.; Head-Gordon, M.; Gonzalez, C.; Pople, J. A. Gaussian 94, Revision C.3; Gaussian, Inc.: Pittsburg, PA, U.S.A., 1995.

26. ACES II is a program product of the Quantum Theory Project, University of Florida. Authors: Stanton, J. F.; Gauss, J.; Watts, J. D.; Nooijen, M.; Oliphant, N.; Perera, S. A.; Szalay, P. G.; Lauderdale, W. J.; Gwaltney, S. R.; Beck, S.; Balkova, A.; Bernholdt, D. E.; Baeck, K.-K.; Rozyczko, P.; Sekino, H.; Hober, C.; Bartlett, R. J. Integral packages included are VMOL (Almlöf, J. and Taylor, P. R.); VPROPS

(Taylor, P.); ABACUS (Helgaker, T.; Jensen, H. J. Aa.; Jørgensen, P.; Olsen, J.; and Taylor, P. R.).

27. PSI 2.0.8, Janssen, C. L.; Seidl, E. T.; Scuseria, G. E.; Hamilton, T. P.; Yamaguchi, Y.; Remington, R. B.; Xie, Y.; Vacek, G.; Sherrill, C. D.; Crawford, T. D.; Fermann, J. T.; Allen, W. D.; Brooks, B. R.; Fitzgerald, G. B.; Fox, D. J.; Gaw, J. F.; Handy, N. C.; Laidig, W. D.; Lee, T. J.; Pitzer, R. M.; Rice, J. E.; Saxe, P.; Scheiner, A. C.; Schaefer, H. F. PSITECH, Inc.: Watkinsville, GA 30677, U.S.A., 1995.
28. Čížek, J. *J. Chem. Phys.* **1966**, *45*, 4256.
29. Čížek, J. *Adv. Chem. Phys.* **1969**, *14*, 35.
30. Čížek, J.; Paldus, J. *Int. J. Quantum Chem.* **1971**, *5*, 359.
31. Pople, J. A.; Krishnan, R.; Schlegel, H. B.; Binkley, J. S. *Int. J. Quantum Chem. Symp.* **1978**, *14*, 545.
32. Bartlett, R. J.; Purvis, G. D. *Int. J. Quantum Chem.* **1978**, *14*, 561.
33. Bartlett, R. J.; Stanton, J. F. *Rev. Comput. Chem.* **1994**, *5*, 65.
34. Noga, J.; Bartlett, R. J. *J. Chem. Phys.* **1987**, *86*, 7041.
35. Noga, J.; Bartlett, R. J. *J. Chem. Phys.* **1988**, *89*, 3401.
36. Monkhorst, H. *Int. J. Quantum Chem. Symp.* **1977**, *11*, 421.
37. Sekino, H.; Bartlett, R. J. *Int. J. Quantum Chem. Symp.* **1984**, *18*, 255.
38. Geertsen, J.; Rittby, M.; Bartlett, R. J. *Chem. Phys. Lett.* **1989**, *164*, 57.
39. Watts, J. D.; Bartlett, R. J. *Chem. Phys. Lett.* **1996**, *258*, 581.

CHAPTER 2

THE GROUND AND TWO LOWEST-LYING SINGLET EXCITED ELECTRONIC STATES OF COPPER HYDROXIDE (CUOH)[1]

---

[1] Suyun Wang, Ankan Paul, Nathan J. DeYonker, Yukio Yamaguchi, and Henry F. Schaefer. 2005. *Journal of Chemical Physics*. 123: Art. No. 014313. Reprinted here with permission of the American Institute of Physics.

2.1 ABSTRACT

Various *ab initio* methods, including Self-Consistent Field (SCF), Configuration Interaction (CI), Coupled Cluster (CC), and Complete-Active-Space SCF (CASSCF), have been employed to study the electronic structure of copper hydroxide, CuOH. Geometries, total energies, dipole moments, harmonic vibrational frequencies, and zero-point vibrational energies are reported for the linear $^1\Sigma^+$ and $^1\Pi$ stationary points, and for the bent ground state $\tilde{X}$ $^1A'$, and excited states 2 $^1A'$ and 1 $^1A''$. Six different basis sets have been used in the study, Wachters/DZP being the smallest, QZVPP being the largest. The ground and excited state bending modes present imaginary frequencies for the linear stationary points, indicating that bent structures are more favorable. The effects of relativity for CuOH are important and have been considered using the Douglas-Kroll approach with cc-pVTZ/cc-pVTZ_DK and cc-pVQZ/cc-pVQZ_DK basis sets. The bent ground and two lowest-lying singlet excited states of the CuOH molecule are indeed energetically more stable than the corresponding linear structures. The optimized geometrical parameters for the $\tilde{X}$ $^1A'$ and 1 $^1A''$ states agree fairly well with available experimental values. However, the 2 $^1A'$ structure and rotational constants are in poor agreement with experiment, and we suggest that the latter are in error. The predicted adiabatic excitation energies are also inconsistent with the experimental values of 45.5 kcal mol^{-1} for the 2 $^1A'$ state and 52.6 kcal mol^{-1} for the 1 $^1A''$ state. The theoretical CC and CASSCF methods show lower adiabatic excitation energies for the 1 $^1A''$ state (53.1 kcal mol^{-1}) than those for the corresponding 2 $^1A'$ state (57.6 kcal mol^{-1}), suggesting that the 1 $^1A''$ state might be the first singlet excited state while the 2 $^1A'$ state might be the second singlet excited state.

2.2 INTRODUCTION

Transition metal hydroxides have applications in corrosion, catalysis, and electrochemistry. Frequently, the formation of transition metal hydroxides has been observed in reactions of water with transition metals (for example Cu, Ag, Ni)[1,2] or metal oxides.[3] Theoretical and experimental investigations of transition metal hydroxides can provide useful information on the covalent/ionic nature of the transition metal bonds, formation mechanism of transition metal hydroxides, and the dissociation mechanism of water on the transition metal surfaces.

However, there is a shortage of high-resolution spectroscopic data for transition metal hydroxides compared to those for corresponding diatomic transition metal compounds (oxides, halides, nitrides, and hydrides). The first rotationally resolved spectrum of a transition metal hydroxide was reported by Trkula and Harris in 1983,[4] who recorded an electronic spectrum of CuOH around 540 nm. The spectrum exhibited the transition from the ground state $^1A'$ to the excited state $^1A''$, and showed clear evidence for a bent structure of CuOH for both ground and excited states. In 1985, Kauffman, Hauge, and Margrave[5] investigated the infrared (IR) vibrational spectrum of CuOH from copper metal atoms condensed with water in an argon matrix at 15K, and observed the vibrational frequencies for the Cu-O stretching and Cu-O-H bending modes. Subsequent high resolution electronic spectra reported by Jarman, Fernando, and Bernath[6,7] in 1990 and 1991 resulted in more accurate rotational constants of the ground and excited states, and revealed two transitions $\tilde{B}\ ^1A''\leftarrow\tilde{X}\ ^1A'$ and $\tilde{A}\ ^1A'\leftarrow\tilde{X}\ ^1A'$ of CuOH. In 1999 and 2000, Whitham, Ozeki, and Saito[8,9] presented the pure microwave rotational spectra of CuOH, which further demonstrated the strongly bent structure of the ground state of CuOH, indicating considerable covalent character in the Cu-O bond.

Some theoretical work has been reported for CuOH.[10-17] In 1991, Mochizuki, Takada, and Murakami[13] performed a singly and doubly excited configuration-interaction (CISD) study with respect to two reference configurations for the geometry optimization of the $\tilde{X}$ ^{1}A′ and 1 ^{1}A″ states. Then, at the optimized $\tilde{X}$ ^{1}A′ geometry, a multi-reference CISD (MRCISD) method was applied to obtain the transition moments and vertical excitation energies. The vertical excitation energy of the 1 ^{1}A″←$\tilde{X}$ ^{1}A′ transition was estimated to be 2.30 eV (53.0 kcal mol^{-1}), which is 0.07 eV (1.7 kcal mol^{-1}) lower than that for the transition 2 ^{1}A′←$\tilde{X}$ ^{1}A′ [2.37 eV (54.7 kcal mol^{-1})]. However, the 2 ^{1}A′ state was assigned as the first electronic excited state, the lowest parallel transition from the $\tilde{X}$ ^{1}A′ state, in order to be consistent with the experimental observation by Jarman *et al.*[7] The most recent study by Ikeda, Nakajima, and Hirao in 2003[17] employed *ab initio* self-consistent-field (SCF) and coupled-cluster methods including single and double excitations and perturbatively applied triple excitations [CCSD(T)] to study the equilibrium geometries, vibrational frequencies, dipole moments, and other properties for the ground state of the molecule, and showed reasonable agreement with experimental data.

In light of the limited theoretical work on the excited states of CuOH, especially the absence of 2 ^{1}A′ excited state information, such as the equilibrium geometry and adiabatic excitation energy, we have applied a range of advanced *ab intio* quantum mechanical methods to investigate the physical properties of the low-lying singlet electronic states of CuOH. The linear $^1\Pi$ state of CuOH is subject to the Renner-Teller effect,[18,19] and the harmonic potential function for such a doubly degenerate electronic state splits into two components when the molecule is bent away from linearity. Therefore, we have considered the lowest $^1\Pi$ state (linear geometry, $C_{\infty v}$ point group symmetry) and corresponding 2 ^{1}A′ and 1 ^{1}A″ states (bent geometry, C_s point group symmetry) for CuOH.

2.3 ELECTRONIC STRUCTURE CONSIDERATIONS

The constrained linear geometry of the CuOH molecule has the electronic configuration

$$[\text{core}](7\sigma)^2(8\sigma)^2(3\pi)^4(1\delta)^4(9\sigma)^2(4\pi)^4,\ \tilde{X}\ {}^1\Sigma^+,$$

where [core] denotes the ten lowest-lying core orbitals (Cu: 1s-, 2s-, 2p-, 3s-, 3p-like and O: 1s-like). An analysis of the SCF molecular orbitals (MOs) indicates that the 7σ and 8σ MOs describe the σ(OH) and σ(CuO) bonds, respectively. The 3π MO is assigned to the CuO π bonding, while the 1δ MO is related to the non-bonding ($3d_{x^2-y^2}$ and $3d_{xy}$-like) orbital localized on the Cu atom. The 9σ MO involves σ(CuO)-σ(OH) anti-bonding, and the 4π MO corresponds to the weak CuO anti-bonding π orbital. The 4π orbital of the $\tilde{X}$ $^1\Sigma^+$ state is depicted in Figure 2.1. Since the $\tilde{X}$ $^1\Sigma^+$ state of CuOH possesses an imaginary degenerate bending frequency, it should have a bent equilibrium structure. The electron configuration for the bent ground state of CuOH may be described as

$$[\text{core}](9a')^2(10a')^2(3a'')^2(11a')^2(4a'')^2(12a')^2(13a')^2(5a'')^2(14a')^2,\ \tilde{X}\ {}^1A'.$$

The 9a′ and 10a′ MOs are associated with OH and CuO σ bonding, while the 3a″ and 11a′ MOs are related to the CuO π bonding. The 4a″ and 12a′ MOs are assigned to the non-bonding σ ($3d_{x^2-y^2}$ and $3d_{xy}$-like) orbitals localized on the Cu atom. The 13a′ MO corresponds to the CuO σ anti-bonding, and the 5a″ and 14a′ MOs depict the CuO anti-bonding π orbital.

The electronic configuration for the constrained linear structure of the first excited singlet state is

$$[\text{core}](7\sigma)^2(8\sigma)^2(3\pi)^4(1\delta)^4(9\sigma)^2(4\pi)^3(10\sigma),\ 1\ {}^1\Pi,$$

which is a 4π → 10σ excitation relative to the closed-shell ground state. The 10σ MO consists of a Cu 4s non-bonding orbital with weak σ anti-bonding character. The 4π and 10σ orbitals of the 1 $^1\Pi$ state are depicted in Figures 2.2 and 2.3, respectively. The 1 $^1\Pi$ state of CuOH is subject to a Renner-Teller splitting, leading to the 2 $^1A'$ and 1 $^1A''$ states in a bent configuration. Overall, the first singlet excited state has the following electron configuration:

$$[\text{core}](9a')^2(10a')^2(3a'')^2(11a')^2(4a'')^2(12a')^2(13a')^2(5a'')^2(14a')(15a'),\ 2\ {}^1A',$$

which involves a single electron excitation 14a′ → 15a′ in the molecular plane with respect to the ground state. The 15a′ MO orbital has CuO π anti-bonding character. The second singlet excited state is represented by

$$[\text{core}](9a')^2(10a')^2(3a'')^2(11a')^2(4a'')^2(12a')^2(13a')^2(5a'')(14a')^2(15a'),\ 1\ {}^1A'',$$

which is a single electron excitation 5a″ → 15a′ from the plane perpendicular to the molecular plane.

2.4 THEORETICAL METHODS

Ab initio methods, including SCF, CISD, CCSD,[20] CCSD(T),[21,22] and CCSD with iteratively applied partial triples (CCSDT-3[23] and CC3[24]), were used to investigate the linear and bent ground states. The equation-of-motion coupled-cluster (EOM-CCSD, EOM-CCSDT-3, EOM-CC3) method [25] was employed to study the low-lying singlet excited electronic states of CuOH, while SCF and CISD were also used for the 1 $^1\Pi$ and 1 $^1A''$ excited states. In addition, the complete-active-space SCF (CASSCF)[26,27] method has been applied to both the ground and excited states of CuOH, with the state-averaged CASSCF (SACASSCF) technique used for the 2 $^1A'$ state. The ACES II,[28] PSI II,[29] and MOLPRO[30] software packages were used in this study. Geometries have been optimized at each level of theory and total energies have been determined at equilibrium geometries, from which the adiabatic excitation energies were computed for the two excited states. Other physical properties, including dipole moments, harmonic vibrational frequencies, and zero-point vibrational energies, have been obtained for the low-lying singlet electronic states at stationary points.

Six different combinations of basis sets have been used in this research. The first basis is the Wachters-Hay-Hood[31-33] set for the Cu (14s11p6d/10s8p3d) atom and the standard Dunning-Huzinaga double-zeta plus polarization (DZP)[34,35] for the O (9s5p1d/4s2p1d) and H (4s1p/2s1p) atoms. For this Wachters-DZP basis set, the ten lowest-lying core MOs (1s, 2s, 2p, 3s, 3p for Cu, 1s for O) and the highest-lying six virtual MOs were deleted at all correlated levels of theory. The 3d orbitals of Cu were NOT frozen following the report by Langhoff and Bauschlicher that the contribution of d-d correlation with a weight greater than 90% dominates the total correlation energy for the ^2S state of Cu.[36] The second basis combines a triple-zeta plus double-polarization set, the first-order polarized basis set (PolCu)[37,38] of Sadlej and coworkers for Cu (16s12p6d4f/9s7p3d2f), with the triple-zeta plus double polarization (TZ2P) basis sets for O (11s6p3d/5s3p2d) and H (5s3p/3s2p).[39]

The third basis PolCu(g)/TZ2P(d,f) was constructed from the PolCu/TZ2P set[37-39] with the addition of higher angular momentum functions: two sets of g functions for Cu (16s12p6d4f4g/9s7p3d2f2g), one set of f functions for O (11s6p3d1f/5s3p2d1f), and one set of d functions for H (5s3p1d/3s2p1d). The fourth basis set cc-pVTZ is also of triple-zeta quality for Cu (20s16p8d2f1g/7s6p4d2f1g), O (10s5p2d1f/4s3p2d1f),[40] and H (5s2p1d/3s2p1d),[40] in which the copper basis set was recently constructed by Balabanov and Peterson.[41] The fifth basis is the correlation consistent polarized valence quadruple-zeta set. For copper this is the (22s18p11d3f2g1h/8s7p5d3f2g1h) set of Balabanov and Peterson.[41] For oxygen (12s6p3d2f1g/5s4p3d2f1g) and hydrogen (6s3p2d1f/4s3p2d1f) we adopt the standard QZ basis sets of Dunning.[40] The final basis is the Ahlrichs QZVPP[42] set for Cu (24s18p10d4f2g/11s6p5d4f2g), O (15s8p3d2f1g/7s4p3d2f1g), and H (7s3p2d1f/4s3p2d1f). The ten lowest-lying core MOs (1s, 2s, 2p, 3s, 3p for Cu, 1s for O) were frozen for the cc-pVTZ and cc-pVQZ basis sets, while the six lowest-lying core MOs (1s, 2s, 2p for Cu, 1s for O) were frozen to include the core-valence MOs for the PolCu/TZ2P, PolCu(g)/TZ2P(d,f), and QZVPP basis sets. No virtual MOs were deleted at correlated levels of theory for the larger five basis sets.

In addition to the non-relativistic studies, Douglas-Kroll relativistic computations[43] at the EOM-CCSD level of theory were also performed to determine equilibrium structures for the ground $\tilde{X}$ $^1A'$ state and excited 2 $^1A'$ and 1 $^1A''$ states. The basis sets used in the Douglas-Kroll relativistic computations are PolCu/cc-pVTZ_DK,[44] cc-pVTZ_DK,[41,44] and cc-pVQZ_DK,[41,44] which have the same number of primitive and contracted functions as the corresponding non-relativistic basis sets. The PolCu basis set used in Douglas-Kroll relativistic study is exactly the same as that in non-relativistic study. The cc-pVXZ_DK (X = T, Q) and cc-pVXZ (X = T, Q) basis sets for oxygen and hydrogen atoms only differ in the contraction coefficients. Of course, the effects of relativistic recontraction of the H atom basis functions are very minor. The cc-pVXZ_DK (X = T, Q) basis sets for the copper atom differ from cc-pVXZ (X = T, Q) in both the contraction coefficients and some of the exponents. Note that the cc-pVXZ_DK (X = T, Q) and cc-pVXZ (X = T, Q) basis sets for Cu were developed by Balabanov and Perterson (unpublished) recently.[41]

For an appropriate zeroth-order description of an open-shell singlet state, two Slater determinants are required. In this context, EOM techniques with high quality CC wave functions are very powerful for the investigation of excited singlet states relative to the reference closed-shell state. In this case, the ground state of CuOH is well described by single reference wave functions, while the two excited singlet states are adequately represented by single excitations relative to the ground state.

The CASSCF and SACASSCF methods used here are based on the partitioning of the MOs into three subsets (inactive orbitals, active orbitals, and external orbitals), corresponding to how they are employed to build the wave function. With these divisions, full CI within the active orbitals was carried out. For the CuOH molecule, the inactive orbitals include 10 MOs coming from the inner atomic orbitals (1s, 2s, 2p, 3s, 3p for Cu, 1s for O), the active orbitals consist of 13 MOs resulting from the valence atomic orbitals (3d, 4s, 4p for Cu, 2s, 2p for O, 1s for H) and 18 valence electrons are distributed in 13 MOs. The external orbitals span the rest of the higher-lying orbital space, defined from the basis set used to build the molecular orbitals. The three states included in SACASSCF for the 2 $^1A'$ state are $\tilde{X}$ $^1A'$, 2 $^1A'$ and 1 $^1A''$ states, since the 2 $^1A'$ state has the same symmetry as the ground state and was found to lie very close in energy to the $1\ ^1A''$ state. The weights in the state averaged CASSCF procedure are the same ($1/\sqrt{3}$) for each of three states.

2.5 RESULTS AND DISCUSSION

In Figure 2.4-2.8 the optimized structures of the five lowest-lying singlet states of CuOH are depicted. In Tables 2.1-2.5.2 the total energies, dipole moments, harmonic vibrational frequencies, and zero-point vibrational energies (ZPVEs) of the five stationary points are presented. In Table 2.6.1 and 2.6.2 the rotational constants of the three bent electronic states are summarized. The relative energies for the five singlet states are shown in Figures 2.9 and 2.10, and Table 2.7.1 and 2.7.2. The available experimental data for bent CuOH are also included in figures and tables for comparison.

2.5.1 GEOMETRIES

2.5.1.1 LINEAR $\tilde{X}\ ^1\Sigma^+$ STATIONARY POINT

The optimized geometries for the constrained linear $\tilde{X}\ ^1\Sigma^+$ state at seven levels of theory with the two basis sets are presented in Figure 2.4. For a given basis set, a more complete inclusion of correlation effects results in a decrease of the CuO separation but an increase of the OH bond distance. The adoption of larger basis sets shortens both CuO and OH bond lengths with the CI and CC methods. With the QZVPP (our largest basis set) coupled-cluster methods that include CC perturbative and iterative partial triple excitations, the linear stationary point geometry is predicted by CCSD(T) to be $R_{\text{Cu-O}}$ = 1.738 Å and $R_{\text{O-H}}$ = 0.945 Å. The equilibrium bond length for the diatomic CuO ($X\ ^2\Pi$) is experimentally determined to be very similar, namely r_e = 1.7243$_7$ Å.[45] The experimentally estimated geometries of the diatomics OH ($X\ ^2\Pi$), OH$^+$ ($X\ ^3\Sigma^-$), and OH$^-$ ($X\ ^1\Sigma^+$) are r_e = 0.9697 Å, 1.0289 Å, and 0.970 Å respectively.[45] Except for the CC3 method with the PolCu(g)/TZ2P(d,f) and QZVPP basis sets, the CuO distance for CuOH is predicted to be longer than for CuO ($X\ ^2\Pi$), while the OH distance in CuOH is seen to be shorter than in OH ($X\ ^2\Pi$), OH$^+$ ($X\ ^3\Sigma^-$), and OH$^-$ ($X\ ^1\Sigma^+$) at all levels of theory. This feature implies that some electron density moves from Cu to O.

2.5.1.2 LINEAR 1 $^1\Pi$ STATIONARY POINT

The OH bond length for the constrained linear 1 $^1\Pi$ state is predicted to be slightly longer than those of the linear ground state except for the CASSCF method, while the predicted CuO bond distance increases or decreases depending on different methods and basis sets, as shown in Figure 2.5. At the QZVPP EOM coupled-cluster level with iterative partial triples, the linear stationary point geometry is predicted (EOM-CCSDT-3) to be $R_{\text{Cu-O}}$ = 1.728 Å and $R_{\text{O-H}}$ = 0.955 Å.

2.5.1.3 BENT $\tilde{X}\ ^1A'$ STATE

In agreement with the experimental findings, our theoretical study demonstrates that the true ground state of CuOH energetically favors a bent structure. This reveals the dramatic shift to covalent character in the balance of ionic/covalent interactions for the CuO bond compared to the alkali and alkali earth metal hydroxides. Since the vibrational analysis performed at the constrained linear stationary point yields a degenerate imaginary bending vibrational frequency (for example, 685i cm^{-1} at the CCSDT-3 level of theory with the QZVPP basis set), the linear structure is a saddle point on the ground state potential energy surface (Table 2.1).

The optimized geometries for the bent $\tilde{X}\ ^1A'$ state at seven levels of theory with the two basis sets are presented in Figure 2.6. The CuO and OH bond distances are significantly longer for the bent structure relative to the linear configuration. The bond angle appears to be surprisingly sensitive (± 5°) to the level of correlation effects. The CuO bond length and the bond angle generally decrease with more advanced treatments of correlation effects, while the OH bond distance increases. Larger basis sets shorten the OH bond lengths but widen the bond angles. With the QZVPP coupled-cluster method including perturbative and iterative partial triples, the equilibrium geometry is predicted by CCSD(T) to be $R_{\text{Cu-O}}$ = 1.776 Å, $R_{\text{O-H}}$ = 0.960 Å, and $\theta_{\text{Cu-O-H}}$ = 110.7°. The CuO distance for $\tilde{X}\ ^1A'$ CuOH is considerably longer than that for diatomic $X\ ^2\Pi$ CuO, while the OH distance is shorter than those of diatomic OH ($X\ ^2\Pi$), OH^+ ($X\ ^3\Sigma^-$), and OH^- ($X\ ^1\Sigma^+$) with the larger basis sets.

In this research, three sophisticated coupled-cluster methods including triple excitations have been employed with the nearly saturated QZVPP basis set of Ahlrichs. All three of these methods give similar OH bond lengths and CuOH bond angles, which are consistent with the experimental values. The CCSD(T) method is considered to be the one that provides the best prediction of the experimental structure of CuOH. In addition, the Douglas-Kroll relativistic study shows a 0.023 Å contraction for $R_{\text{Cu-O}}$, 1.0° decrease for $\theta_{\text{Cu-O-H}}$, and 0.001 Å increase for $R_{\text{O-H}}$ at the cc-pVQZ_DK EOM-CCSD level of theory, compared to the corresponding non-relativistic predictions. The 0.023 Å bond contraction of $R_{\text{Cu-O}}$ is consistent with Pyykkö's conclusions concerning relativistic effects for Cu compounds.[46] Taking relativity into account, the cc-pVQZ_DK EOM-CCSD result ($R_{\text{Cu-O}}$ = 1.771 Å, $R_{\text{O-H}}$ = 0.956 Å, and $\theta_{\text{Cu-O-H}}$ = 111.1°) provides full agreement with experiment, considering the spread among the three experimental structures.[4,6,9] It does appear to us that the experimental OH distance of Trkula and Harris[4] is too short by at least 0.01 Å.

2.5.1.4 SINGLET EXCITED STATE 2 ^{1}A′

The 2 ^{1}A′ state is expected to be non-linear due to the existence of the two distinct imaginary vibrational frequencies at the linear geometry of the 1 $^1\Pi$ state (Table 2.2.1 and 2.2.2). For example, at the EOM-CCSD level of theory with the QZVPP basis set, the bending frequency is 455i cm^{-1} on the ^{1}A″ potential surface and 366i cm^{-1} on the ^{1}A′ potential surface.

The optimized geometries for the 2 ^{1}A′ state at the SACASSCF and three EOM-CC levels of theory are depicted in Figure 2.7. An increase of basis set size generally shortens both the CuO and OH bond distances, while it opens the bond angle, except for the cc-pVTZ EOM-CC methods. At the QZVPP EOM-CCSD level of theory, the optimized geometry is $R_{\text{Cu-O}}$ = 1.793 Å, $R_{\text{O-H}}$ = 0.954 Å, and $\theta_{\text{Cu-O-H}}$ = 124.8°. At the PolCu(g)/TZ2P(d,f) EOM-CCSDT-3 level of theory, the optimized geometry is $R_{\text{Cu-O}}$ = 1.775 Å, $R_{\text{O-H}}$ = 0.959 Å, and $\theta_{\text{Cu-O-H}}$ = 125.6°. The CuO bond length of the 2 ^{1}A′ state is considerably longer than that of the linear $\tilde{X}$ $^1\Sigma^+$ and 1 $^1\Pi$ structures, but close to that of the $\tilde{X}$ ^{1}A′ ground state. Relative to the $\tilde{X}$ ^{1}A′ state, the 2 ^{1}A′ state has a slightly shorter $R_{\text{O-H}}$, and a significantly larger angle $\theta_{\text{Cu-O-H}}$, about 12° for the QZVPP EOM-CCSD method and 16° for the PolCu(g)/TZ2P(d,f) EOM-CCSDT-3 method. The Douglas-Kroll relativistic study shows a 0.001 Å increase for $R_{\text{Cu-O}}$, 0.2° decrease for θ_{CuOH}, and almost the same $R_{\text{O-H}}$ at the cc-pVQZ_DK EOM-CCSD level of theory compared to the corresponding non-relativistic predictions.

Although in seemingly perfect agreement with the experimental $R_{\text{Cu-O}}$ value of 1.7748(32) Å, the theoretical equilibrium geometries for the 2 ^{1}A′ state at the EOM-CC level of theory present large deviations of $R_{\text{O-H}}$ (0.07 Å) and $\theta_{\text{Cu-O-H}}$ (12°~16°) from the experimental values. Although we have much respect for Bernath's research group, their 2 ^{1}A′ OH distance of 1.035 Å is unreasonably long. Jarman, Fernando, and Bernath[7] seem to recognize this, but state "The simplistic ionic model also cannot explain the large increase (~ 8%) in the O-H bond length between the $\tilde{X}$ ^{1}A′ and $\tilde{A}$ ^{1}A′ states. The only appropriate model is therefore one in which covalent bonding and electron correlation are fully taken into account."

2.5.1.5 SINGLET EXCITED STATE 1 ^{1}A″

Similar to the 2 ^{1}A′ state, the 1 ^{1}A″ state has a bent equilibrium structure. The CuO bond distance for the 1 ^{1}A″ state is again longer (by about 0.04 Å) than that for the $\tilde{X}$ $^1\Sigma^+$ and 1 $^1\Pi$ states, but comparable to that for the $\tilde{X}$ ^{1}A′ state, as shown in Figure 2.8. The bent 1 ^{1}A″ state of CuOH has a smaller bond angle by 5° and 10° compared to that of the 2 ^{1}A′ state with the QZVPP EOM-CCSD and PolCu(g)/TZ2P(d,f) EOM-CCSDT-3 methods, respectively. However, the bond angle is still 7° larger than that of the bent ground $\tilde{X}$ ^{1}A′ state at the QZVPP CCSD level of theory, and 6° larger at the PolCu(g)/TZ2P(d,f) CCSDT-3 level of theory. At the QZVPP EOM-CCSD level of theory, the optimized geometry is $R_{\text{Cu-O}}$ = 1.780 Å, $R_{\text{O-H}}$ = 0.958 Å, and $\theta_{\text{Cu-O-H}}$ = 120.3°.

At the PolCu(g)/TZ2P(d,f) EOM-CCSDT-3 level of theory, the optimized geometry is $R_{\text{Cu-O}} = 1.769$ Å, $R_{\text{O-H}} = 0.965$ Å, and $\theta_{\text{Cu-O-H}} = 115.6°$.

The Douglas-Kroll relativistic results show a 0.009 Å contraction for $R_{\text{Cu-O}}$, 1.2° decrease for θ_{CuOH}, and negligible change to $R_{\text{O-H}}$ at the cc-pVQZ_DK EOM-CCSD level of theory compared to the corresponding non-relativistic predictions. This 0.009 Å relativistic contraction of the CuO bond length for the 1 ^{1}A″ state is 0.014 Å smaller than that for the $\tilde{X}$ ^{1}A′ state (0.023 Å). Overall, the predicted equilibrium structure appears to be surprisingly sensitive to the level of correlation effects. However, the theoretical predictions reasonably agree with the available experimental geometrical parameters for the 1 ^{1}A″ state. The 1 ^{1}A″ cc-pVQZ_DK relativistic EOM-CCSD CuO distance is 0.0063 Å shorter than that for the experimental structure of Bernath,[6] which we consider to be the more reliable experiment. The theoretical CuOH angle is 0.23° more than the best experiment, while the OH distance is 0.008 Å longer than experiment. Given the differences between r_e structures (this work) and vibrationally averaged (experimental) structures, this agreement must be considered very good.

2.5.2 DIPOLE MOMENTS

The dipole moment of the constrained linear ground $\tilde{X}$ $^1\Sigma^+$ state is predicted to be 3.68 debye at the QZVPP coupled-cluster level with perturbative partial triples, i.e., CCSD(T). Improved treatment of correlation effects generally decreases the magnitude of the dipole moment. The electronegativity of Cu (1.9) is close to that of H (2.1), but much smaller than that of O (3.5). Thus, the direction of the dipole moment is $^+$CuOH$^-$. The dipole moment of the linear 1 $^1\Pi$ stationary point is predicted to be 0.76 debye at the

QZVPP SCF level of theory and 0.43 debye at the PolCu/TZ2P CISD level of theory, which is much smaller than that for the $\tilde{X}\ ^1\Sigma^+$ state. The single excitation 4π (a weakly anti-bonding π orbital or a non-bonding O 2p orbital in Figure 2.1) → 10σ (a weakly anti-bonding σ orbital or a non-bonding Cu 4s orbital) decreases the polarity of the CuOH molecule.

The bent ground $\tilde{X}\ ^1A'$ state has a slightly larger dipole moment (for example, 3.98 debye at the QZVPP CCSDT-3 level of theory) than the linear $\tilde{X}\ ^1\Sigma^+$ state. As was the case for the linear $\tilde{X}\ ^1\Sigma^+$ state, improved treatments of correlation effects generally decrease the magnitude of the dipole moment. Similar to the comparison of the linear excited 1 $^1\Pi$ state to the linear ground $\tilde{X}\ ^1\Sigma^+$ state, both the bent excited 2 $^1A'$ state and the 1 $^1A''$ state have considerably smaller dipole moments (1.69 debye and 1.34 debye at the PolCu(g)/TZ2P(d,f) EOM-CCSDT-3 level of theory, respectively) than the bent ground $\tilde{X}\ ^1A'$ state.

2.5.3 VIBRATIONAL FREQUENCIES

The linear $\tilde{X}\ ^1\Sigma^+$ state possesses a degenerate imaginary vibrational bending frequency at all levels of theory (see Table 2.1). Therefore, this linear structure is an inversion transition state that connects the two equivalent bent equilibrium structures. The CuO harmonic stretching frequency (ω_3) for the diatomic $X\ ^2\Pi$ CuO is experimentally determined to be ω_e = 640 cm^{-1}.[45] The corresponding theoretical CuO stretching frequency of 677 cm^{-1} at the QZVPP CCSD(T) level of theory for CuOH is higher than the diatomic value.

The OH stretching frequency (ω_1) is lower for the 1 $^1\Pi$ state of CuOH than that for the $\tilde{X}$ $^1\Sigma^+$ state, owing to the elongated OH bond distance. The linear 1 $^1\Pi$ state presents two distinct imaginary bending frequencies at all levels of theory (in Table 2.2.1 and 2.2.2). The magnitude of the imaginary frequencies is significantly smaller than that for the linear ground $\tilde{X}$ $^1\Sigma^+$ state, indicating that the two bent equilibrium singlet excited states are expected to have larger equilibrium bond angles and smaller energy barriers to linearity.

For the bent ground $\tilde{X}$ $^1A'$ state in Table 2.3.1, 2.3.2, and 2.3.3, all levels of theory overestimate ω_1 compared to the experimental value, but this feature lessens as higher levels of theory are used. The three real harmonic vibrational frequencies of the $\tilde{X}$ $^1A'$ state are predicted to be ω_1 (OH stretch) = 3856 cm^{-1}, ω_2 (bend) = 737 cm^{-1}, and ω_3 (CuO stretch) = 624 cm^{-1} at the QZVPP CCSD(T) level of theory. The CuO stretching frequency in CuOH is generally lower than that for diatomic CuO (X $^2\Pi$) except at the CCSDT-3 and CC3 levels of theory, reflecting the longer CuO bond distances. While the SCF method underestimates both ω_2 and ω_3 by around 10%, all the other methods produce results comparable to the available experimental frequencies.

The theoretical OH stretching (ω_1) and CuO stretching (ω_3) vibrational frequencies (for example, 3896 cm^{-1} and 696 cm^{-1} at the PolCu(g)/TZ2P(d,f) EOM-CCSDT-3 level of theory) for the 2 $^1A'$ state (in Table 2.4) are higher than the corresponding modes of the ground $\tilde{X}$ $^1A'$ state. However, the theoretical CuOH bending (ω_2) frequency (for example, 436 cm^{-1} at the PolCu(g)/TZ2P(d,f) EOM-CCSDT-3 level of theory) of the 2 $^1A'$ state is much lower than the corresponding mode of the ground $\tilde{X}$ $^1A'$ state, due to the much wider bond angle. According to the present vibrational analysis, there is a strong coupling between the bending and CuO stretching vibrations. Therefore, it may be more appropriate to assign the 696 cm^{-1} vibration to a [CuO stretch + bend] mode and the 436 cm^{-1} vibration to a [CuO stretch – bend] mode.

The theoretical 1 $^1A''$ state OH stretching (ω_1) frequencies using CC methods (for example 3805 cm^{-1} at the PolCu(g)/TZ2P(d,f) EOM-CCSDT-3 level of theory) (in Table 2.5.1 and 2.5.2) are lower than the corresponding modes of the ground $\tilde{X}$ $^1A'$ state, while the predicted CuO stretching (ω_3) frequencies (675 cm^{-1} at the PolCu(g)/TZ2P(d,f) EOM-CCSCT-3 level of theory) are very close to those of the ground $\tilde{X}$ $^1A'$ state. Both the ω_1 and ω_3 stretches of the 1 $^1A''$ state are lower than the corresponding modes of the 2 $^1A'$ state. In addition, the theoretical CuOH bending (ω_2) frequencies of the 1 $^1A''$ state at all levels of theory (for example, 626 cm^{-1} at the PolCu(g)/TZ2P(d,f) EOM-CCSDT-3 level of theory) are lower than the corresponding modes of the ground $\tilde{X}$ $^1A'$ state and higher than those of the 2 $^1A'$ state, reflecting the intermediate bond angle between those of the $\tilde{X}$ $^1A'$ and 2 $^1A'$ states. Again, it may be more appropriate to assign the 675 cm^{-1} vibration to a [CuO stretch + bend] mode and the 626 cm^{-1} vibration to a [CuO stretch – bend] mode.

2.5.4 ROTATIONAL CONSTANTS

The three rotational constants of the bent ground $\tilde{X}$ $^1A'$ state are predicted to be $A_e = 22.65$ cm^{-1}, $B_e = 0.39$ cm^{-1}, and $C_e = 0.38$ cm^{-1} at the QZVPP CCSD(T) level, which agrees fairly well with the available experimental observations ($A_0 = 23.0391$ cm^{-1}, $B_0 = 0.3922$ cm^{-1}, $C_0 = 0.3846$ cm^{-1}), as shown in Table 2.6.1 and 2.6.2. Note, of course, that one cannot expect precise agreement between equilibrium and vibrationally averaged rotational constants. Improved treatments of correlation effects generally decrease the magnitude of the rotational constant A_e, while increasing the magnitude of the rotational constants B_e and C_e. In addition, extension of the basis set generally increases the rotational constant A_e.

For the bent excited 2 $^1A'$ state the rotational constants are predicted to be A_e = 30.57 cm^{-1}, B_e = 0.38 cm^{-1}, and C_e = 0.38 cm^{-1} at the PolCu(g)/TZ2P(d,f) EOM-CCSDT-3 level of theory. The theoretical A_e value presents a large deviation from the experimental finding of 18.3160 cm^{-1}, resulting in the geometrical parameters different from the experimental structures, as discussed above in Section IV.A.iv. Most seriously, the equilibrium geometries of the 2 $^1A'$ state at EOM-CC levels of theory are 0.07 Å shorter for $R_{\text{O-H}}$ and 12°~16° larger for $\theta_{\text{Cu-O-H}}$ compared with the available experimental values. As implied above, it would appear that the experimental rotational constant A is incorrect.

Finally we consider the rotational constants of the bent excited 1 $^1A''$ state. These are predicted to be A_e = 24.25 cm^{-1}, B_e = 0.39 cm^{-1}, and C_e = 0.38 cm^{-1} at the PolCu(g)/TZ2P(d,f) EOM-CCSDT-3 level of theory, which exhibits reasonable agreement with the experimental observations (A_0 = 25.8982 cm^{-1}, B_0 = 0.3822 cm^{-1}, C_0 = 0.3760 cm^{-1}). Improved treatments of correlation effects generally decrease the magnitude of the rotational constants A_e, while extension of the basis set generally increases the rotational constants B_e and C_e. Furthermore, the Douglas-Kroll relativistic study shows only small differences for the three rotational constants of the $\tilde{X}$ $^1A'$, 2 $^1A'$, and 1 $^1A''$ states compared to the corresponding non-relativistic predictions.

2.5.5 ENERGETICS

At all levels of theory the bent 1 $^1A'$ state is predicted to be the electronically lowest-lying singlet isomer of CuOH, as shown in Table 2.7.1 and 2.7.2. The linear $^1\Sigma^+$ stationary point is an inversion transition state and lies 9.2 kcal mol^{-1} (at the QZVPP CCSD(T) level) above the bent equilibrium $\tilde{X}$ $^1A'$ ground state (Figure 2.9). This barrier to linearity is predicted to be 11.0 kcal mol^{-1} from the CCSDT-3 method with the PolCu(g)/TZ2P(d,f) basis set. The linear 1 $^1\Pi$ structure is a Renner-Teller state that splits into two bent equilibrium structures. Using the QZVPP basis set, the 1 $^1\Pi$ state is predicted to lie 59.4 kcal mol^{-1} (EOM-CCSDT-3) above the bent electronic ground state.

The bent singlet excited state 2 $^1A'$ is predicted to lie 49.3 (EOM-CCSD) and 57.9 kcal mol^{-1} (EOM-CCSDT-3) above the ground $\tilde{X}$ $^1A'$ state with the PolCu(g)/TZ2P(d,f) basis set. The 2 $^1A' \leftarrow \tilde{X}$ $^1A'$ adiabatic energy separation from the EOM-CCSDT-3 method with the PolCu(g)/TZ2P(d,f) basis set is predicted to be T_0 = 57.6 kcal mol^{-1}, which is 12.1 kcal mol^{-1} higher than Bernath's experimental value[7] of T_0 = 45.5 kcal mol^{-1}.

The bent singlet excited state 1 $^1A''$ is predicted to lie 9.2 (SCF), 34.9 (CASSCF), 47.4 (CISD), 46.7 (EOM-CCSD), 53.3 (EOM-CCSDT-3), and 57.3 kcal mol^{-1} (EOM-CC3) above the ground $\tilde{X}$ $^1A'$ state using the PolCu(g)/TZ2P(d,f) basis set. The adiabatic excitation energy T_0 of 9.1 ~ 9.8 kcal mol^{-1} at the SCF level of theory is much lower than the experimental value[4,6] of 52.6 kcal mol^{-1} for the 1 $^1A''$ state. However, all correlated methods yield energy separations which are in much better agreement with the experiments, demonstrating the significance of electron correlation for CuOH. The 1 $^1A''$ $\leftarrow \tilde{X}$ $^1A'$ vibrationally corrected adiabatic excitation energy from the EOM-CCSDT-3 method with the PolCu(g)/TZ2P(d,f) basis set is predicted to be T_0 = 53.1 kcal mol^{-1} which is only 0.5 kcal mol^{-1} higher than the experimental value of T_0 = 52.6 kcal mol^{-1}.

It should be noted that the 1 ^{1}A″ state is predicted to have a smaller T_e (T_0) value than the 2 ^{1}A′ state at the same level of theory, as shown in Table 2.7.1 and 2.7.2. The energy difference of T_e (T_0) between the 1 ^{1}A″ and 2 ^{1}A′ states is about 1-5 kcal mol^{-1}, and an increase occurs as the higher level of theory is used for computations (Figure 2.10), which implies that 1 ^{1}A″ state might lies lower than 2 ^{1}A′ state. The Douglas-Kroll relativistic single point energies at the EOM-CCSD equilibrium structures for the ground and excited states give rise to the adiabatic excitation energies with relativistic corrections, as shown in Table 2.7.2. Note that the addition of relativistic effects always increases the energy separation between the 2 ^{1}A′ and 1 ^{1}A″ states, making the 1 ^{1}A″ state lying even more lower than the 2 ^{1}A′ state. For example, the relativistic results show decreases of 3.0 and 4.5 kcal mol^{-1} in the adiabatic excitation energies T_e for the 2 ^{1}A′ and 1 ^{1}A″ states, respectively, indicating that the 1 ^{1}A″ state lies 2.2 kcal mol^{-1} lower than 2 ^{1}A′ state at the cc-pVQZ_DK EOM-CCSD level of theory. This 2.2 kcal mol^{-1} energy difference between the 2 ^{1}A′ and 1 ^{1}A″ excited states is 1.5 kcal mol^{-1} larger than that (0.7 kcal mol^{-1}) of the corresponding non-relativistic prediction. The barriers to linearity are determined to be small, 0.8 kcal mol^{-1} for the 2 ^{1}A′ state, and 5.4 kcal mol^{-1} for the 1 ^{1}A″ state from the EOM-CCSDT-3 wave function with the PolCu(g)/TZ2P(d,f) basis set.

2.6 CONCLUDING REMARKS

Two constrained linear ($\widetilde{X}$ $^1\Sigma^+$ and 1 $^1\Pi$) stationary points and three bent ($\widetilde{X}$ ^{1}A′, 2 ^{1}A′ and 1 ^{1}A″) equilibrium structures for CuOH have been investigated using *ab initio* quantum mechanical techniques. The ground state of CuOH has been confirmed to be strongly bent with bond angle of about 110° with coupled-cluster methods. The CuO and OH bond distances of the 2 $^1A'$ state are slightly elongated and shortened, respectively, relative to the ground state. There is little change of bond lengths for the 1 $^1A''$ state compared to the ground state. The predicted bond angles for the excited singlet state 2 $^1A'$ (123°) and the excited singlet state 1 $^1A''$ (118°) are wider than that of the ground state (111°). The experimental rotational constants and deduced geometry for the 2 $^1A'$ state appear to be in error.

The ZPVE-corrected adiabatic excitation energies are predicted to be 57.6 kcal mol^{-1} for the 2 $^1A'$ state and 53.1 kcal mol^{-1} for the 1 $^1A''$ state with the PolCu(g)/TZ2P(d,f) EOM-CCSDT-3 method. The Douglas-Kroll relativistic corrections to these excitation energies are substantial.

The barrier heights to linearity for the ground and two singlet excited states are predicted to be 11.0 kcal mol^{-1} for the $\tilde{X}$ $^1A'$ state, 0.8 kcal mol^{-1} for the 2 $^1A'$ state, and 5.4 kcal mol^{-1} for the 1 $^1A''$ state from the CCSDT-3/EOM-CCSDT-3 wave function with the PolCu(g)/TZ2P(d,f) basis set.

The great mystery that remains is the identity of the observed electronic state[7] at 45.5 kcal. This spectral feature does not appear to be the CuOH 2 $^1A'$ electronic state, which we predict to lie at 57.6 kcal mol^{-1}. A plausible alternative is the lowest triplet state of CuOH, either the $^3A''$ state or the $^3A'$ state. With the cc-pVTZ basis set, the CCSD(T) method predicts the lowest $^3A''$ state to lie at 47.2 kcal mol^{-1}. However, the $^3A''$ rotational constants (24.24, 0.39, and 0.38 cm^{-1}) are a poor fit to the experimental values (18.32, 0.39, and 0.38 cm^{-1}). Similarly, CCSD(T) predicts the lowest $^3A'$ state to lie at 43.5 kcal mol^{-1}, with rotational constants (24.34, 0.39, and 0.38 cm^{-1}) again in poor agreement with experiment. Thus the identity of the observed feature at 45.5 kcal mol^{-1} is unclear.

2.7 ACKNOWLEDGEMENTS

We thank Professor Kirk Peterson (Washington State University) for transmission of basis sets prior to publication. The authors would like to thank Dr. Kurt W. Sattelmeyer and Justin M. Turney for very helpful discussions on ACES and PSI software packages. This research was performed in part using the Molecular Science Computing Facility (MSCF) in the William R. Wiley Environmental Molecular Sciences Laboratory, a national scientific user facility sponsored by the U.S. Department of Energy's Office of Biological and Environmental Research and located at the Pacific Northwest National Laboratory. Pacific Northwest is operated for the Department of Energy by Battelle. This research was supported by the National Science Foundation, Grant CHE-0451445.

2.8 REFERENCES

1. Thiel, P. A.; Madey, T. F. *Surf. Sci. Rep.* **1987**, *7*, 211.
2. Fisher, G. B.; Sexton, B. A. *Phys. Rev. Lett.* **1980**, *44*, 683.
3. Andersson, S.; Davenport, J. W. *Solid State Commun.* **1978**, *28*, 677.
4. Trkula, M.; Harris, D. O. *J. Chem. Phys.* **1983**, *79*, 1138.
5. Kauffman, J. W.; Hauge, R. H.; Margrave, J. L. *J. Phys. Chem.* **1985**, *89*, 3541.
6. Jarman, C. N.; Fernando, W. T. M. L.; Bernath, P. F. *J. Mol. Spectrosc.* **1990**, *144*, 286.

7. Jarman, C. N.; Fernando, W. T. M. L.; Bernath, P. F. *J. Mol. Spectrosc.* **1991**, *145*, 151.

8. Whitham, C. J.; Ozeki, H.; Saito, S. *J. Chem. Phys.* **1999**, *110*, 11109.

9. Whitham, C. J.; Ozeki, H.; Saito, S. *J. Chem. Phys.* **2000**, *112*, 641.

10. Illas, F.; Rubio, J.; Centellas, F.; Virgili, J. *J. Phys. Chem.* **1984**, *88*, 5225.

11. Illas, F.; Rubio, J. *Chem. Phys. Lett.* **1985**, *119*, 397.

12. Bauschlicher, C. W. *Int. J. Quant. Chem.: Quant. Chem. Symp.* **1986**, *20*, 563.

13. Mochizuki, Y.; Takada, T.; Murakami, A. *Chem. Phys. Lett.* **1991**, *185*, 535.

14. Pápai, I. *J. Chem. Phys.* **1995**, *103*, 1860.

15. Bera, J. K.; Samuelson, A. G.; Chandrasekhar, J. *Organometallics* **1998**, *17*, 4136.

16. Trachtman, M.; Markham, G. D.; Glusker, J. P.; George, P.; Bock, C. W. *Inorg. Chem.* **2001**, *40*, 4230.

17. Ikeda, S.; Nakajima, T.; Hirao, K. *Mol. Phys.* **2003**, *101*, 105.

18. Herzberg, G.; Teller, E. *Z. Phys. Chem. Abt. B* **1933**, *21*, 410.

19. Renner, R. *Z. Phys.* **1934**, *92*, 172.

20. Purvis, G. D.; Bartlett, R. J. *J. Chem. Phys.* **1982**, *76*, 1910.

21. Raghavachari, K.; Trucks, G. W.; Pople, J. A.; Head-Gordon, M. *Chem. Phys. Lett.* **1989**, *157*, 479.

22. Bartlett, R. J.; Watts, J. D.; Kucharski, S. A.; Noga, J. *Chem. Phys. Lett.* **1990**, *165*, 513.

23. Noga, J.; Bartlett, R. J.; Urban, M. *Chem. Phys. Lett.* **1987**, ***134***, 126.

24. Koch, H.; Christiansen, O.; Jørgensen, P.; Sanchez de Merás, A. M.; Helgaker, T. *J. Chem. Phys.* **1997**, *106*, 1808.

25. Stanton, J. F.; Bartlett, R. J. *J. Chem. Phys.* **1993**, *98*, 7029.

26. Werner, H. J.; Knowles, P. J. *J. Chem. Phys.* **1985**, *82*, 5053.

27. Knowles, P. J.; Werner, H. J. *Chem. Phys. Lett.* **1985**, *115*, 259.

28. ACES II is a program product of the Quantum Theory Project, University of Florida. Authors: Stanton, J. F.; Gauss, J.; Watts, J. D.; Nooijen, M.; Oliphant, N.; Perera, S. A.; Szalay, P. G.; Lauderdale, W. J.; Gwaltney, S. R.; Beck, S.; Balkova, A.; Bernholdt, D. E.; Baeck, K.-K.; Rozyczko, P.; Sekino, H.; Hober, C.; Bartlett, R. J. Integral packages included are VMOL (Almlöf, J. and Taylor, P. R.); VPROPS (Taylor, P.); ABACUS (Helgaker, T.; Jensen, H. J. Aa.; Jørgensen, P.; Olsen, J.; and Taylor, P. R.).

29. PSI 2.0.8, Janssen, C. L.; Seidl, E. T.; Scuseria, G. E.; Hamilton, T. P.; Yamaguchi, Y.; Remington, R. B.; Xie, Y.; Vacek, G.; Sherrill, C. D.; Crawford, T. D.; Fermann, J. T.; Allen, W. D.; Brooks, B. R.; Fitzgerald, G. B.; Fox, D. J.; Gaw, J. F.; Handy, N. C.; Laidig, W. D.; Lee, T. J.; Pitzer, R. M.; Rice, J. E.; Saxe, P.; Scheiner, A. C.; Schaefer, H. F. PSITECH, Inc.: Watkinsville, GA 30677, U.S.A., 1995.

30. MOLPRO, a package of *ab initio* programs designed by Werner, H.-J. and Knowles, P. J., version 2002.1, Amos, R. D.; Bernhardsson, A.; Berning, A.; Celani, P.; Cooper, D. L.; Deegan, M. J. O.; Dobbyn, A. J.; Eckert, F.; Hampel, C.; Hetzer, G.; Knowles, P. J.; Korona, T.; Lindh, R.; Lloyd, A. W.; McNicholas, S. J.; Manby, F. R.; Meyer, W.; Mura, M. E.; Nicklass, A.; Palmieri, P.; Pitzer, R. M.; Rauhut, G.; Schütz, M.; Schumann, U.; Stoll, H.; Stone, A. J.; Tarroni, R.; Thorsteinsson, T.; Werner, H.-J.

31. Wachters, A. J. H. *J. Chem. Phys.* **1970**, *52*, 1033.

32. Hay, P. J. *J. Chem. Phys.* **1977**, *66*, 4377.

33. Hood, D. M.; Pitzer, R. M.; Schaefer, H. F. *J. Chem. Phys.* **1979**, *71*, 705.

34. Huzinaga, S. *J. Chem. Phys.* **1965**, *42*, 1293.

35. Dunning, T. H. *J. Chem. Phys.* **1970**, *53*, 2823.

36. Langhoff, S. R.; Bauschlicher, C. W. *J. Chem. Phys.* **1986**, *84*, 4485.

37. Neogrády, P.; Kellö, V.; Urban, M.; Sadlej, A. J. *Theoret. Chim. Acta* **1996**, *93*, 101.

38. Kellö, V.; Sadlej, A. J. *Theoret. Chim. Acta* **1996**, *94*, 93.

39. Dunning, T. H. *J. Chem. Phys.* **1971**, *55*, 716.

40. Dunning, T. H. *J. Chem. Phys.* **1989**, *90*, 1007.

41. Balabanov, N. B.; Peterson, K. A. *J. Chem. Phys.* submitted.

42. Weigend, F.; Furche, F.; Ahlrichs, R. *J. Chem. Phys.* **2003**, *119*, 12753.

43. Douglas, M.; Kroll, N. M. *Ann. Phys.* **1974**, *82*, 89.

44. De Jong, W. A.; Harrison, R. J.; Dixon, D. A. *J. Chem. Phys.* **2001**, *114*, 48.

45. Huber, K. P.; Herzberg, G. *Molecular Spectra and Molecular Structure. IV. Constants of Diatomic Molecules.* Van Nostrand Reinhold: New York, 1979.

46. Pyykkö, P. *Chem. Rev.* **1988**, *88*, 563.

Table 2.1: Theoretical predictions of the total energy (in hartree), dipole moment (in debye), harmonic vibrational frequencies (in cm^{-1}), and zero-point vibrational energy (ZPVE in kcal mol^{-1}) for the linear $\tilde{X}\ {}^1\Sigma^+$ stationary point of the CuOH molecule.

Level of Theory	Energy	μ	ω_1	ω_2	ω_3	ZPVE
cc-pVTZ SCF	-1714.419 957	4.598	4313	523i	615	7.05
cc-pVTZ CASSCF	-1714.558 284	···	···	···	···	···
QZVPP SCF	-1714.432 559	4.762	4317	512i	597	7.02
QZVPP CASSCF	-1714.573 564	···	···	···	···	···
cc-pVTZ CISD	-1715.058 146	4.036	4222	594i	658	6.98
QZVPP CISD	-1715.354 811	4.172	4265	577i	656	7.03
cc-pVTZ CCSD	-1715.124 971	3.730	4108	650i	670	6.83
QZVPP CCSD	-1715.468 094	3.865	4120	640i	671	6.85
cc-pVTZ CCSD(T)	-1715.153 280	3.494	4072	677i	680	6.79
QZVPP CCSD(T)	-1715.504 442	3.681	4075	663i	677	6.79
cc-pVTZ CCSDT-3	-1715.156 020	3.350	4076	689i	689	6.81
QZVPP CCSDT-3	-1715.511 755	3.434	4081	685i	697	6.83
cc-pVTZ CC3	-1715.162 804	···	4069	700i	697	6.81
QZVPP CC3	-1715.522 029	···	4073	697i	712	6.84

Table 2.2.1: Theoretical predictions of the total energy (in hartree), dipole moment (in debye), harmonic vibrational frequencies (in cm^{-1}), and zero-point vibrational energy (ZPVE in kcal mol^{-1}) for the linear 1 $^1\Pi$ stationary point of the CuOH molecule.

Level of Theory	Energy	μ	ω_1	ω_2 ($^1A''$)	ω_2 ($^1A'$)	ω_3	ZPVE
cc-pVTZ SCF	-1714.410 159	0.618	4317	470i	···	709	7.19
cc-pVTZ CASSCF	-1714.503 483	···	···	···	···	···	···
QZVPP SCF	-1714.421 145	0.757	4318	467i	···	695	···
QZVPP CASSCF	-1714.516 270	···	···	···	···	···	···
Wachters/DZP CISD	-1714.668 591	0.389	4154	522i	···	727	6.98
PolCu/TZ2P CISD	-1715.033 935	0.426	4212	528i	···	736	7.07
PolCu(g)/TZ2P(d,f) CISD	-1715.113 656	···	4218	509i	···	749	7.10
cc-pVTZ CISD	-1714.988 315	···	4187	496i	···	730	7.03
Wachters/DZP EOM-CCSD	-1714.710 105	···	3980	487i	254i	692	6.68
PolCu/TZ2P EOM-CCSD	-1715.130 251	···	3990	499i	283i	702	6.71
PolCu(g)/TZ2P(d,f) EOM-CCSD	-1715.218 853	···	3993	483i	248i	718	6.73
cc-pVTZ EOM-CCSD	-1715.048 289	···	3977	466i	430i	754	6.76
QZVPP EOM-CCSD	-1715.394 556	···	3988	455i	366i	700	6.70

Table 2.2.2: Theoretical predictions of the total energy (in hartree), dipole moment (in debye), harmonic vibrational frequencies (in cm^{-1}), and zero-point vibrational energy (ZPVE in kcal mol^{-1}) for the linear 1 $^1\Pi$ stationary point of the CuOH molecule. (Continued)

Level of Theory	Energy	μ	ω_1	ω_2 ($^1A''$)	ω_2 ($^1A'$)	ω_3	ZPVE
Wachters/DZP EOM-CCSDT-3	-1714.725 538	···	3946	540i	···	697	6.64
PolCu/TZ2P EOM-CCSDT-3	-1715.157 795	···	3911	543i	···	683	6.57
PolCu(g)/TZ2P(d,f) EOM-CCSDT-3	-1715.249 736	···	3915	528i	···	708	6.61
cc-pVTZ EOM-CCSDT-3	-1715.079 106	···	3930	500i	···	767	6.71
QZVPP EOM-CCSDT-3	-1715.432 477	···	3915	···	···	701	
Wachters/DZP EOM-CC3	-1714.729 890	···	3937	554i	···	700	6.63
PolCu/TZ2P EOM-CC3	-1715.160 926	···	3893	505i	···	642	6.48
PolCu(g)/TZ2P(d,f) EOM-CC3	-1715.253 246	···	3900	···	···	680	6.55
cc-pVTZ EOM-CC3	-1715.085 433	···	3894	509i	···	681	6.54
QZVPP EOM-CC3	-1715.438 665	···	3904	···	···	697	

Table 2.3.1: Theoretical predictions of the total energy (in hartree), dipole moment (in debye), harmonic vibrational frequencies (in cm^{-1}), and zero-point vibrational energy (ZPVE in kcal mol^{-1}) for the bent $\tilde{X}$ ^{1}A′ ground state of the CuOH molecule.

Level of Theory	Energy	μ	ω_1	ω_2	ω_3	ZPVE
Wachters/DZP SCF	-1714.353 573	5.528	4200	657	588	7.78
Wachters/DZP CASSCF	-1714.487 089	···	···	···	···	···
PolCu/TZ2P SCF	-1714.373 682	5.423	4213	654	586	7.80
PolCu/TZ2P CASSCF	-1714.515 686	···	···	···	···	···
PolCu(g)/TZ2P(d,f) SCF	-1714.375 063	5.394	4223	637	587	7.79
PolCu(g)/TZ2P(d,f) CASSCF	-1714.516 946	···	···	···	···	···
cc-pVTZ SCF	-1714.427 278	5.392	4192	639	587	7.74
cc-pVTZ CASSCF	-1714.567 518	···	···	···	···	···
QZVPP SCF	-1714.439 334	5.477	4205	631	575	7.73
QZVPP CASSCF	-1714.581 942	···	···	···	···	···
Wachters/DZP CISD	-1714.742 720	4.826	4007	722	609	7.63
PolCu/TZ2P CISD	-1715.116 667	4.786	4089	727	630	7.79
PolCu(g)/TZ2P(d,f) CISD	-1715.195 865	4.754	4108	716	643	7.82
cc-pVTZ CISD	-1715.069 190	4.829	4063	700	618	7.69
QZVPP CISD	-1715.364 464	4.884	4123	687	625	7.77
Wachters/DZP CCSD	-1714.785 408	4.466	3875	739	611	7.47
PolCu/TZ2P CCSD	-1715.210 657	4.354	3900	755	631	7.56
PolCu(g)/TZ2P(d,f) CCSD	-1715.299 797	4.327	3913	746	646	7.58
cc-pVTZ CCSD	-1715.138 987	4.446	3897	725	618	7.49
QZVPP CCSD	-1715.480942	4.493	3919	718	627	7.53

Table 2.3.2: Theoretical predictions of the total energy (in hartree), dipole moment (in debye), harmonic vibrational frequencies (in cm^{-1}), and zero-point vibrational energy (ZPVE in kcal mol^{-1}) for the bent $\tilde{X}$ $^1A'$ ground state of the CuOH molecule. (Continued)

Level of Theory	Energy	μ	ω_1	ω_2	ω_3	ZPVE
Wachters/DZP CCSD(T)	-1714.801 305	4.260	3836	748	607	7.42
PolCu/TZ2P CCSD(T)	-1715.239 414	4.175	3841	768	618	7.47
PolCu(g)/TZ2P(d,f) CCSD(T)	-1715.331 732	4.130	3852	762	635	7.50
cc-pVTZ CCSD(T)	-1715.169 137	4.150	3840	739	621	7.44
QZVPP CCSD(T)	-1715.519126	4.250	3856	737	624	7.46
Wachters/DZP CCSDT-3	-1714.808 924	3.986	3835	756	628	7.46
PolCu/TZ2P CCSDT-3	-1715.250 889	3.832	3835	780	646	7.52
PolCu(g)/TZ2P(d,f) CCSDT-3	-1715.343 230	3.799	3846	772	663	7.55
cc-pVTZ CCSDT-3	-1715.172 234	3.987	3839	742	632	7.45
QZVPP CCSDT-3	-1715.527 141	3.981	3851	747	647	7.50
Wachters/DZP CC3	-1714.815 394	···	3822	761	639	7.47
PolCu/TZ2P CC3	-1715.261 084	···	3816	787	657	7.52
PolCu(g)/TZ2P(d,f) CC3	-1715.353 635	···	3826	779	674	7.55
cc-pVTZ CC3	-1715.179 578	···	3823	747	641	7.45
QZVPP CC3	-1715.538 128	···	3830	756	661	7.50

Table 2.3.3: Theoretical predictions of the total energy (in hartree), dipole moment (in debye), harmonic vibrational frequencies (in cm^{-1}), and zero-point vibrational energy (ZPVE in kcal mol^{-1}) for the bent $\tilde{X}\ ^1A'$ ground state of the CuOH molecule. (Continued)

Level of Theory	Energy	μ	ω_1	ω_2	ω_3	ZPVE
PolCu/cc-pVTZ CCSD	-1715.228 380	···	···	···	···	···
PolCu/cc-pVTZ_DK Rel. CCSD	-1726.638 391	···	···	···	···	···
cc-pVTZ CCSD	-1715.138 987	···	···	···	···	···
cc-pVTZ_DK Rel. CCSD	-1729.355 693	···	···	···	···	···
cc-pVQZ CCSD	-1715.201 767	···	···	···	···	···
cc-pVQZ_DK Rel. CCSD	-1729.418 841	···	···	···	···	···
Experiment Ref. 4 (fundamentals).	···	···	···	743(1)	···	···
Experiment Ref. 5 (fundamentals).	···	···	···	727.7	632.7	···
Ref. 9 (estimated harmonics).	···	···	3738	744	628	···

Table 2.4: Theoretical predictions of the total energy (in hartree), dipole moment (in debye), harmonic vibrational frequencies (in cm^{-1}), and zero-point vibrational energy (ZPVE in kcal mol^{-1}) for the bent 2 $^1A'$ state of the CuOH molecule.

Level of Theory	Energy	μ	ω_1	ω_2	ω_3	ZPVE
cc-pVTZ SACASSCF	-1714.506 008	···	···	···	···	···
QZVPP SACASSCF	-1714.518 341	···	···	···	···	···
Wachters/DZP EOM-CCSD	-1714.713 095	1.959	3917	514	678	7.30
PolCu/TZ2P EOM-CCSD	-1715.133 474	1.846	3934	530	682	7.36
PolCu(g)/TZ2P(d,f) EOM-CCSD	-1715.221 270	1.842	3950	492	691	7.34
cc-pVTZ EOM-CCSD	-1715.052 952	1.801	3919	543	687	7.36
QZVPP EOM-CCSD	-1715.398 086	1.772	3944	515	683	7.35
Wachters/DZP EOM-CCSDT-3	-1714.727 897	1.745	3886	491	681	7.23
PolCu/TZ2P EOM-CCSDT-3	-1715.159 507	1.675	3882	479	681	7.21
PolCu(g)/TZ2P(d,f) EOM-CCSDT-3	-1715.250 890	1.692	3896	436	696	7.19
cc-pVTZ EOM-CCSDT-3	-1715.082 259	1.714	3873	511	682	7.24
Wachters/DZP EOM-CC3	-1714.730 999	···	3894	421	686	7.15
cc-pVTZ EOM-CC3	-1715.087 058	···	3871	454	683	7.16
PolCu/cc-pVTZ EOM-CCSD	-1715.151 390	···	···	···	···	···
PolCu/cc-pVTZ_DK Rel. EOM-CCSD	-1726.564 915	···	···	···	···	···
cc-pVTZ EOM-CCSD	-1715.052 952	···	···	···	···	···
cc-pVTZ_DK Rel. EOM_CCSD	-1729.273 891	···	···	···	···	···
cc-pVQZ EOM-CCSD	-1715.112 740	···	···	···	···	···
cc-pVQZ_DK Rel. EOM-CCSD	-1729.334 510	···	···	···	···	···

Table 2.5.1: Theoretical predictions of the total energy (in hartree), dipole moment (in debye), harmonic vibrational frequencies (in cm^{-1}), and zero-point vibrational energy (ZPVE in kcal mol^{-1}) for the bent 1 $^1A''$ state of the CuOH molecule.

Level of Theory	Energy	μ	ω_1	ω_2	ω_3	ZPVE
cc-pVTZ SCF	-1714.415 072	1.843	4209	592	677	7.83
cc-pVTZ CASSCF	-1714.515 167	···	···	···	···	···
QZVPP SCF	-1714.425 904	1.859	···	···	···	···
QZVPP CASSCF	-1714.527 338	···	···	···	···	···
Wachters/DZP CISD	-1714.676 308	1.842	4007	637	678	7.61
PolCu/TZ2P CISD	-1715.041 415	1.729	4083	656	694	7.77
PolCu(g)/TZ2P(d,f) CISD	-1715.120 316	···	4103	635	707	7.78
cc-pVTZ CISD	-1714.994 946	···	4058	619	684	7.66
Wachters/DZP EOM-CCSD	-1714.717 155	1.476	3861	600	652	7.31
PolCu/TZ2P EOM-CCSD	-1715.137 548	1.353	3878	617	666	7.38
PolCu(g)/TZ2P(d,f) EOM-CCSD	-1715.225 398	1.339	3892	597	680	7.39
cc-pVTZ EOM-CCSD	-1715.054 665	1.290	3864	579	653	7.28
QZVPP EOM-CCSD	-1715.400 091	1.322	3896	561	666	7.32
Wachters/DZP EOM-CCSDT-3	-1714.734 475	1.310	3811	625	657	7.28
PolCu/TZ2P EOM-CCSDT-3	-1715.167 051	1.339	3792	637	657	7.27
PolCu(g)/TZ2P(d,f) EOM-CCSDT-3	-1715.258 255	1.341	3805	626	675	7.30
cc-pVTZ EOM-CCSDT-3	-1715.086 854	1.363	3801	596	648	7.21

Table 2.5.2: Theoretical predictions of the total energy (in hartree), dipole moment (in debye), harmonic vibrational frequencies (in cm^{-1}), and zero-point vibrational energy (ZPVE in kcal mol^{-1}) for the bent 1 $^1A''$ state of the CuOH molecule. (Continued)

Level of Theory	Energy	μ	ω_1	ω_2	ω_3	ZPVE
Wachters/DZP EOM-CC3	-1714.739 559	···	3796	636	666	7.29
PolCu/TZ2P EOM-CC3	-1715.170 739	···	3782	637	667	7.27
PolCu(g)/TZ2P(d,f) EOM-CC3	-1715.262 348	···	3794	644	676	7.31
cc-pVTZ EOM-CC3	-1715.093 635	···	3784	602	652	7.20
PolCu/cc-pVTZ EOM-CCSD	-1715.155 562	···	···	···	···	···
PolCu/cc-pVTZ_DK Rel. EOM-CCSD	-1726.571 969	···	···	···	···	···
cc-pVTZ EOM-CCSD	-1715.054 665	···	···	···	···	···
cc-pVTZ_DK Rel. EOM-CCSD	-1729.278 296	···	···	···	···	···
cc-pVQZ EOM-CCSD	-1715.113 736	···	···	···	···	···
cc-pVQZ_DK Rel. EOM-CCSD	-1729.338 076	···	···	···	···	···

Table 2.6.1: Predicted equilibrium rotational constants (A_e, B_e, C_e values) in cm^{-1} for the $\tilde{X}\ ^1A'$, 2 $^1A'$, and 1 $^1A''$ states of the CuOH molecule.

Level of Theory	$\tilde{X}\ ^1A'$	2 $^1A'$	1 $^1A''$
cc-pVTZ SCF	27.35, 0.36, 0.35	···	31.34, 0.37, 0.37
QZVPP SCF	28.14, 0.36, 0.35	···	···
cc-pVTZ CISD	24.39, 0.38, 0.37	···	27.36, 0.38, 0.38
QZVPP CISD	25.64, 0.38, 0.38	···	···
cc-pVTZ CCSD/EOM-CCSD	22.80, 0.38, 0.38	28.55, 0.38, 0.37	25.60, 0.38, 0.38
QZVPP CCSD/EOM-CCSD	23.52, 0.39, 0.38	30.26, 0.38, 0.37	27.00, 0.38, 0.38
Wachters/DZP CCSD(T)	21.60, 0.38, 0.37	···	···
PolCu/TZ2P CCSD(T)	22.15, 0.38, 0.38	···	···
PolCu(g)/TZ2P(d,f) CCSD(T)	22.20, 0.39, 0.38	···	···
cc-pVTZ CCSD(T)	22.07, 0.39, 0.38	···	···
QZVPP CCSD(T)	22.65, 0.39, 0.38	···	···
Wachters/DZP CCSDT-3/EOM-CCSDT-3	21.63, 0.39, 0.38	27.97, 0.37, 0.37	23.88, 0.38, 0.37
PolCu/TZ2P CCSDT-3/EOM-CCSDT-3	22.16, 0.39, 0.38	29.12, 0.38, 0.37	23.98, 0.38, 0.38
PolCu(g)/TZ2P(d,f) CCSDT-3/EOM-CCSDT-3	22.20, 0.39, 0.39	30.57, 0.38, 0.38	24.25, 0.39, 0.38
cc-pVTZ CCSDT-3/EOM-CCSDT-3	22.06, 0.39, 0.38	28.11, 0.38, 0.37	24.24, 0.39, 0.38
QZVPP CCSDT-3/EOM-CCSDT-3	22.63, 0.39, 0.39	···	···

Table 2.6.2: Predicted equilibrium rotational constants (A_e, B_e, C_e values) in cm^{-1} for the $\tilde{X}$ $^1A'$, 2 $^1A'$, and 1 $^1A''$ states of the CuOH molecule. (Continued)

Level of Theory	$\tilde{X}$ $^1A'$	2 $^1A'$	1 $^1A''$
Wachters/DZP CC3/EOM-CC3	21.51, 0.39, 0.38	29.78, 0.37, 0.37	23.51, 0.38, 0.38
PolCu/TZ2P CC3/EOM-CC3	21.98, 0.39, 0.38	⋯	23.48, 0.39, 0.38
PolCu(g)/TZ2P(d,f) CC3/EOM-CC3	22.02, 0.40, 0.39	⋯	23.73, 0.40, 0.39
cc-pVTZ CC3/EOM-CC3	21.90, 0.39, 0.39	29.35, 0.38, 0.38	23.92, 0.39, 0.38
QZVPP CC3/EOM-CC3	22.43, 0.40, 0.39	⋯	⋯
PolCu/cc-pVTZ CCSD/EOM-CCSD	22.69, 0.38, 0.38	28.80, 0.37, 0.37	25.46, 0.38, 0.37
PolCu/cc-pVTZ_DK Rel. CCSD/EOM-CCSD	22.41, 0.39, 0.39	30.37, 0.37, 0.37	24.89, 0.38, 0.38
cc-pVTZ CCSD/EOM-CCSD	22.80, 0.38, 0.38	28.55, 0.38, 0.37	25.60, 0.38, 0.38
cc-pVTZ_DK Rel. CCSD/EOM-CCSD	22.47, 0.39, 0.39	28.46, 0.37, 0.37	25.04, 0.38, 0.38
cc-pVQZ CCSD/EOM-CCSD	23.29, 0.38, 0.37	28.85, 0.38, 0.37	26.26, 0.38, 0.37
cc-pVQZ_DK Rel. CCSD/EOM-CCSD	22.93, 0.39, 0.38	28.71, 0.37, 0.37	25.65, 0.38, 0.38
Experiment Ref. 4 (A_0, B_0, C_0)	22.95, 0.39, 0.38	⋯	25.85, 0.38, 0.38
Experiment Ref. 6,7 (A_0, B_0, C_0)	23.04, 0.39, 0.38	18.32, 0.39, 0.38	25.90, 0.38, 0.38
Experiment Ref. 6,7 (A_s, B_s, C_s)[a]	22.87, 0.39, 0.39	19.34, 0.39, 0.38	25.96, 0.38, 0.38
Experiment Ref. 9 (A_Z, B_Z, C_Z)	22.26, 0.39, 0.38	⋯	⋯

[a] A_s, B_s, C_s are computed from the experimental r_s structure.

Table 2.7.1: Energies and adiabatic excitation energies in kcal mol^{-1} (ZPVE-corrected values in parentheses) relative to the $\tilde{X}$ $^{1}A'$ bent electronic ground state of the CuOH molecule.

Level of Theory	$\tilde{X}$ $^{1}A'$	$\tilde{X}$ $^{1}\Sigma^{+}$	1 $^{1}\Pi$	2 $^{1}A'$	1 $^{1}A''$
cc-pVTZ SCF	0.0 (0.0)	4.6 (3.9)	10.7 (10.2)	···	7.7 (7.7)
cc-pVTZ CASSCF/SACASSCF	0.0 (0.0)	5.8 (-)	40.2 (-)	38.6 (-)	32.9 (-)
QZVPP SCF	0.0 (0.0)	4.3 (3.5)	11.4 (-)	···	8.4 (-)
QZVPP CASSCF/SACASSCF	0.0 (0.0)	5.3 (-)	41.2 (-)	39.9 (-)	34.3 (-)
Wachters/DZP CISD	0.0 (0.0)	8.2 (7.5)	46.5 (45.9)	···	41.7 (41.7)
PolCu/TZ2P CISD	0.0 (0.0)	7.4 (6.6)	51.9 (51.2)	···	47.2 (47.2)
PolCu(g)/TZ2P(d,f) CISD	0.0 (0.0)	7.0 (6.2)	51.6 (50.9)	···	47.4 (47.4)
cc-pVTZ CISD	0.0 (0.0)	6.9 (6.2)	50.7 (50.1)	···	46.6 (46.6)
QZVPP CISD	0.0 (0.0)	6.1 (5.3)	···	···	···
Wachters/DZP CCSD/EOM-CCSD	0.0 (0.0)	9.9 (9.3)	47.3 (46.5)	45.4 (45.2)	42.8 (42.7)
PolCu/TZ2P CCSD/EOM-CCSD	0.0 (0.0)	9.7 (9.0)	50.5 (49.6)	48.4 (48.2)	45.9 (45.7)
PolCu(g)/TZ2P(d,f) CCSD/EOM-CCSD	0.0 (0.0)	9.3 (8.6)	50.8 (49.9)	49.3 (49.0)	46.7 (46.5)
cc-pVTZ CCSD/EOM-CCSD	0.0 (0.0)	8.8 (8.1)	56.9 (56.2)	54.0 (53.9)	52.9 (52.7)
QZVPP CCSD/EOM-CCSD	0.0 (0.0)	8.1 (7.4)	54.2 (53.4)	52.0 (51.8)	50.7 (50.5)
Wachters/DZP CCSD(T)	0.0 (0.0)	10.8 (10.2)	···	···	···
PolCu/TZ2P CCSD(T)	0.0 (0.0)	10.8 (10.2)	···	···	···
PolCu(g)/TZ2P(d,f) CCSD(T)	0.0 (0.0)	10.4 (9.8)	···	···	···
cc-pVTZ CCSD(T)	0.0 (0.0)	10.0 (9.3)	···	···	···
QZVPP CCSD(T)	0.0 (0.0)	9.2 (8.5)	···	···	···

Table 2.7.2: Energies and adiabatic excitation energies in kcal mol^{-1} (ZPVE-corrected values in parentheses) relative to the $\tilde{X}$ $^1A'$ bent electronic ground state of the CuOH molecule. (Continued)

Level of Theory	$\tilde{X}$ $^1A'$	$\tilde{X}$ $^1\Sigma^+$	1 $^1\Pi$	2 $^1A'$	1 $^1A''$
Wachters/DZP CCSDT-3/EOM-CCSDT-3	0.0 (0.0)	11.2 (10.6)	52.3 (51.5)	50.8 (50.6)	46.7 (46.5)
PolCu/TZ2P CCSDT-3/EOM-CCSDT-3	0.0 (0.0)	11.4 (10.7)	58.4 (57.5)	57.3 (57.0)	52.6 (52.4)
PolCu(g)/TZ2P(d,f) CCSDT-3/EOM-CCSDT-3	0.0 (0.0)	11.0 (10.3)	58.7 (57.7)	57.9 (57.6)	53.3 (53.1)
cc-pVTZ CCSDT-3/EOM-CCSDT-3	0.0 (0.0)	10.2 (9.5)	58.4 (57.7)	56.5 (56.3)	53.6 (53.3)
QZVPP CCSDT-3/EOM-CCSDT-3	0.0 (0.0)	9.7 (9.0)	59.4 (-)	···	···
Wachters/DZP CC3/EOM-CC3	0.0 (0.0)	11.5 (10.9)	53.7 (52.8)	53.0 (52.6)	47.6 (47.4)
PolCu/TZ2P CC3/EOM-CC3	0.0 (0.0)	11.9 (11.2)	62.9 (61.8)	···	56.7 (56.4)
PolCu(g)/TZ2P(d,f) CC3/EOM-CC3	0.0 (0.0)	11.4 (10.7)	63.0 (62.0)	···	57.3 (57.0)
cc-pVTZ CC3/EOM-CC3	0.0 (0.0)	10.5 (9.9)	59.1 (58.2)	58.1 (57.8)	53.9 (53.7)
QZVPP CC3/EOM-CC3	0.0 (0.0)	10.1 (9.4)	62.4 (-)	···	···
PolCu/cc-pVTZ EOM-CCSD	0.0 (0.0)	···	···	48.3 (-)	45.7 (-)
PolCu/cc-pVTZ_DK Rel. EOM-CCSD	0.0 (0.0)	···	···	46.1 (-)	41.7 (-)
cc-pVTZ EOM-CCSD	0.0 (0.0)	···	···	54.0 (-)	52.9 (-)
cc-pVTZ_DK Rel. EOM-CCSD	0.0 (0.0)	···	···	51.3 (-)	48.6 (-)
cc-pVQZ EOM-CCSD	0.0 (0.0)	···	···	55.9 (-)	55.2 (-)
cc-pVQZ_DK Rel. EOM-CCSD	0.0 (0.0)	···	···	52.9 (-)	50.7 (-)
Experiment Ref. 7	0.0 (0.0)	···	···	(45.49)	···
Experiment Ref. 4, 6	0.0 (0.0)	···	···	···	(52.63)

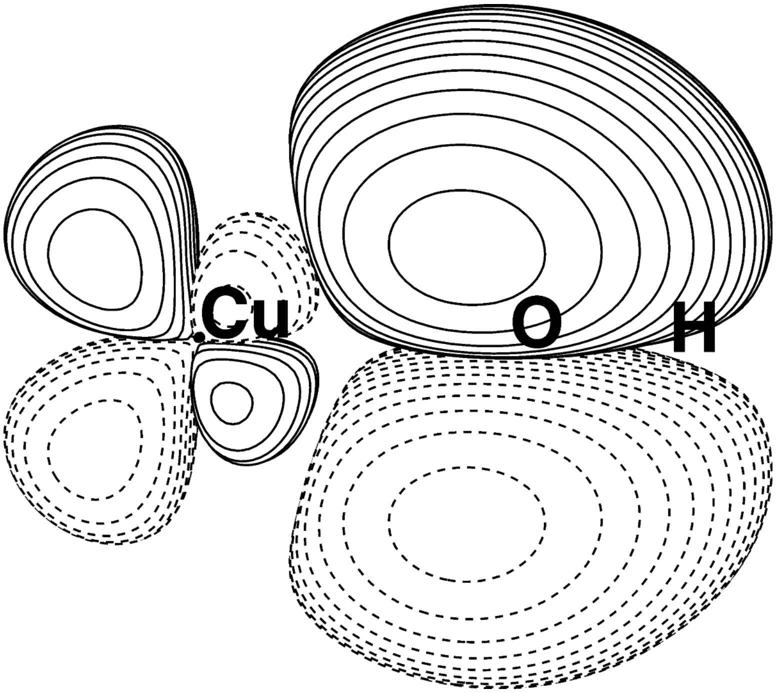

Figure 2.1: The 4π Hartree-Fock orbital for the $\tilde{X}$ $^1\Sigma^+$ stationary point using the PolCu/TZ2P basis set.

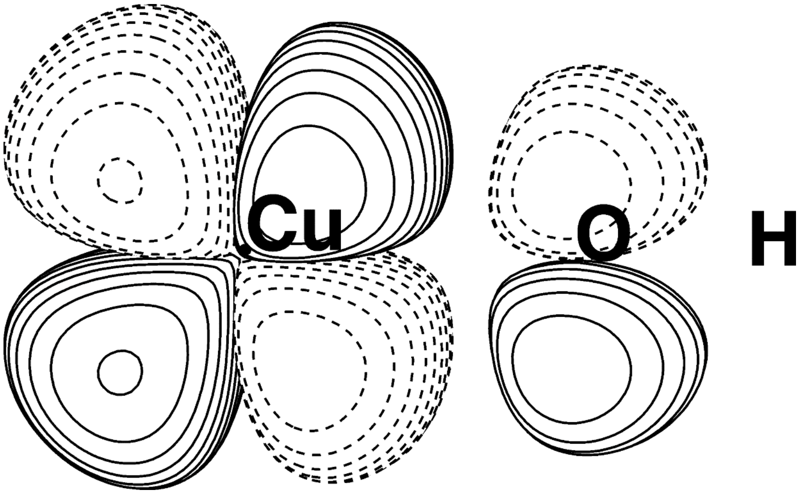

Figure 2.2: The 4π Hartree-Fock orbital for the lowest energy $^1\Pi$ stationary point using the PolCu/TZ2P basis set. Note the remarkable difference with respect to the 4π orbital in Figure 2.1.

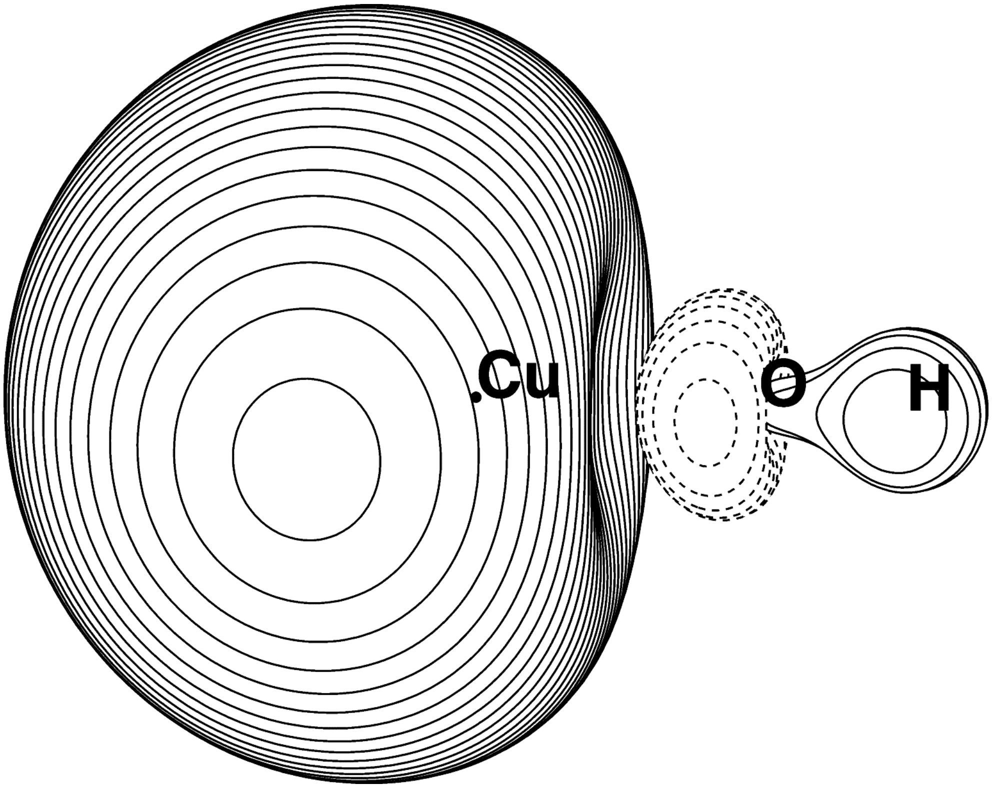

Figure 2.3: The 10σ Hartree-Fock orbital for the lowest energy $^1\Pi$ stationary point using the PolCu/TZ2P basis set.

$\tilde{X}\ ^1\Sigma^+$

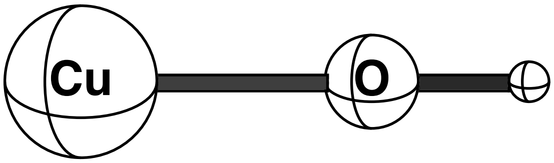

		$R_{\text{Cu-O}}$(Å)	$R_{\text{O-H}}$(Å)
cc-pVTZ	SCF	1.8060	0.9308
	CASSCF	1.8184	0.9496
	CISD	1.7597	0.9371
	CCSD	1.7485	0.9442
	CCSD(T)	1.7389	0.9464
	CCSDT-3	1.7333	0.9462
	CC3	1.7265	0.9467
QZVPP	SCF	1.8168	0.9299
	CASSCF	1.8344	0.9496
	CISD	1.7565	0.9336
	CCSD	1.7448	0.9426
	CCSD(T)	1.7377	0.9454
	CCSDT-3	1.7279	0.9451
	CC3	1.7193	0.9456

Figure 2.4: Optimized geometrical parameters for the $\tilde{X}\ ^1\Sigma^+$ stationary point of the CuOH molecule.

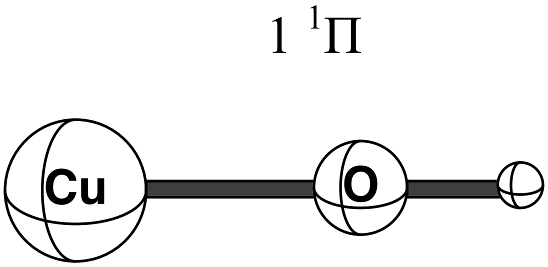

		$R_{\text{Cu-O}}$(Å)	$R_{\text{O-H}}$(Å)
cc-pVTZ	SCF	1.7723	0.9311
	CASSCF	1.7863	0.9365
	CISD	1.7416	0.9397
	EOM-CCSD	1.7472	0.9535
	EOM-CCSDT-3	1.7365	0.9567
	EOM-CC3	1.7297	0.9574
QZVPP	SCF	1.7788	0.9304
	CASSCF	1.7963	0.9363
	EOM-CCSD	1.7436	0.9507
	EOM-CCSDT-3	1.7283	0.9551
	EOM-CC3	1.7162	0.9556

Figure 2.5: Optimized geometrical parameters for the $1\ ^1\Pi$ stationary point of the CuOH molecule.

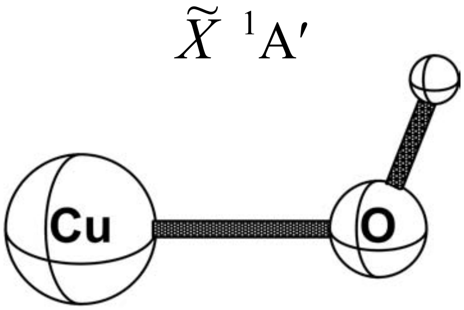

		$R_{\text{Cu-O}}$(Å)	$\theta_{\text{Cu-O-H}}$(°)	$R_{\text{O-H}}$(Å)
cc-pVTZ	SCF	1.8396	119.00	0.9379
	CASSCF	1.8630	114.84	0.9610
	CISD	1.7962	113.85	0.9474
	CCSD	1.7898	110.92	0.9580
	CCSD(T)	1.7815	109.16	0.9618
	CCSDT-3	1.7756	109.14	0.9620
	CC3	1.7692	108.76	0.9631
QZVPP	SCF	1.8468	120.24	0.9366
	CASSCF	1.8742	116.53	0.9598
	CISD	1.7872	116.13	0.9426
	CCSD	1.7810	112.64	0.9556
	CCSD(T)	1.7757	110.74	0.9600
	CCSDT-3	1.7657	110.71	0.9604
	CC3	1.7581	110.29	0.9618
PolCu/cc-pVTZ	CCSD	1.7860	110.65	0.9585
PolCu/cc-pVTZ_DK	Rel. CCSD	1.7630	109.85	0.9591
cc-pVTZ	CCSD	1.7898	110.92	0.9580
cc-pVTZ_DK	Rel. CCSD	1.7668	109.98	0.9586
cc-pVQZ	CCSD	1.7937	112.06	0.9558
cc-pVQZ_DK	Rel. CCSD	1.7705	111.06	0.9564
Experiment	Ref. 4 (r_0)	1.774(3)	111(1)	0.933(6)
	Ref. 6, 7 (r_s)	1.76893(25)	110.245(80)	0.9520(50)
	Ref. 9 (r_z)	1.77182(3)	110.12(30)	0.9646(3)

Figure 2.6: Optimized geometrical parameters for the $\tilde{X}\ ^1\mathrm{A}'$ electronic state of the CuOH molecule.

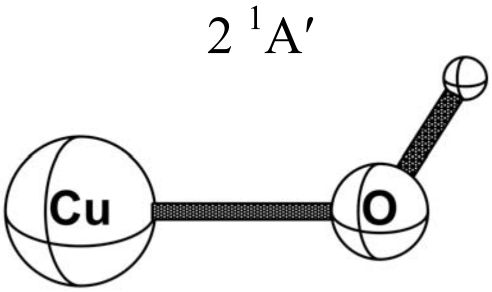

		$R_{\text{Cu-O}}$(Å)	$\theta_{\text{Cu-O-H}}$(°)	$R_{\text{O-H}}$(Å)
cc-pVTZ	SACASSCF	1.8562	117.83	0.9633
	EOM-CCSD	1.7940	122.67	0.9567
	EOM-CCSDT-3	1.7847	122.26	0.9599
	EOM-CC3	1.7778	124.07	0.9600
QZVPP	SACASSCF	1.8613	119.21	0.9622
	EOM-CCSD	1.7933	124.82	0.9541
PolCu/cc-pVTZ	EOM-CCSD	1.8041	123.00	0.9561
PolCu/cc-pVTZ_DK	Rel. EOM-CCSD	1.7973	125.05	0.9551
cc-pVTZ	EOM-CCSD	1.7940	122.67	0.9567
cc-pVTZ_DK	Rel. EOM-CCSD	1.7954	122.51	0.9563
cc-pVQZ	EOM-CCSD	1.7932	122.96	0.9550
cc-pVQZ_DK	Rel. EOM-CCSD	1.7945	122.73	0.9546
Experiment	Ref. 7 (r_s)	1.7748(32)	110.0(16)	1.0348(40)

Figure 2.7: Optimized geometrical parameters for the 2 ^{1}A′ electronic state of the CuOH molecule.

$1\ ^1A''$

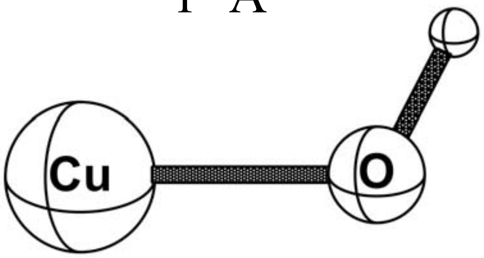

		$R_{\text{Cu-O}}$(Å)	$\theta_{\text{Cu-O-H}}$(°)	$R_{\text{O-H}}$(Å)
cc-pVTZ	SCF	1.8070	124.89	0.9377
	CASSCF	1.8394	114.94	0.9649
	CISD	1.7819	119.96	0.9481
	EOM-CCSD	1.7866	118.03	0.9610
	EOM-CCSDT-3	1.7776	115.61	0.9654
	EOM-CC3	1.7713	114.97	0.9665
QZVPP	SCF	1.8115	125.47	0.9366
	CASSCF	1.8454	116.01	0.9637
	EOM-CCSD	1.7801	120.27	0.9577
PolCu/cc-pVTZ	EOM-CCSD	1.7892	117.67	0.9602
PolCu/cc-pVTZ_DK	Rel. EOM-CCSD	1.7797	116.47	0.9601
cc-pVTZ	EOM-CCSD	1.7866	118.03	0.9610
cc-pVTZ_DK	Rel. EOM-CCSD	1.7778	116.85	0.9608
cc-pVQZ	EOM-CCSD	1.7867	119.10	0.9590
cc-pVQZ_DK	Rel. EOM-CCSD	1.7778	117.90	0.9588
Experiment	Ref. 4 (r_0)	1.781(3)	119(1)	0.942(6)
	Ref. 6, 7 (r_s)	1.78414(46)	117.670(98)	0.9508(27)

Figure 2.8: Optimized geometrical parameters for the $1\ ^1A''$ electronic state of the CuOH molecule.

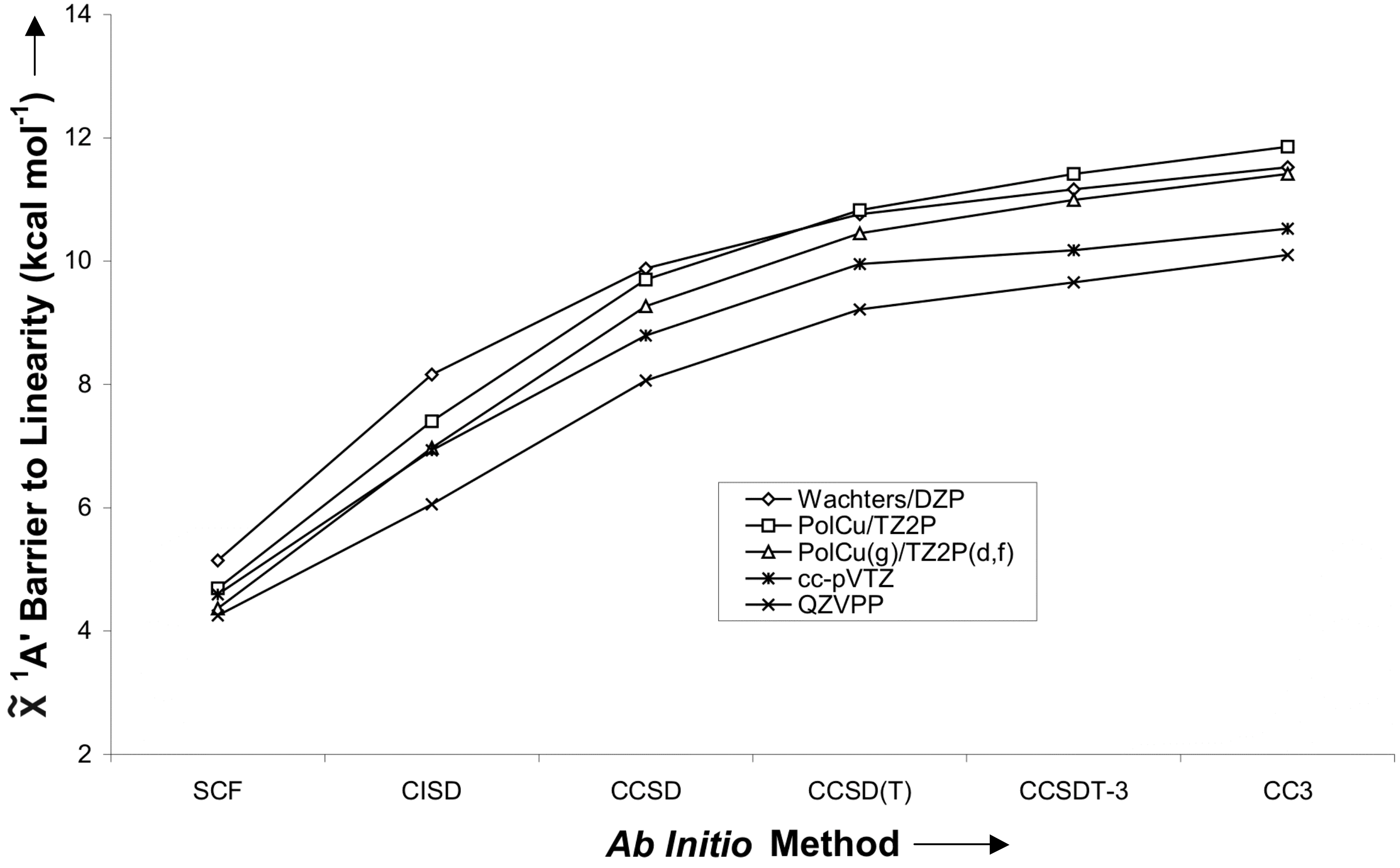

Figure 2.9: The relative energies (in kcal mol^{-1}) for the linear $\tilde{X}$ $^1\Sigma^+$ stationary point of the CuOH molecule with respect to the bent $\tilde{X}$ ^{1}A′ state equilibrium geometry, with a variety of *ab initio* methods and basis sets. This energy difference is the barrier to linearity for the CuOH ground electronic state.

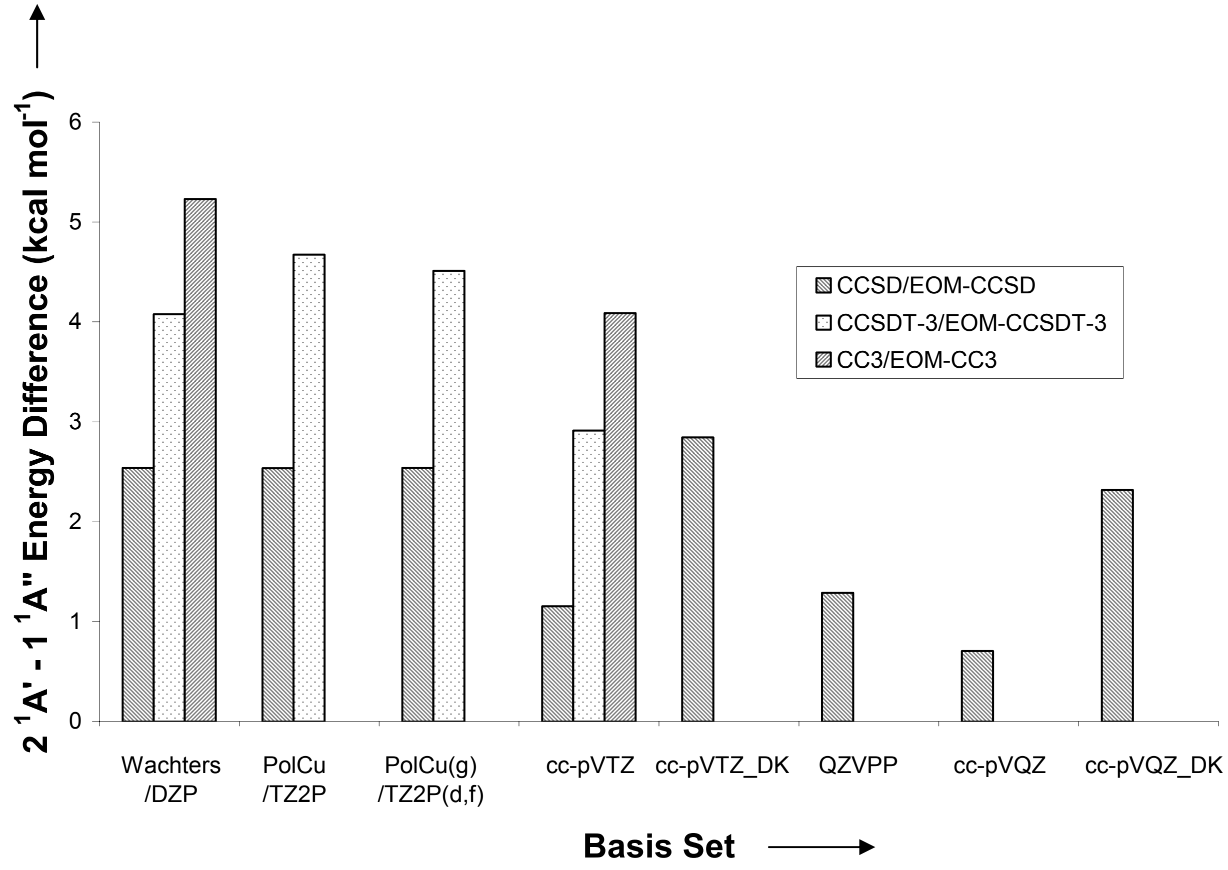

Figure 2.10: The ZPVE-corrected energy differences (in kcal mol^{-1}) between the 2 ^{1}A′ and 1 ^{1}A" states of the CuOH molecule, with a variety of *ab initio* methods and basis sets. For the EOM-CCSD method with cc-pVTZ_DK, cc-pVQZ, and cc-pVQZ_DK basis sets, the cc-pVTZ ZPVE corrections were used.

CHAPTER 3

THE EXOTHERMIC PNC → PCN REACTION[1]

---

[1] Suyun Wang, Yukio Yamaguchi, and Henry F. Schaefer. Accepted by *Journal of Theoretical and Computational Chemistry*. Reprinted here with permission of the World Scientific Publishing Co. Pte. Ltd, Singapore, 2/28/2006.

3.1 ABSTRACT

PCN and PNC are possible interstellar species that have not been experimentally characterized. With various *ab initio* methods, including multireference and restricted open-shell single-reference electronic structure theory, the PCN / PNC species and the transition state for the isomerization reaction PCN ↔ PNC have been studied. The Dunning series of correlation-consistent basis sets, cc-pVXZ and aug-cc-pVXZ (X = T and Q), have been used. Geometries, total energies, dipole moments, harmonic vibrational frequencies, infrared intensities, and zero-point vibrational energies are reported for the PCN / PNC isomers and the transition state. Both PCN and PNC are linear with $^3\Sigma^-$ ground states, and linear PNC ($\tilde{X}\,^3\Sigma^-$) is predicted to lie 13.7 kcal mol^{-1} (13.5 kcal mol^{-1} with ZPVE correction) above linear PCN ($\tilde{X}\,^3\Sigma^-$) at the aug-cc-pVQZ CCSD(T) level of theory. The CN bond distance in PCN ($\tilde{X}\,^3\Sigma^-$) is predicted to be 1.174 Å, only 0.002 Å longer than the experimental value of 1.172 Å for diatomic CN ($X\,^2\Sigma^+$), suggesting that CN has triple bond character in PCN ($\tilde{X}\,^3\Sigma^-$). The isomerization transition state is found to be cyclic PCN ($\tilde{X}\,^3A''$) with angles θ_e (PCN) = 82.2°, θ_e (CNP) = 63.1°, and θ_e (NPC) = 34.7°. The isomerization barrier is predicted to be 35.7 kcal mol^{-1} (34.5 kcal mol^{-1} with the ZPVE correction) relative to linear PCN ($\tilde{X}\,^3\Sigma^-$). The predicted dipole moments are substantial, 2.79 debye (polarity $^+$PCN$^-$) and 2.51 debye (polarity $^+$PNC$^-$).

3.2 INTRODUCTION

Phosphorus-bearing compounds have been identified in astronomical sources for many years. In 1976, Ridgway[1] detected PH_3 in Jupiter's atmosphere, and the presence of

PH_3 there was confirmed by Larson, *et al.* in 1977.[2] Turner and Bally,[3] and Ziurys[4] detected the PN molecule in the Orion molecular cloud in 1987. In 1990, Guelin *et al.*[5] observed the PC molecule in the envelope of a carbon star. Consequently, the phosphorus cyanide (PCN) / phosphorus isocyanide (PNC) isomers have been assumed to be plausible interstellar species.

Basco and Yee[6] studied the flash photolysis of $PH_3 - C_2N_2 - N_2$ mixtures and reported absorption spectra which might be attributed to PCN and the HPCN free radical. Thorne, Anicich, and Huntress[7] detected $PCNH^+$ in the reaction of PH^+ with HCN in 1983 using ion cyclotron resonance (ICR) mass spectrometry. In 1989, Smith, McIntosh, and Adams[8] observed $HCN{\cdot}P^+$, $HCN{\cdot}PH^+$, and $HCN{\cdot}PH_2^+$ in the reactions of P^+, PH^+, and PH_2^+ with HCN using the selected ion flow tube technique. In 1991, Largo and Barrientos[9] proposed that the subsequent dissociative recombination processes of the phosphorus-bearing products of the reactions of PH_n^+ (n = 0-2) with HCN could lead to PCN. Similarly, using HNC instead of HCN in reactions with PH_n^+ (n = 0-2) might result in the production of the PNC molecule.

A few theoretical studies have been reported for the PCN / PNC isomers. Thomson[10] employed self-consistent-field (SCF) method to investigate the ground states of PCN / PNC in 1976, and concluded that PCN ($\tilde{X}\,^3\Sigma^-$) is more stable than PNC ($\tilde{X}\,^3\Sigma^-$). In 1991, Largo and Barrientos[9] performed the unrestricted Hartree-Fock (UHF) geometry optimizations and Møller-Plesset (MP) single point energy predictions on PCN / PNC. Their results suggested that PNC ($\tilde{X}\,^3\Sigma^-$) lies about 15 kcal mol^{-1} above PCN ($\tilde{X}\,^3\Sigma^-$) at the projected MP3 level, and the isomerization barrier is about 23 kcal mol^{-1} relative to PNC at the MP4 level. Further, in 1997 El-Yazal, Martin, and Francois[11] employed B3LYP density functional theory (DFT) for geometry optimizations and the coupled-cluster method with single, double, and perturbatively applied triple excitations [CCSD(T)] for single point energies to study the low-lying electronic states of the PCN / PNC isomers and their transition states. PNC ($\tilde{X}\,^3\Sigma^-$) was predicted to lie 14.2 kcal mol^{-1} above PCN ($\tilde{X}\,^3\Sigma^-$), and the isomerization transition state ($\tilde{X}\,^3A''$) with a cyclic structure was estimated to lie 36.2 kcal mol^{-1} above PCN ($\tilde{X}\,^3\Sigma^-$).

Due to the absence of the high-level theoretical research on the geometries and physical properties of the PCN / PNC isomers and their isomerization transition state, we have applied a range of advanced correlated *ab initio* quantum mechanical methods in this research.

3.3 ELECTRONIC STRUCTURE CONSIDERATIONS

The linear ground state of PCN has the electronic configuration

$$[\text{core}](6\sigma)^2(7\sigma)^2(8\sigma)^2(9\sigma)^2(2\pi)^4(3\pi)^2,\ \tilde{X}\,^3\Sigma^-,$$

where [core] denotes the seven lowest-lying core orbitals (P: 1s-, 2s-, 2p-like and C, N: 1s-like). An analysis of the SCF MOs indicates that the 6σ and 7σ MOs have the σ(CN) and σ(PC) bonding character, respectively. The 8σ MO is associated with the non-bonding (3*s*-like) orbital localized on the P atom plus the CN anti-bonding σ orbital. The 9σ MO corresponds to the σ*(PC)-σ*(CN) bonding. The 2π MO is assigned to the CN π bond, while the 3π MO is related to the non-bonding ($3p_x$ and $3p_y$-like) orbital localized on the P atom.

The electron configuration for the ground state of PNC may likewise be described as

$$[\text{core}](6\sigma)^2(7\sigma)^2(8\sigma)^2(2\pi)^4(9\sigma)^2(3\pi)^2,\ \tilde{X}\,^3\Sigma^-.$$

The 6σ and 7σ MOs are assigned to the σ(NC) and σ(PN)-σ(NC) bonds, respectively. The 8σ MO is related to the non-bonding (3*s*-like) orbital localized on the P atom plus the NC anti-bonding σ orbital. The 2π MO is associated with NC π bonding. The 9σ MO involves a non-bonding (2*s* and $2p_z$-like) orbital localized on the C atom. The 3π MO describes the non-bonding ($3p_x$ and $3p_y$-like) orbital localized on the P atom. It should be noted that the ordering of the 2π and 9σ MOs is reversed for PNC.

The necessarily lower symmetry transition state for the isomerization reaction PCN ↔ PNC has the following electron configuration:

$$[\text{core}](7a')^2(8a')^2(9a')^2(2a'')^2(10a')^2(11a')^2(3a'')(12a'),\ \tilde{X}\,^3A''.$$

The 7a′ MO describes the σ(CN) bond. The 8a′ MO is primarily assigned to the σ(PC) bond. The 9a′ MO is mainly associated with the CN anti-bonding σ orbital. The 2a″ MO is related to the CN π bond. The 10a′ MO is the non-bonding (3*s*-like) orbital localized on the P atom plus the CN π bonding orbital. The 11a′ MO primarily comes from the non-bonding (2*s* and 2*p*-like) orbital localized on the C atom. The 3a″ and 12a′ MOs are related to the non-bonding (3*p*-like) orbital localized on the P atom.

3.4 THEORETICAL METHODS

Ab initio methods, including SCF (restricted open-shell Hartree-Fock),[12, 13] configuration interaction with single and double excitations (CISD),[14, 15] coupled cluster with single and double excitations (CCSD),[16-18] and CCSD(T)[19, 20] were used to investigate the ground states of the PCN / PNC isomers and the isomerization transition state between the two isomers. In addition to the above single-reference methods, the complete-active-space SCF (CASSCF)[21, 22] and multi-reference CISD (MRCISD)[23] techniques have been applied for PCN / PNC and their transition state. The MOLPRO[24] software package was used in this study. Geometries have been optimized at each level of theory except MRCISD and total energies have been determined at stationary-point geometries (MRCISD single point energies were evaluated at the optimized CCSD geometries). Also predicted were the energy difference between the PCN and PCN molecules and the barrier for the isomerization reaction. Other physical properties, including dipole moments, harmonic vibrational frequencies, and zero-point vibrational energies, have been obtained for the ground states of the PCN – PNC system.

Two series of basis sets have been used in this research. One was the Dunning series of correlation-consistent polarized valence basis sets cc-pVXZ[25, 26] [X=D (P: 12s8p1d/4s3p1d; C, N: 9s4p1d/3s2p1d), X=T (P: 15s9p2d1f/5s4p2d1f; C, N: 10s5p2d1f/4s3p2d1f), and X=Q (P: 16s11p3d2f1g/6s5p3d2f1g; C, N: 12s6p3d2f1g/5s4p3d2f1g)]. The other series was the augmented correlation-consistent polarized valence basis sets aug-cc-pVXZ[25-27] (X=D, T, and Q) by adding an additional diffuse function to each angular momentum in the cc-pVXZ sets. The seven lowest-lying core molecular orbitals (MOs) (1s, 2s, and 2p for P, 1s for C and N) were frozen at all correlated levels of theory.

The T_1 diagnostic values (defined as the norm of the single excitation coupled cluster amplitudes divided by the square root of the number of active electrons in the correlation procedure)[28] of the aug-cc-pVQZ CCSD(T) wave functions for PCN, PNC, and the isomerization transition state are 0.0221, 0.0216, and 0.0269, respectively. Therefore, this PCN – PNC system may be reasonably well described by the single-reference methods. However, in order to investigate performance of the multi-reference methods for the current system, the CASSCF and MRCISD methods were also examined in this research.

The CASSCF method used here are based on the partitioning of the MOs into three subsets (inactive orbitals, active orbitals, and external orbitals), corresponding to how they are employed to build the wave function. For the PCN / PNC isomers and their transition state, the inactive orbitals include 7 MOs coming from the inner atomic orbitals (AOs) (1s, 2s, and 2p for P, 1s for C and N), the active orbitals (active space) consist of the 12 MOs resulting from the valence AOs (3s and 3p for P, 2s and 2p for C and N), and 14 valence electrons are distributed in these 12 MOs. The external orbitals span the rest of the higher-lying orbital space, defined from the basis set used to build the MOs. With these divisions, full CI within the active orbitals was carried out. Using the CASSCF optimized MOs, internally contracted MRCISD method was used to obtain the single-point energies at the optimized CCSD geometries for the PCN – PNC system.

3.5 RESULTS AND DISCUSSION

In Figures 3.1-3.3, the optimized structures of the PCN / PNC isomers and their isomerization transition state are depicted. The potential energy surface of the PCN – PNC system is illustrated in Figure 3.4. In Tables 3.1.1-3.3.2 the total energies, dipole moments, harmonic vibrational frequencies, infrared intensities, and zero-point vibrational energies (ZPVEs) of the three stationary points are presented, while their relative energies are summarized in Table 3.4.1 and 3.4.2. The available previous theoretical data are also included in the figures and tables for comparison.

3.5.1 GEOMETRIES

3.5.1.1 THE $\tilde{X}\,^3\Sigma^-$ STATE OF LINEAR PCN

The optimized geometries for the $\tilde{X}\,^3\Sigma^-$ state of the linear PCN isomer at the five levels of theory with the four basis sets are depicted in Figure 3.1. The previous theoretical predictions are also included in the figure. For a given basis set, a more complete inclusion of correlation effects results in a surprising decrease in the PC internuclear separation but an expected increase of the CN bond distance. The CASSCF method leads to the PC bond distances shorter than the SCF result but longer than the CISD prediction, and gives rise to the longest CN bond separation among all methods. The adoption of larger basis sets shortens both the PC and CN bond lengths at a given level of theory. The aug-cc-pVXZ (X = T and Q) basis gives similar geometries to the corresponding cc-pVXZ results, indicating insignificant influence of the diffuse functions on the PC and CN bond distances.

With the aug-cc-pVQZ CCSD(T) method (our highest level of theory), the linear PCN geometry is predicted to be $R_{\text{P-C}}$ = 1.740 Å and $R_{\text{C-N}}$ = 1.174 Å. The equilibrium bond distances for the diatomic PC ($X\ ^2\Sigma^+$) and CN ($X\ ^2\Sigma^+$) radicals have been experimentally determined to be r_e(PC) = 1.562 Å and r_e(CN) = 1.172 Å, respectively.[29] The PC bond length in PCN is predicted to be substantially longer than that for PC ($X\ ^2\Sigma^+$), while the CN distance in PCN is seen to be similar to that for CN ($X\ ^2\Sigma^+$), implying single bond character for PC and triple bond character for CN, yielding for the PCN isomer a valence structure

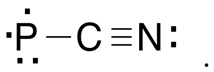

$$\cdot\dot{\underset{\cdot\cdot}{\mathrm{P}}}-\mathrm{C}\equiv\mathrm{N}\colon\ .$$

3.5.1.2 THE $\tilde{X}\,^3\Sigma^-$ STATE OF LINEAR PNC

In Figure 3.2, the optimized geometries for the $\tilde{X}\,^3\Sigma^-$ state of the linear PNC isomer with various methods and basis sets are illustrated along with previous theoretical results. With a given basis set, the single-reference correlation methods [CISD, CCSD, and CCSD(T)] predict remarkably similar PN bond lengths which are slightly shorter than that at the SCF level. For the CN bond in contrast, a more complete inclusion of correlation effects results in the expected increases. The CASSCF method shows longer PN bond distances than do the single-reference methods, with the CASSCF CN internuclear separation close to the CCSD(T) predictions. Using larger basis sets shortens both the PN and CN bond lengths at a given level of theory. Again, the aug-cc-pVXZ (X = T and Q) basis sets lead to geometries similar to the corresponding cc-pVXZ sets, indicating the insignificant influence of the diffuse functions on the PN and CN bond distances.

At the aug-cc-pVQZ CCSD(T) level of theory, the linear PNC geometry is predicted to be $R_{\text{P-N}}$ = 1.675 Å and $R_{\text{C-N}}$ = 1.191 Å. As noted earlier, experimental equilibrium bond distances for the diatomics PN ($X\,^1\Sigma^+$) and CN ($X\,^2\Sigma^+$) are r_e(PN) = 1.491 Å and r_e(CN) = 1.172 Å, respectively.[29] Both the PN and CN bond distances in PNC are predicted to be longer than those for PN ($X\,^1\Sigma^+$) and CN ($X\,^2\Sigma^+$). Compared to the PCN isomer, the CN bond in PNC is significantly longer. Therefore, the CN bond in PNC may have double bond or elongated triple bond character. The double bond character perhaps has some contribution from

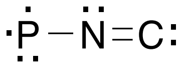

or

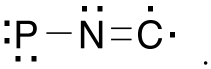

3.5.1.3 THE $\tilde{X}\,^3A''$ TRANSITION STATE

The optimized geometries for the bent (triangular) $\tilde{X}\,^3A''$ isomerization transition state at the five levels of theory with the four basis sets are presented in Figure 3.3. With a given basis set, the PC and PN bond lengths generally shorten, while the CN bond distance elongates with more advanced treatments of correlation effects. Accordingly, the PCN and PNC angles decrease but the CPN angle increases with more sophisticated treatments of correlation effects. The CASSCF method leads to the longest PC and CN distances but the shortest PN separation among all methods. Therefore, the CASSCF PNC and CPN angles are the largest and the PCN angle is the smallest among all methods. The larger basis sets usually shorten all bond lengths except the PN bond with the CCSD(T) method, but provide very little change for the CPN angle. Again, the aug-cc-pVXZ (X = T and Q) basis leads to similar geometries to the corresponding cc-pVXZ sets, indicating the small influence of the diffuse functions on the structural features.

With the aug-cc-pVQZ CCSD(T) method, the transition state geometry is predicted to be $R_{\text{P-C}} = 1.882$ Å, $R_{\text{P-N}} = 2.091$ Å, $R_{\text{C-N}} = 1.201$ Å, $\theta_{\text{P-C-N}} = 82.2°$, and $\theta_{\text{C-P-N}} = 34.7°$. All three bond distances in the transition state are predicted to be substantially longer than the experimental r_e values for the diatomics PC ($X\,^2\Sigma^+$), PN ($X\,^1\Sigma^+$), and CN ($X\,^2\Sigma^+$). Compared to the PCN and PNC isomers, all three bonds at the transition state are longer, with the PN bond presenting the largest elongation.

3.5.2 DIPOLE MOMENTS

The dipole moment of the linear PCN isomer generally decreases with more sophisticated treatments of correlation effects. The CASSCF method yields the dipole moments of the smallest magnitude. The cc-pVXZ dipole moments increase while the aug-cc-pVXZ dipole moments decrease with increasing basis set size. Compared to the cc-pVXZ sets, the aug-cc-pVXZ basis gives larger dipole moments. The dipole moment of PCN is predicted to be 2.79 debye at the aug-cc-pVQZ CCSD(T) level of theory. The direction of the dipole moments is $^{+}$PCN^{-} for the PCN isomer. Although triplet states are difficult to observe by microwave spectroscopy, the substantial magnitude of the PCN dipole moment should provide encouragement to experimental efforts.

For the linear PNC species, the dipole moment usually increases with advanced treatments of correlation effects from SCF to CCSD. The CCSD(T) level of theory shows similar dipole moments to the CCSD method, and the CASSCF method presents the largest values for the dipole moments. The dipole moments decrease with increasing basis set size. Compared to the cc-pVXZ sets, the aug-cc-pVXZ basis leads to larger dipole moments except for the SCF method. The dipole moment of PNC is predicted to be 2.51 debye at the aug-cc-pVQZ CCSD(T) level of theory. The direction of the dipole moment is $^{+}$PNC^{-} for the PNC isomer.

For the isomerization transition state, improved treatments of correlation effects generally decrease the magnitude of the dipole moment. The CASSCF dipole moments are similar to those from the CCSD(T) method. The dipole moments decrease as the basis set size increases, and the dipole moments with the aug-cc-pVXZ basis are usually larger than those with the cc-pVXZ sets. The dipole moment of the transition state is predicted to be 1.43 debye at the aug-cc-pVQZ CCSD(T) level of theory, which is significantly smaller than those for the PCN and PNC isomers, indicating the diminished polarity of the transition state.

3.5.3 VIBRATIONAL FREQUENCIES

The vibrational analyses performed for both the linear PCN ($\tilde{X}\,^3\Sigma^-$) and PNC ($\tilde{X}\,^3\Sigma^-$) molecules yield a degenerate real bending vibrational frequency [for example, 312 cm^{-1} and 243 cm^{-1} at the aug-cc-pVQZ CCSD(T) level of theory for PCN and PNC, respectively]. This confirms that there must be a transition state ($\tilde{X}\,^3A''$) on the ground state potential energy surface for the PCN – PNC system (Table 3.1.1-3.2.2).

3.5.3.1 THE $\tilde{X}\,^3\Sigma^-$ STATE OF LINEAR PCN

The CN stretching frequency (ω_1) for PCN in Table 3.1.1 decreases with advanced treatments of correlation effects, reflecting the longer CN bond distance. The PCN bending frequency (degenerate ω_2) also decreases with improved treatments of correlation effects. The ω_1 and PC stretching frequency (ω_3) slightly increase with the expansion of the basis set (except for the cc-pVXZ SCF method), corresponding to the shortened CN and PC bond distances. However, the bending frequency ω_2 shows relatively consistent results at a same level of theory with different basis sets. Inclusion of diffuse functions (aug-cc-pVXZ basis sets) does not provide a major influence on the frequencies, compared to the original cc-pVXZ basis. In addition, the PC stretching mode has significantly higher infrared intensity than the CN stretching mode and PCN bending mode, as shown in Table 3.1.1.

The harmonic vibrational frequencies are predicted to be ω_1 = 2046 cm^{-1}, ω_2 = 312 cm^{-1}, and ω_3 = 635 cm^{-1} at the aug-cc-pVQZ CCSD(T) level of theory. The PC and CN harmonic stretching frequencies for the diatomics PC ($X\ ^2\Sigma^+$) and CN ($X\ ^2\Sigma^+$) have been experimentally determined[29] to be ω_e(PC) = 1240 cm^{-1} and ω_e(CN) = 2069 cm^{-1}. The PCN ω_1 prediction is close to the experimental diatomic frequency, reflecting the theoretical CN bond length (1.174 Å) of PCN compared to experiment (1.172 Å) for the CN ($X\ ^2\Sigma^+$) radical.[29] The harmonic frequency ω_3 is seen to be much lower than the experimental diatomic PC stretching frequency, consistent with the predicted PC bond distance (1.740 Å) for PCN being much longer than the experimental r_e value (1.562 Å) of diatomic PC ($X\ ^2\Sigma^+$).[29] All this is consistent with a picture in which the PC bond in PCN is a single bond while that in diatomic PC is a triple bond

$$:\mathrm{P}\equiv\mathrm{C}\cdot\quad .$$

3.5.3.2 THE $\tilde{X}\ ^3\Sigma^-$ STATE OF LINEAR PNC

The CN stretching frequency (ω_1) for PNC in Table 3.2.1 decreases with more sophisticated treatments of correlation effects, owing to the elongated CN bond distance. The PN stretching frequency (ω_3) also decreases somewhat with improved descriptions of electron correlation. Both ω_1 and ω_3 slightly increase with larger basis sets (except with the cc-pVXZ SCF method), corresponding to the shortened CN and PN bond distances. However, the PNC bending frequency (degenerate ω_2) shows relatively consistent results at a given level of theory with different basis sets. Again, addition of diffuse functions (aug-cc-pVXZ basis sets) leads to a small effect on the frequencies, compared to the original cc-pVXZ basis. Additionally, the CN stretching mode has substantially larger infrared intensity than the PN stretching mode, and the infrared intensity of the PNC bending mode is negligible, as shown in Table 3.2.1. If PNC can be made, the infrared spectrum should be observable in the ω_1 range (~ 1900 cm^{-1}).

The PNC harmonic vibrational frequencies are predicted to be ω_1 = 1976 cm^{-1}, ω_2 = 243 cm^{-1}, and ω_3 = 686 cm^{-1} at the aug-cc-pVQZ CCSD(T) level of theory. The PN and CN stretching frequencies for the diatomics PN ($X\ ^1\Sigma^+$) and CN ($X\ ^2\Sigma^+$) are experimentally known to be ω_e(PN) = 1337 cm^{-1} and ω_e(CN) = 2069 cm^{-1}.[29] The ω_1 and ω_3 values are lower than the experimental CN and PN stretching frequencies, reflecting CN and PN bond distance predictions (1.191 Å and 1.675 Å, respectively) longer than the experimental values (1.172 Å and 1.491 Å, respectively) for the diatomics PN ($X\ ^1\Sigma^+$) and CN ($X\ ^2\Sigma^+$).[29] Compared to the PCN molecule (2046 cm^{-1}), the PNC species gives the lower CN frequency prediction (1976 cm^{-1}), with the CN bond length (1.191 Å) of PNC longer than that (1.174 Å) of PCN.

3.5.3.3 THE $\tilde{X}\ ^3A''$ TRANSITION STATE

For the transition state, the CN stretching (ω_1) frequency (see Table 3.3.1 and 3.3.2) decreases with advanced treatments of correlation effects, due to the longer CN bond distance. The single imaginary PCN bending frequency (ω_2) also decreases with more complete descriptions of electron correlation. Both ω_1 and the PC stretching frequency (ω_3) increase with basis set size (except for the SCF method), corresponding to the shortened CN and PC bond distances. For a given method, the bending frequency ω_2 increases with basis set size as well. Again, addition of diffuse functions (aug-cc-pVXZ) to the cc-pVXZ basis affects the frequencies very slightly.

The three harmonic vibrational frequencies of the transition state are predicted to be ω_1 = 1883 cm^{-1}, ω_2 = 229i cm^{-1}, and ω_3 = 576 cm^{-1} at the aug-cc-pVQZ CCSD(T) level of theory. Both ω_1 and ω_3 are predicted to be significantly lower than the experimental CN and PC stretching frequencies for the diatomics CN ($X\ ^2\Sigma^+$) and PC ($X\ ^2\Sigma^+$),[29] respectively. This reflects the fact that the theoretical transition state CN and PC bond distances (1.201 Å and 1.882 Å) are longer than the experimental diatomic r_e values (1.172 Å and 1.562 Å). In addition, the CN stretching frequency ω_1 is lower than that of the PCN and PNC isomers, and ω_3 is lower than that for PCN as well, indicating the longer CN and PC internuclear separations at the transition state compared to the two isomers.

3.5.4 ENERGETICS

A one-dimensional depiction of the predicted potential energy surface for the PCN – PNC system is provided in Figure 3.4. This depiction is composed of 181 energy points corresponding to one degree increments in the PCN angle from 0° to 180° along optimized bond distances at the cc-pVTZ CCSD level of theory. This figure shows the two lowest stationary points corresponding to the linear ground states ($\tilde{X}\ ^3\Sigma^-$) of the two isomers and a single saddle point associated with the isomerization transition state ($\tilde{X}\ ^3A''$). Also illustrated in the figure are the energy separations of the PCN / PNC isomers and their transition state at the aug-cc-pVQZ CCSD(T) level of theory.

The total energies of PCN, PNC, and the transition state are reported in Tables 3.1.1-3.3.2, respectively. It is seen that the MRCISD method does not recover quite as much correlation energy compared to the CCSD and CCSD(T) methods. However, it must be noted that the CCSD and CCSD(T) methods are not variational. Based on the total energies of three stationary points, Table 3.4.1 and 3.4.2 report the relative energies of the two isomers and the transition state. The earlier theoretical studies[9, 11] are included in Table 3.4.2 as well. At all levels of theory, the $\tilde{X}\,^3\Sigma^-$ PCN species is predicted to be lower lying than the $\tilde{X}\,^3\Sigma^-$ PNC isomer, in the manner seen in Figure 3.4. For a given basis set, the energy difference between the two isomers increases with improved treatments of correlation effects. The CASSCF method gives higher energy separations than the single-reference methods. The MRCISD single-point energy separations evaluated at the optimized CCSD geometries are somewhat larger than the CASSCF prediction. The energy difference between the two isomers generally decreases with increasing basis set size. The effect of the diffuse functions is not too significant, since the aug-cc-pVXZ predictions of the energy separation are similar to those with the cc-pVXZ basis sets. At the aug-cc-pVQZ CCSD(T) level of theory, the PNC isomer is predicted to lie 13.7 kcal mol^{-1} [13.5 kcal mol^{-1} with zero-point vibrational energy (ZPVE) correction] higher than the PCN isomer. The predicted energy separation is mostly consistent with the previous cc-pVTZ CCSD(T) single-point result (at the cc-pVTZ B3LYP geometries) of 14.2 kcal mol^{-1} (14.0 kcal mol^{-1} with ZPVE correction),[11] but larger than those of the other theoretical studies.

With a given basis set, the isomerization barrier relative to the $\tilde{X}\,^3\Sigma^-$ PCN isomer (energy difference between the $\tilde{X}\,^3\Sigma^-$ PCN isomer and the $\tilde{X}\,^3A''$ transition state) decreases with advanced treatments of correlation effects. Consistent with the increasing energy separation of the PCN / PNC isomers, the isomerization energy barrier relative to the $\tilde{X}\,^3\Sigma^-$ PNC isomer (energy difference between the $\tilde{X}\,^3\Sigma^-$ PNC isomer and the $\tilde{X}\,^3A''$

transition state) also decreases with more sophisticated treatments of correlation. The CASSCF method gives much higher energy barriers (by ~ 7 kcal mol^{-1}) than the more reliable single-reference methods. On the other hand, the MRCISD single-point energy barriers evaluated at the optimized CCSD geometries are very close to those with the CISD and CCSD methods. The energy barrier slightly decreases with addition of diffuse functions (aug-cc-pVXZ) to the cc-pVXZ basis sets. At the aug-cc-pVQZ CCSD(T) level of theory, the forward (PNC → PCN) isomerization energy barrier is predicted to be 21.9 kcal mol^{-1} (21.0 kcal mol^{-1} with ZPVE-correction) (relative to the PCN isomer), and the reverse isomerization energy barrier is 35.7 kcal mol^{-1} (34.5 kcal mol^{-1} with ZPVE-correction) (relative to the PNC isomer). The predicted energy barrier is closer to the recent 36.2 kcal mol^{-1} with the single-point cc-pVTZ CCSD(T) method (at the cc-pVTZ B3LYP geometries)[11] than to the earlier theoretical studies.

3.6 CONCLUDING REMARKS

The PCN / PNC isomers and isomerization transition state structures have been investigated using *ab initio* quantum mechanical techniques. Both isomers have been confirmed to be linear with $\tilde{X}\,^3\Sigma^-$ ground states, and PCN is located 13.7 kcal mol^{-1} (13.5 kcal mol^{-1} with ZPVE correction) below PNC. The PCN molecule exhibits triple bond character for CN, while the PNC species presents double or elongated triple bond character for CN. The transition state for the PCN ↔ PNC system has been found to have a cyclic structure ($\tilde{X}\,^3A''$) with PCN and NPC bond angles of 82.2° and 34.7°, respectively. The forward (PNC → PCN) isomerization barrier is predicted to be 21.9 kcal mol^{-1} (21.0 kcal mol^{-1} with ZPVE-correction). A barrier of 35.7 kcal mol^{-1} (34.5 kcal mol^{-1} with ZPVE-correction) is found for the reverse (PCN → PNC) isomerization reaction. The optimized geometries and energetics for the PCN – PNC system presented in this study are the most reliable quantities to date.

3.7 ACKNOWLEDGEMENTS

This research was supported by the National Science Foundation, Grant CHE-0451445.

3.8 REFERENCES

1. Ridgway, S. T.; Wallace, L.; Smith, G. R. *Astrophys. J.* **1976**, *207*, 1002.
2. Larson, H. P.; Treffers, R. R.; Fink, U. *Astrophys. J.* **1977**, *211*, 972.
3. Turner, B. E.; Bally, J. *Astrophys. J.* **1987**, *321*, L75.
4. Ziurys, L. M. *Astrophys. J.* **1987**, *321*, L81.
5. Guelin, M.; Cernicharo, J.; Paubert, G.; Turner, B. E. *Astron. Astrophys.* **1990**, *230*, L9.
6. Basco, N.; Yee, K. K. *Chem. Comm.* **1968**, 152.
7. Thorne, L. R.; Anicich, V. G.; Huntress, W. T. *Chem. Phys. Lett.* **1983**, *98*, 162.
8. Smith, D.; McIntosh, B. J.; Adams, N. G. *J. Chem. Phys.* **1989**, *90*, 6213.
9. Largo, A.; Barrientos, C. *J. Phys. Chem.* **1991**, *95*, 9864.
10. Thomson, C. *Int. J. Quantum Chem. Symp.* **1976**, *10*, 85.
11. El-Yazal, J.; Martin, J. M. L.; Francois, J.-P. *J. Phys. Chem. A* **1997**, *101*, 8319.
12. Hurley, A. C. *Introduction to the Electron Theory of Small Molecules*. Academic Press: New York, 1976.

13. Roothaan, C. C. J. *Rev. Mod. Phys.* **1960**, *32*, 179.

14. Shavitt, I. In *Methods of Electronic Structure Theory*, Schaefer, H. F. Ed. Plenum: New York, 1977.

15. Brooks, B. R.; Schaefer, H. F. *J. Chem. Phys.* **1979**, *70*, 5092.

16. Purvis, G. D.; Bartlett, R. J. *J. Chem. Phys.* **1982**, *76*, 1910.

17. Bartlett, R. J. *J. Phys. Chem. A* **1989**, *93*, 1697.

18. Crawford, T. D.; Schaefer, H. F. *Rev. Comput. Chem.* **2000**, *14*, 33.

19. Raghavachari, K.; Trucks, G. W.; Pople, J. A.; Head-Gordon, M. *Chem. Phys. Lett.* **1989**, *157*, 479.

20. Bartlett, R. J.; Watts, J. D.; Kucharski, S. A.; Noga, J. *Chem. Phys. Lett.* **1990**, *165*, 513.

21. Werner, H.-J.; Knowles, P. J. *J. Chem. Phys.* **1985**, *82*, 5053.

22. Knowles, P. J.; Werner, H.-J. *Chem. Phys. Lett.* **1985**, *115*, 259.

23. Werner, H.-J.; Knowles, P. J. *J. Chem. Phys.* **1988**, *89*, 5803.

24. MOLPRO, a package of *ab initio* programs designed by Werner, H.-J. and Knowles, P. J., version 2002.1. Amos, R. D.; Bernhardsson, A.; Berning, A.; Celani, P.; Cooper, D. L.; Deegan, M. J. O.; Dobbyn, A. J.; Eckert, F.; Hampel, C.; Hetzer, G.; Knowles, P. J.; Korona, T.; Lindh, R.; Lloyd, A. W.; McNicholas, S. J.; Manby, F. R.; Meyer, W.; Mura, M. E.; Nicklass, A.; Palmieri, P.; Pitzer, R. M.; Rauhut, G.; Schütz, M.; Schumann, U.; Stoll, H.; Stone, A. J.; Tarroni, R.; Thorsteinsson, T.; Werner, H.-J.

25. Dunning, T. H. *J. Chem. Phys.* **1989**, *90*, 1007.

26. Woon, D. E.; Dunning, T. H. *J. Chem. Phys.* **1993**, *98*, 1358.

27. Kendall, R. A.; Dunning, T. H.; Harrison, R. J. *J. Chem. Phys.* **1992**, *96*, 6796.

28. Lee, T. J.; Taylor, P. R. *Int. J. Quantum Chem. Symp.* **1989**, *23*, 199.

29. Huber, K. P.; Herzberg, G. *Molecular Spectra and Molecular Structure. IV. Constants of Diatomic Molecules*. Van Nostrand Reinhold: New York, 1979.

Table 3.1.1: Theoretical predictions of the total energy (in hartree), dipole moment (in debye), harmonic vibrational frequencies (in cm^{-1}), infrared intensities (in parentheses in km mol^{-1}), and zero-point vibrational energy (ZPVE in kcal mol^{-1}) for the linear $\tilde{X}\ ^3\Sigma^-$ state of the PCN molecule. The infrared intensities for ω_2 were doubled.

Level of Theory	Energy	μ	ω_1 (σ)	ω_2 (π)	ω_3 (σ)	ZPVE
cc-pVTZ SCF	-433.055 829	3.125	2492 (2.7)	355 (10.7)	640 (43.4)	5.49
cc-pVQZ SCF	-433.065 461	3.162	2491 (2.2)	353 (10.7)	641 (42.8)	5.49
aug-cc-pVTZ SCF	-433.057 104	3.185	2488 (1.9)	353 (10.1)	639 (43.8)	5.48
aug-cc-pVQZ SCF	-433.065 703	3.176	2489 (1.8)	353 (10.2)	641 (43.0)	5.48
cc-pVTZ CISD	-433.457 963	2.927	2297 (-)	334 (-)	640 (-)	5.15
cc-pVQZ CISD	-433.488 905	2.976	2304 (-)	334 (-)	645 (-)	5.17
aug-cc-pVTZ CISD	-433.464 036	3.014	2293 (-)	332 (-)	639 (-)	5.14
aug-cc-pVQZ CISD	-433.491 263	3.002	2303 (-)	333 (-)	645 (-)	5.16
cc-pVTZ CCSD	-433.509 731	2.803	2144 (-)	324 (-)	632 (-)	4.89
cc-pVQZ CCSD	-433.543 201	2.854	2150 (-)	323 (-)	638 (-)	4.91
aug-cc-pVTZ CCSD	-433.516 832	2.898	2138 (-)	320 (-)	630 (-)	4.87
aug-cc-pVQZ CCSD	-433.545 877	2.885	2148 (-)	321 (-)	637 (-)	4.90
cc-pVTZ CCSD(T)	-433.535 529	2.700	2046 (-)	314 (-)	629 (-)	4.72
cc-pVQZ CCSD(T)	-433.571 317	2.752	2050 (-)	314 (-)	636 (-)	4.74
aug-cc-pVTZ CCSD(T)	-433.543 582	2.804	2039 (-)	311 (-)	628 (-)	4.70
aug-cc-pVQZ CCSD(T)	-433.574 365	2.788	2046 (-)	312 (-)	635 (-)	4.72

Table 3.1.2: Theoretical predictions of the total energy (in hartree), dipole moment (in debye), harmonic vibrational frequencies (in cm^{-1}), infrared intensities (in parentheses in km mol^{-1}), and zero-point vibrational energy (ZPVE in kcal mol^{-1}) for the linear $\widetilde{X}\ {}^3\Sigma^-$ state of the PCN molecule. The infrared intensities for ω_2 were doubled. (Continued)

Level of Theory	Energy	μ	ω_1 (σ)	ω_2 (π)	ω_3 (σ)	ZPVE
cc-pVTZ CASSCF	-433.214 406	2.605	···	···	···	···
cc-pVQZ CASSCF	-433.223 823	2.638	···	···	···	···
aug-cc-pVTZ CASSCF	-433.215 517	2.654	···	···	···	···
aug-cc-pVQZ CASSCF	-433.224 052	2.648	···	···	···	···
cc-pVTZ MRCISD[a]	-433.505 109	···	···	···	···	···
cc-pVQZ MRCISD[a]	-433.536 776	···	···	···	···	···
aug-cc-pVTZ MRCISD[a]	-433.511 446	···	···	···	···	···
aug-cc-pVQZ MRCISD[a]	-433.539 230	···	···	···	···	···
Ref. 9: 6-31G* UHF	···	2.42	1771 (119.6)	332 (4.4)	681 (45.1)	···
Ref. 11: cc-pVTZ B3LYP	···	2.68	2037 (11)	333 (3)	649 (24)	···

[a] At the CCSD geometries optimized with the same basis set.

Table 3.2.1: Theoretical predictions of the total energy (in hartree), dipole moment (in debye), harmonic vibrational frequencies (in cm^{-1}), infrared intensities (in parentheses in km mol^{-1}), and zero-point vibrational energy (ZPVE in kcal mol^{-1}) for the linear $\tilde{X}\ ^3\Sigma^-$ state of the PNC molecule. The infrared intensities for ω_2 were doubled.

Level of Theory	Energy	μ	ω_1 (σ)	ω_2 (π)	ω_3 (σ)	ZPVE
cc-pVTZ SCF	-433.045 063	2.275	2290 (476.0)	244 (0.1)	712 (102.4)	4.99
cc-pVQZ SCF	-433.055 153	2.234	2288 (487.3)	243 (0.1)	712 (103.1)	4.98
aug-cc-pVTZ SCF	-433.046 411	2.259	2286 (505.0)	243 (0.1)	709 (105.5)	4.98
aug-cc-pVQZ SCF	-433.055 447	2.225	2287 (502.2)	242 (0.1)	711 (104.5)	4.98
cc-pVTZ CISD	-433.439 433	2.486	2157 (-)	248 (-)	702 (-)	4.80
cc-pVQZ CISD	-433.470 967	2.437	2163 (-)	249 (-)	707 (-)	4.81
aug-cc-pVTZ CISD	-433.445 731	2.493	2153 (-)	245 (-)	697 (-)	4.77
aug-cc-pVQZ CISD	-433.473 557	2.440	2161 (-)	247 (-)	705 (-)	4.80
cc-pVTZ CCSD	-433.488 307	2.544	2059 (-)	248 (-)	689 (-)	4.64
cc-pVQZ CCSD	-433.522 349	2.498	2063 (-)	249 (-)	696 (-)	4.65
aug-cc-pVTZ CCSD	-433.495 695	2.561	2054 (-)	244 (-)	684 (-)	4.61
aug-cc-pVQZ CCSD	-433.525 298	2.507	2060 (-)	247 (-)	694 (-)	4.64
cc-pVTZ CCSD(T)	-433.512 819	2.538	1977 (-)	244 (-)	681 (-)	4.50
cc-pVQZ CCSD(T)	-433.549 162	2.496	1980 (-)	245 (-)	688 (-)	4.51
aug-cc-pVTZ CCSD(T)	-433.521 252	2.560	1971 (-)	240 (-)	675 (-)	4.47
aug-cc-pVQZ CCSD(T)	-433.552 512	2.508	1976 (-)	243 (-)	686 (-)	4.50

Table 3.2.2: Theoretical predictions of the total energy (in hartree), dipole moment (in debye), harmonic vibrational frequencies (in cm^{-1}), infrared intensities (in parentheses in km mol^{-1}), and zero-point vibrational energy (ZPVE in kcal mol^{-1}) for the linear $\tilde{X}$ $^3\Sigma^-$ state of the PNC molecule. The infrared intensities for ω_2 were doubled. (Continued)

Level of Theory	Energy	μ	ω_1 (σ)	ω_2 (π)	ω_3 (σ)	ZPVE
cc-pVTZ CASSCF	-433.190 574	2.818	···	···	···	···
cc-pVQZ CASSCF	-433.200 353	2.804	···	···	···	···
aug-cc-pVTZ CASSCF	-433.191 765	2.831	···	···	···	···
aug-cc-pVQZ CASSCF	-433.200 636	2.807	···	···	···	···
cc-pVTZ MRCISD[a]	-433.480 520	···	···	···	···	···
cc-pVQZ MRCISD[a]	-433.512 555	···	···	···	···	···
aug-cc-pVTZ MRCISD[a]	-433.487 081	···	···	···	···	···
aug-cc-pVQZ MRCISD[a]	-433.515 237	···	···	···	···	···
Ref. 9: 6-31G* UHF	···	2.16	2210 (221.7)	275 (0.1)	722 (81.3)	···
Ref. 11: cc-pVTZ B3LYP	···	2.48	1974 (125)	264 (0.28)	693 (30)	···

[a] At the CCSD geometries optimized with the same basis set.

Table 3.3.1: Theoretical predictions of the total energy (in hartree), dipole moment (in debye), harmonic vibrational frequencies (in cm^{-1}), and zero-point vibrational energy (ZPVE in kcal mol^{-1}) for the $\tilde{X}$ $^3A''$ isomerization transition state of the PCN – PNC system.

Level of Theory	Energy	μ	ω_1 (a′)	ω_2 (a′)	ω_3 (a′)	ZPVE
cc-pVTZ SCF	-432.995 058	1.907	2229	380i	537	3.95
cc-pVQZ SCF	-433.004 699	1.883	2230	381i	535	3.95
aug-cc-pVTZ SCF	-432.996 694	1.915	2226	380i	534	3.95
aug-cc-pVQZ SCF	-433.005 096	1.885	2229	381i	534	3.95
cc-pVTZ CISD	-433.397 588	1.622	2081	322i	565	3.78
cc-pVQZ CISD	-433.428 694	1.583	2090	327i	574	3.81
aug-cc-pVTZ CISD	-433.404 426	1.650	2079	324i	563	3.78
aug-cc-pVQZ CISD	-433.431 475	1.595	2089	328i	574	3.81
cc-pVTZ CCSD	-433.450 213	1.519	1966	260i	559	3.61
cc-pVQZ CCSD	-433.484 022	1.485	1975	269i	574	3.64
aug-cc-pVTZ CCSD	-433.458 233	1.553	1963	263i	558	3.60
aug-cc-pVQZ CCSD	-433.487 206	1.501	1974	272i	576	3.64
cc-pVTZ CCSD(T)	-433.477 643	1.439	1877	204i	551	3.47
cc-pVQZ CCSD(T)	-433.513 946	1.413	1885	224i	574	3.52
aug-cc-pVTZ CCSD(T)	-433.486 711	1.481	1872	210i	551	3.46
aug-cc-pVQZ CCSD(T)	-433.517 555	1.434	1883	229i	576	3.52

Table 3.3.2: Theoretical predictions of the total energy (in hartree), dipole moment (in debye), harmonic vibrational frequencies (in cm^{-1}), and zero-point vibrational energy (ZPVE in kcal mol^{-1}) for the $\tilde{X}$ ^{3}A″ isomerization transition state of the PCN – PNC system. (Continued)

Level of Theory	Energy	μ	ω_1 (a′)	ω_2 (a′)	ω_3 (a′)	ZPVE
cc-pVTZ CASSCF	-433.146 103	1.450	···	···	···	···
cc-pVQZ CASSCF	-433.155 511	1.428	···	···	···	···
aug-cc-pVTZ CASSCF	-433.147 549	1.460	···	···	···	···
aug-cc-pVQZ CASSCF	-433.155 894	1.433	···	···	···	···
cc-pVTZ MRCISD[a]	-433.445 019	···	···	···	···	···
cc-pVQZ MRCISD[a]	-433.476 986	···	···	···	···	···
aug-cc-pVTZ MRCISD[a]	-433.452 196	···	···	···	···	···
aug-cc-pVQZ MRCISD[a]	-433.479 909	···	···	···	···	···
Ref. 9: 6-31G* UHF	···	···	2200	346i	529	···
Ref. 11: cc-pVTZ B3LYP	···	1.54	1938	213i	571	···

[a] At the CCSD geometries optimized with the same basis set.

Table 3.4.1: Energies in kcal mol^{-1} (ZPVE-corrected values in parentheses) for the linear PNC ($\tilde{X}$ $^3\Sigma^-$) isomer and the $\tilde{X}$ $^3A''$ isomerization transition state relative to the linear PCN ($\tilde{X}$ $^3\Sigma^-$) isomer.

Level of Theory	$\tilde{X}$ $^3\Sigma^-$ PCN	$\tilde{X}$ $^3\Sigma^-$ PNC	$\tilde{X}$ $^3A''$ TS
cc-pVTZ SCF	0.0 (0.0)	6.76 (6.26)	38.13 (36.59)
cc-pVQZ SCF	0.0 (0.0)	6.47 (5.96)	38.13 (36.59)
aug-cc-pVTZ SCF	0.0 (0.0)	6.71 (6.21)	37.91 (36.38)
aug-cc-pVQZ SCF	0.0 (0.0)	6.44 (5.94)	38.03 (36.50)
cc-pVTZ CISD	0.0 (0.0)	11.63 (11.28)	37.89 (36.52)
cc-pVQZ CISD	0.0 (0.0)	11.26 (10.90)	37.78 (36.42)
aug-cc-pVTZ CISD	0.0 (0.0)	11.49 (11.12)	37.41 (36.05)
aug-cc-pVQZ CISD	0.0 (0.0)	11.11 (10.75)	37.52 (36.17)
cc-pVTZ CCSD	0.0 (0.0)	13.44 (13.19)	37.35 (36.07)
cc-pVQZ CCSD	0.0 (0.0)	13.08 (12.82)	37.14 (35.87)
aug-cc-pVTZ CCSD	0.0 (0.0)	13.26 (13.00)	36.77 (35.50)
aug-cc-pVQZ CCSD	0.0 (0.0)	12.91 (12.65)	36.82 (35.56)
cc-pVTZ CCSD(T)	0.0 (0.0)	14.25 (14.03)	36.32 (35.07)
cc-pVQZ CCSD(T)	0.0 (0.0)	13.90 (13.67)	36.00 (34.78)
aug-cc-pVTZ CCSD(T)	0.0 (0.0)	14.01 (13.78)	35.69 (34.45)
aug-cc-pVQZ CCSD(T)	0.0 (0.0)	13.71 (13.49)	35.65 (34.45)

Table 3.4.2: Energies in kcal mol^{-1} (ZPVE-corrected values in parentheses) for the linear PNC ($\tilde{X}$ $^3\Sigma^-$) isomer and the $\tilde{X}$ $^3A''$ isomerization transition state relative to the linear PCN ($\tilde{X}$ $^3\Sigma^-$) isomer. (Continued)

Level of Theory	$\tilde{X}$ $^3\Sigma^-$ PCN	$\tilde{X}$ $^3\Sigma^-$ PNC	$\tilde{X}$ $^3A''$ TS
cc-pVTZ CASSCF	0.0 (-)	14.95 (-)	42.86 (-)
cc-pVQZ CASSCF	0.0 (-)	14.73 (-)	42.87 (-)
aug-cc-pVTZ CASSCF	0.0 (-)	14.90 (-)	42.65 (-)
aug-cc-pVQZ CASSCF	0.0 (-)	14.69 (-)	42.77 (-)
cc-pVTZ MRCISD[a]	0.0 (-)	15.43 (-)	37.71 (-)
cc-pVQZ MRCISD[a]	0.0 (-)	15.20 (-)	37.52 (-)
aug-cc-pVTZ MRCISD[a]	0.0 (-)	15.29 (-)	37.18 (-)
aug-cc-pVQZ MRCISD[a]	0.0 (-)	15.06 (-)	37.22 (-)
Ref. 9: MC-311G* MP4[b]	0.0 (-)	9.4 (-)	32.2 (-)
Ref. 9: MC-311G* PMP3[b]	0.0 (-)	15.0 (-)	39.4 (-)
Ref. 11: cc-pVTZ B3LYP	0.0 (-)	12.9 (-)	36.8 (-)
Ref. 11: cc-pVTZ CCSD(T)[c]	0.0 (0.0)	14.2 (14.0)	36.2 (35.0)

[a] At the CCSD geometries optimized with the same basis set.

[b] At the 6-31G* UHF geometries.

[c] At the cc-pVTZ B3LYP geometries. Zero-point vibrational energy differences were obtained from the cc-pVTZ B3LYP harmonic frequencies.

$\widetilde{X}\ {}^3\Sigma^-$

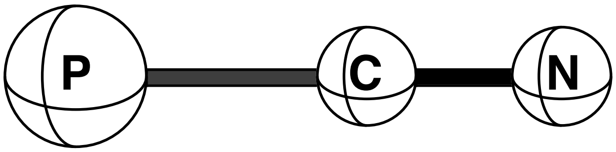

cc-pVTZ SCF	1.7810	1.1322
cc-pVQZ SCF	1.7778	1.1307
aug-cc-pVTZ SCF	1.7815	1.1318
aug-cc-pVQZ SCF	1.7776	1.1308
cc-pVTZ CISD	1.7597	1.1533
cc-pVQZ CISD	1.7530	1.1497
aug-cc-pVTZ CISD	1.7600	1.1530
aug-cc-pVQZ CISD	1.7531	1.1500
cc-pVTZ CCSD	1.7527	1.1671
cc-pVQZ CCSD	1.7449	1.1635
aug-cc-pVTZ CCSD	1.7528	1.1670
aug-cc-pVQZ CCSD	1.7450	1.1638
cc-pVTZ CCSD(T)	1.7486	1.1773
cc-pVQZ CCSD(T)	1.7402	1.1740
aug-cc-pVTZ CCSD(T)	1.7487	1.1775
aug-cc-pVQZ CCSD(T)	1.7403	1.1744
cc-pVTZ CASSCF	1.7704	1.1792
cc-pVQZ CASSCF	1.7665	1.1774
aug-cc-pVTZ CASSCF	1.7708	1.1785
aug-cc-pVQZ CASSCF	1.7664	1.1775
Ref. 9: 6-31G* UHF	1.724	1.174
Ref. 11: cc-pVTZ B3LYP	1.724	1.170

Figure 3.1: Predicted geometries for the linear $\widetilde{X}\ {}^3\Sigma^-$ state of the PCN isomer. Bond lengths are in Å.

$\tilde{X}\ ^3\Sigma^-$

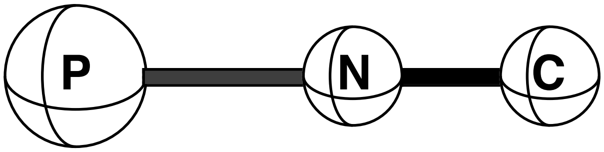

cc-pVTZ SCF	1.6864	1.1577
cc-pVQZ SCF	1.6822	1.1561
aug-cc-pVTZ SCF	1.6873	1.1571
aug-cc-pVQZ SCF	1.6823	1.1561
cc-pVTZ CISD	1.6821	1.1741
cc-pVQZ CISD	1.6740	1.1707
aug-cc-pVTZ CISD	1.6835	1.1736
aug-cc-pVQZ CISD	1.6747	1.1708
cc-pVTZ CCSD	1.6824	1.1847
cc-pVQZ CCSD	1.6733	1.1813
aug-cc-pVTZ CCSD	1.6838	1.1844
aug-cc-pVQZ CCSD	1.6740	1.1815
cc-pVTZ CCSD(T)	1.6831	1.1939
cc-pVQZ CCSD(T)	1.6736	1.1908
aug-cc-pVTZ CCSD(T)	1.6848	1.1939
aug-cc-pVQZ CCSD(T)	1.6745	1.1911
cc-pVTZ CASSCF	1.7060	1.1925
cc-pVQZ CASSCF	1.7018	1.1906
aug-cc-pVTZ CASSCF	1.7069	1.1917
aug-cc-pVQZ CASSCF	1.7020	1.1905
Ref. 9: 6-31G* UHF	1.680	1.170
Ref. 11: cc-pVTZ B3LYP	1.665	1.188

Figure 3.2: Predicted geometries for the linear $\tilde{X}\ ^3\Sigma^-$ state of the PNC isomer. Bond lengths are in Å.

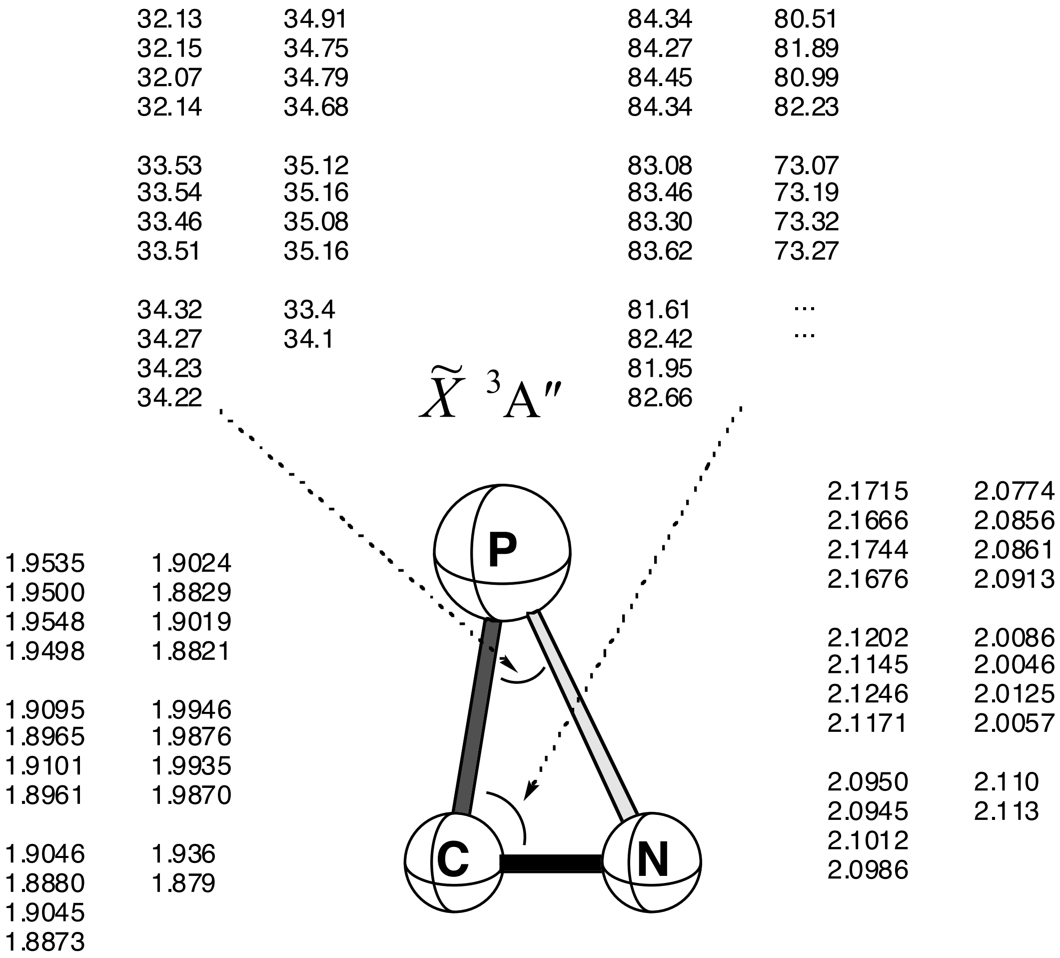

cc-pVTZ SCF	1.1605	cc-pVTZ CCSD(T)	1.2053
cc-pVQZ SCF	1.1586	cc-pVQZ CCSD(T)	1.2009
aug-cc-pVTZ SCF	1.1600	aug-cc-pVTZ CCSD(T)	1.2052
aug-cc-pVQZ SCF	1.1587	aug-cc-pVQZ CCSD(T)	1.2011
cc-pVTZ CISD	1.1799	cc-pVTZ CASSCF	1.2080
cc-pVQZ CISD	1.1759	cc-pVQZ CASSCF	1.2060
aug-cc-pVTZ CISD	1.1794	aug-cc-pVTZ CASSCF	1.2074
aug-cc-pVQZ CISD	1.1760	aug-cc-pVQZ CASSCF	1.2060
cc-pVTZ CCSD	1.1940	Ref. 9: 6-31G* UHF	1.173
cc-pVQZ CCSD	1.1897	Ref. 11: cc-pVTZ B3LYP	...
aug-cc-pVTZ CCSD	1.1937		
aug-cc-pVQZ CCSD	1.1899		

Figure 3.3: Predicted geometries of the $\widetilde{X}\ ^3A''$ transition state for the PCN ↔ PNC isomerization reaction. Bond lengths are in Å, and angles are in degrees.

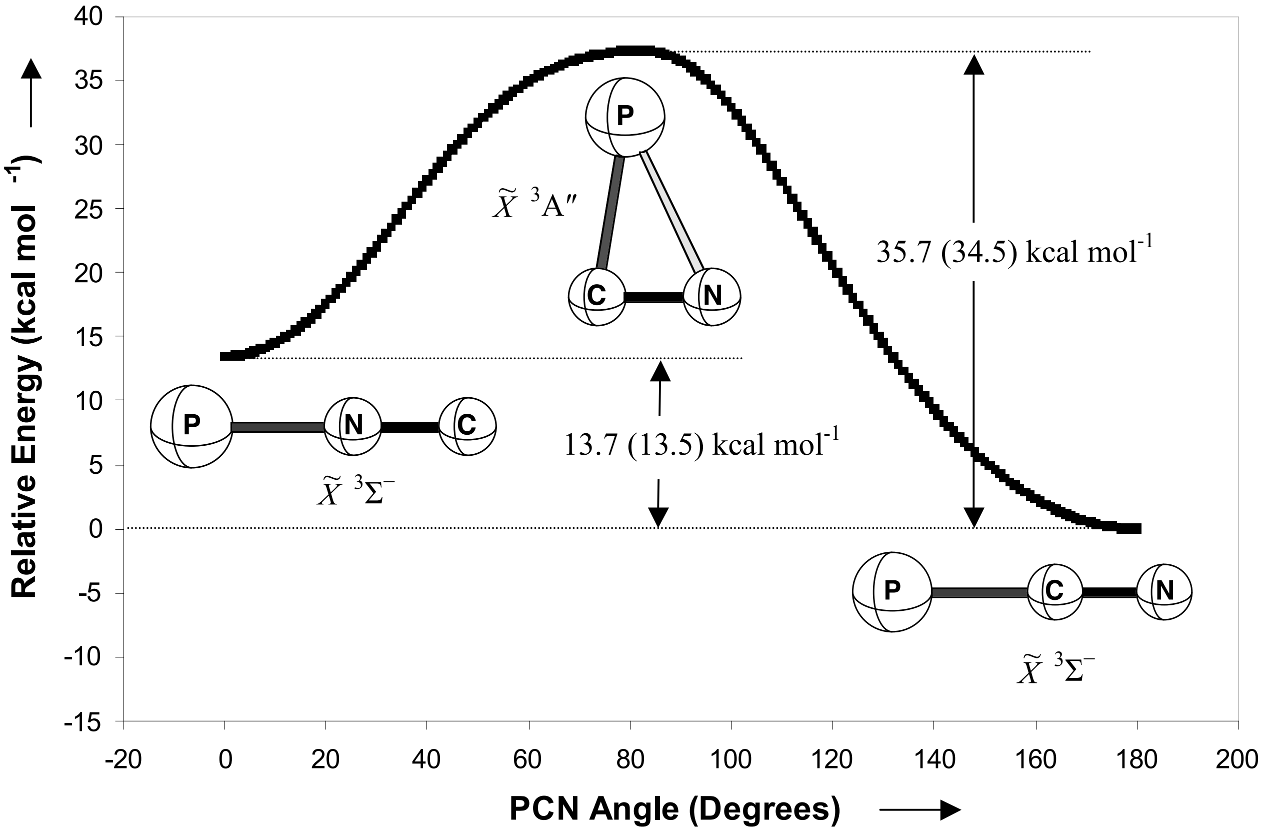

Figure 3.4: Predicted pathway for the PCN – PNC system with the cc-pVTZ CCSD method. This surface consists of 181 energy points (with energies in kcal mol^{-1} relative to the PCN isomer) corresponding to PCN angles from 0° to 180° along with the optimized bond distances. The energy separations (ZPVE-corrected values in parentheses) of the PCN / PNC isomers and their transition state explicitly labeled in the figure were evaluated at the aug-cc-pVQZ CCSD(T) level of theory.

CHAPTER 4

THE SMALL PLANARIZATION BARRIERS FOR THE AMINO GROUP IN THE NUCLEIC ACID BASES[1]

---

[1] Suyun Wang and Henry F. Schaefer. 2006. *Journal of Chemical Physics*. 124: Art. No. 044303. Reprinted here with permission of the American Institute of Physics.

4.1 ABSTRACT

The amino group in the nucleic acid bases frequently interacts with other bases or with other molecular systems. Thus any nonplanarity of the amino group may affect the molecular recognition of nucleic acids. *Ab initio* Hartree-Fock (HF) and second-order Møller-Plesset perturbation (MP2) levels of theory have been used to obtain the equilibrium geometries of the C_1 and C_s structures for five common nucleic acid bases. The energy barriers between the C_1 and C_s structures have also been predicted. A series of correlation consistent basis sets up to cc-pCVQZ and aug-cc-pVQZ has been used to systematically study the dependence of the amino group nonplanarity. The equilibrium geometries of the nucleic acid bases with an amino group, including adenine, guanine, and cytosine, are examined carefully. At the MP2 level of theory, larger basis sets decrease the extent of nonplanarity of the amino group, but the decrease slows down when the QZ basis sets are used, demonstrating the intrinsic property of nonplanarity for guanine. For adenine and cytosine the situation is less clear; as the HF limit is approached, these two structures become planar. Addition of core correlation effects or diffuse functions further decreases the degree of nucleic acid (NA) base nonplanarity, in comparison to the original cc-pVXZ (X = D, T, and Q) basis sets. The aug-cc-pVXZ basis shows smaller degrees of nonplanarity than the cc-pCVXZ sets. The aug-cc-pVXZ basis is less size-dependent than the cc-pVXZ and cc-pCVXZ sets in the prediction of the amino group related bond angles and dihedral angles and energy barriers for adenine, guanine, and cytosine. The cc-pCVQZ and aug-cc-pVQZ MP2 results may be regarded as benchmark predictions for the five common bases. The predicted classical barriers to planarization are 0.02 (adenine), 0.74 (guanine), and 0.03 (cytosine) kcal mol^{-1}.

4.2 INTRODUCTION

The five nucleic acid (NA) bases adenine, guanine, cytosine, thymine (in DNA), and uracil (in RNA) are common components of nucleotides, the building blocks of the NA strands. These five NA bases can form hydrogen bonds with each other to yield base pairs in both double-stranded and single-stranded NAs, or interact with other molecules to form complexes. The nonplanarity of the bases will influence the structure, and consequently the molecular recognition of NAs.

The isolated NA bases had been expected to be planar for many years. Accordingly, the empirical force fields used in many theoretical NA conformational and dynamics analyses assume planar geometries for the NA bases. However, *ab initio* quantum mechanical studies have consistently predicted nonplanar amino groups for the NA bases.[1, 2] Direct experimental results for the NA base amino moieties are not available, but indirect experimental evidence does exist.

The first indirect experimental evidence was connected with the excellent agreement between the theoretical[3] anharmonic and experimental[4-6] inversion-torsion vibrational frequencies for the fundamental, overtone, and combination modes of the model system aniline. Accurate gas phase inversion splitting data for aniline were reported by Kydd and Krueger[4, 5] and Larsen *et al.*,[6] and the related *ab initio* Hartree-Fock (HF), second-order Møller-Plesset perturbation (MP2) and single-point coupled-cluster including single and double excitations and perturbatively applied triple excitations [CCSD(T)] studies on aniline were performed by Bludsky and coworkers.[3] This agreement provided evidence concerning the nature of the predicted aniline potential energy surface, consistent with a strong nonplanarity of the amino group.[7-9] The second piece of indirect experimental evidence came from an unexpected blue shift of the amino N-H stretch vibrational frequency in the gas-phase IR spectra of the guanine dimer (Nir *et al.*[10] in 2002). This blue shift was explained by Hobza and Spirko[11] in 2003 based on the contraction of the amino N-H bonds from the planarization of the amino group in the guanine dimer. The increase of the guanine amino N-H stretch frequency occurring with guanine dimerization represented the first spectroscopic manifestation of the fact that the amino group in a NA base is nonplanar. Indirect experimental evidence was associated with the vibrational transition moment angles (VTMAs) of adenine reported in 2002 by Dong and Miller.[12] Their VTMAs were extremely sensitive to the molecular structure, and the IR spectroscopic results were only reproduced by methods that assumed a nonplanar amino group for adenine.

In addition, crystallographic and database studies[13-16] have revealed that the amino group hydrogen atoms can form very efficient out-of-plane hydrogen bonds and the amino group nitrogen atom can serve as a weak H-bond acceptor. The mismatched G(*anti*) · A(*anti*) base pair[17] is an example exhibiting the strong out-of-plane H-bond character related to the nonplanar guanine amino group. Thus, the base amino group is often activated to adopt a partial sp^3 geometry and exhibit bifurcated hydrogen bonds[18, 19] and close amino group contacts[13, 20, 21] when another group interacts with the amino group.

In the early 1990s, theoretical studies[13, 22-25] at the HF level of theory with polarized basis sets provided the first respectable suggestion that a weak nonplanarity of amino groups of bases could occur. In 1994, Sponer and Hobza[26] applied both the HF and MP2 methods to cytosine. They concluded that the inclusion of electron correlation significantly increases the nonplanarity of the cytosine amino group compared to the HF level of theory. In the same year, Sponer and Hobza[27] published their correlated MP2 study of the DNA bases. Their results showed that the degree of nonplanarity of guanine is greater than that of cytosine and adenine, and the amino group of guanine is substantially rotated due to the repulsion between the H_1 hydrogen and the amino group hydrogen. Later *ab initio* studies[28-32] confirmed the original results. The 1996 reference values of NA base amino group nonplanarity were those of Sponer, Leszczynski, and Hobza[28] at the 6-311G(2df,p) MP2 level of theory. A new reference set was presented by Ryjacek, Kubar, and Hobza[30] in 2003 using the RIMP2 method.

In addition to HF and MP2 methods, density functional theory (DFT) and single-point coupled-cluster computations have been used for the study of the nonplanarity of NA bases. However, the DFT approach showed a rather wide range of results for the NA base amino group nonplanarities.[20, 33] In 2004, Preuss and coworkers[34] applied the PW91 DFT method using ultrasoft pseudopotentials to this problem. Very different from the *ab initio* results, the amino dihedral angles were predicted to be zero for adenine, 11.2° for cytosine, and 2.3° for guanine.

In this paper, a systematic exploration of base amino group nonplanarity with respect to different basis sets has been performed by using a series of correlation consistent basis sets in conjunction with the MP2 method. The cc-pCVQZ and aug-cc-pVQZ benchmark results for amino group nonplanarities have been obtained for comparison with previous theoretical research.

4.3 THEORETICAL METHODS

The *ab initio* HF and MP2 methods were used to investigate the C_1 and constrained C_s structures for the five common NA bases, namely adenine, guanine, cytosine, thymine, and uracil. The Gaussian 94[35] and NWChem[36] software packages were used in this study. Equilibrium geometries have been optimized with various basis sets for the C_1 and constrained C_s structures, and the energy barriers between the C_1 and constrained C_s structures were predicted for the five common NA bases. Harmonic vibrational frequencies have been obtained at stationary points.

A series of correlation consistent polarized valence basis sets were used for the five NA bases. This approach was adopted to systematically investigate the dependence of the base amino group nonplanarity and energy barriers on the different basis sets. These basis sets include cc-pVDZ (C, N, O: 9s4p1d/3s2p1d; H: 4s1p/2s1p),[37] cc-pCVDZ (C, N, O: 10s5p1d/4s3p1d),[37, 38] aug-cc-pVDZ (C, N, O: 10s5p2d/4s3p2d; H: 5s2p/3s2p),[37, 39] cc-pVTZ (C, N, O: 10s5p2d1f/4s3p2d1f; H: 5s2p1d/3s2p1d),[37] cc-pCVTZ (C, N, O: 12s7p3d1f/6s5p3d1f),[37, 38] aug-cc-pVTZ (C, N, O: 11s6p3d2f/5s4p3d2f; H: 6s3p2d/4s3p2d),[37, 39] cc-pVQZ (C, N, O: 12s6p3d2f1g/5s4p3d2f1g; H: 6s3p2d1f/4s3p2d1f),[37] cc-pCVQZ (15s9p5d3f1g/8s7p5d3f1g),[37, 38] and aug-cc-pVQZ (C, N, O: 13s7p4d3f2g/6s5p4d3f2g; H: 7s4p3d2f/5s4p3d2f).[37, 39] The cc-pCVXZ (X = D, T, and Q) basis extended the cc-pVXZ set by including extra functions designed for core-core and core-valence correlation. When using the cc-pCVXZ basis sets, no C, N, O core orbitals were frozen at the MP2 level of theory, and the cc-pVXZ basis sets were adopted for H atoms. The aug-cc-pVXZ basis was constructed by augmenting the cc-pVXZ set with diffuse functions.

The largest computations involve the guanine molecule with the aug-cc-pVQZ basis set. There are 1110 contracted Gaussian functions in the HF and MP2 optimizations. In addition, there are 1797 contracted Gaussian functions in the aug-cc-pV5Z HF single-point energy predictions.

4.4 RESULTS AND DISCUSSION

Qualitatively, the atoms of the molecular rings for adenine, guanine, and cytosine provide ten, ten, and six π electrons, respectively, satisfying the 4n+2 (n = 2 for adenine and guanine, n = 1 for cytosine) Hückel rule of aromaticity. The molecular structures and the numbering of the amino group related atoms for the adenine, guanine, and cytosine bases are illustrated in Figure 4.1. The amino group nitrogen atoms of adenine, guanine, and cytosine do not participate in the π system, leading the amino group hydrogens out of the plane of the molecular ring. Having no amino group, thymine and uracil are expected to be planar if the methyl group of thymine is not considered.

4.4.1 NONPLANARITY OF ADENINE, GUANINE, AND CYTOSINE

4.4.1.1 BOND DISTANCES

The optimized C_1 and constrained C_s geometries of adenine, guanine, and cytosine are presented in Figures 4.2, 4.3, and 4.4, respectively, using various basis sets with the MP2 method. The DZ basis sets (cc-pVDZ, cc-pCVDZ, and aug-cc-pVDZ) significantly overestimate the bond distances for the C_1 and constrained C_s structures of these three NA bases compared to other basis sets. The use of larger basis sets generally shortens the bond distances for both the C_1 and C_s structures. Compared to the cc-pVXZ basis sets, the cc-pCVXZ basis (adding core correlation) usually shortens the bond lengths, while the aug-cc-pVXZ basis (adding diffuse functions) only slightly changes the bond lengths for all structures. With the cc-pVQZ MP2 method, the optimized C_1 structure bond distances of guanine are consistent with the theoretical results of Pulay, Saebo, Malagoli, and Baker.[31]

The optimized amino group related bond distances (C_6-N_6, N_6-H_{6a}, and N_6-H_{6b} bonds for adenine; C_2-N_2, N_2-H_{2a}, and N_2-H_{2b} bonds for guanine; C_4-N_4, N_4-H_{4a}, and N_4-H_{4b} bonds for cytosine) indicate substantial changes between the C_1 and C_s structures compared to the other structural features of these three bases. All basis sets predict longer amino group related bond distances for the C_1 structure than for the C_s structure. The difference in amino group bond lengths between the C_1 and C_s structures tends to decrease with the increased size of the basis sets.

With the aug-cc-pVQZ MP2 method, the equilibrium bond lengths for the amino group of adenine are predicted to be $r_e(C_6N_6)$ = 1.353 Å, $r_e(N_6H_{6a})$ = 1.004 Å, $r_e(N_6H_{6b})$ = 1.004 Å for the C_1 structure, and $r_e(C_6N_6)$ = 1.348 Å, $r_e(N_6H_{6a})$ = 1.002 Å, $r_e(N_6H_{6b})$ = 1.003 Å for the constrained C_s structure (Figure 4.2). For guanine, the amino group bond distances are computed to be $r_e(C_2N_2)$ = 1.376 Å, $r_e(N_2H_{2a})$ = 1.007 Å, $r_e(N_2H_{2b})$ = 1.006 Å for the C_1 structure, and $r_e(C_2N_2)$ = 1.358 Å, $r_e(N_2H_{2a})$ = 1.002 Å, $r_e(N_2H_{2b})$ = 1.000 Å for the constrained C_s structure (Figure 4.3). For cytosine, the amino group bond distances are $r_e(C_4N_4)$ = 1.357 Å, $r_e(N_4H_{4a})$ = 1.005 Å, $r_e(N_4H_{4b})$ = 1.002 Å for the C_1 structure, and $r_e(C_4N_4)$ = 1.352 Å, $r_e(N_4H_{4a})$ = 1.004 Å, $r_e(N_4H_{4b})$ = 1.000 Å for the constrained C_s structure (Figure 4.4). It turns out that guanine has larger differences in amino group bond lengths between the C_1 and C_s structures (0.018 Å for the C_2-N_2 bond, 0.005 Å for the N_2-H_{2a} bond, and 0.006 Å for the N_2-H_{2b} bond) than the adenine and cytosine bases (0.005 Å for the C-N bonds, 0.001 ~ 0.002 Å for the N-H bonds). This demonstrates that the optimized guanine amino group geometry possesses the most significant deviation from the constrained coplanar structure.

The C-N single bond length for methylamine (CH_3NH_2) is experimentally known to be $r_0 = 1.471(3)$ Å[40] and $r_g = 1.472(3)$ Å.[41] These C-N bond distances are much longer than the amino group C-N bonds of adenine, guanine, and cytosine, primarily due to the partial sp^3 hybridization of amino group nitrogen in bases. The partial sp^3 hybridization of the amino nitrogen atom leads to the deviation of the amino group hydrogen atoms from the base plane in one direction and the slightly shifted amino group nitrogen atom in the opposite direction. The experimentally deduced N-H equilibrium bond distance of ammonia (NH_3) is $r_e = 1.011(3)$ Å[42] which is less than 0.01 Å longer than the amino group N-H bond of adenine, guanine, and cytosine.

4.4.1.2 BOND ANGLES AND DIHEDRAL ANGLES

Tables 4.1, 4.2, and 4.3 summarize the optimized bond angles around the amino group nitrogen atoms and the amino group related dihedral angles for the nonplanar C_1 structures of adenine, guanine, and cytosine, respectively. The three amino group related valence bond angles are defined as the C_6-N_6-H_{6a}, C_6-N_6-H_{6b}, and H_{6a}-N_6-H_{6b} angles for adenine; the C_2-N_2-H_{2a}, C_2-N_2-H_{2b}, and H_{2a}-N_2-H_{2b} angles for guanine; and the C_4-N_4-H_{4a}, C_4-N_4-H_{4b}, and H_{4a}-N_4-H_{4b} angles for cytosine. The summation of these three angles for each basis set is also listed in the tables. The larger the predicted deviation of this summation from 360°, the more pronounced is the nonplanarity of the NA base amino group. The amino group related dihedral angles are the N_1-C_6-N_6-H_{6b} and C_5-C_6-N_6-H_{6a} angles for adenine; the N_1-C_2-N_2-H_{2b} and N_3-C_2-N_2-H_{2a} angles for guanine; and the N_3-C_4-N_4-H_{4a} and C_5-C_4-N_4-H_{4b} angles for cytosine (see Figure 4.1 for atom numbering).

At the MP2 level of theory, the extension of the basis set size usually widens the bond angles, and consequently increases the sum of valence bond angles, while decreasing the dihedral angles, which means diminishing the nonplanarity of the amino group. However, the decrease in the degree of nonplanarity becomes less pronounced when the larger QZ basis sets are used, demonstrating the intrinsic nonplanarity of the NA base amino groups. Addition of core-core and core-valence correlation (cc-pCVXZ basis sets) or diffuse functions (aug-cc-pVXZ basis sets) broadens the valence bond angles and decreases the dihedral angles compared to the original cc-pVXZ basis sets. Furthermore, the aug-cc-pVXZ basis gives larger changes in the valence bond angles and dihedral angles with respect to the cc-pVXZ values than do the cc-pCVXZ sets, reflecting a lesser degree of the amino group nonplanarity with the aug-cc-pVXZ bases than with the cc-pCVXZ bases. Note that all basis sets for guanine lead to values of the dihedral angle N_1-C_2-N_2-H_{2b} about three times as large as N_3-C_2-N_2-H_{2a} due to the repulsion of the H_{2b} and H_1 (connected with N_1) atoms. In addition, the optimized C_1 bond angles and dihedral angles of guanine at the cc-pVQZ MP2 level of theory are consistent with the theoretical results of Pulay, Saebo, Malagoli, and Baker.[31]

With the aug-cc-pVQZ MP2 method, the equilibrium bond angles are predicted to be $\theta_e(C_6N_6H_{6a}) = 118.4^\circ$, $\theta_e(C_6N_6H_{6b}) = 117.6^\circ$, and $\theta_e(H_{6a}N_6H_{6b}) = 119.2^\circ$ (sum = 355.2°) for adenine (Table 4.1); $\theta_e(C_2N_2H_{2a}) = 112.2^\circ$, $\theta_e(C_2N_2H_{2b}) = 116.4^\circ$, and $\theta_e(H_{2a}N_2H_{2b}) = 113.4^\circ$ (sum = 342.0°) for guanine (Table 4.2); and $\theta_e(C_4N_4H_{4a}) = 116.7^\circ$,

$\theta_e(C_4N_4H_{4b})$ = 120.2°, and $\theta_e(H_{4a}N_4H_{4b})$ = 118.5° (sum = 355.4°) for cytosine (Table 4.3). The optimized dihedral angles (absolute values only) are determined to be $\varphi_e(N_1C_6N_6H_{6b})$ = 12.9° and $\varphi_e(C_5C_6N_6H_{6a})$ = 13.3° for adenine (Table 4.1); $\varphi_e(N_1C_2N_2H_{2b})$ = 36.5° and $\varphi_e(N_3C_2N_2H_{2a})$ = 13.3° for guanine (Table 4.2); and $\varphi_e(N_3C_4N_4H_{4a})$ = 10.1° and $\varphi_e(C_5C_4N_4H_{4b})$ = 15.7° for cytosine (Table 4.3). The cc-pVQZ and cc-pCVQZ results are broadly consistent with the previous theoretical work [sum = 352.9°, $\varphi_e(N_1C_6N_6H_{6b})$ = 16.5° and $\varphi_e(C_5C_6N_6H_{6a})$ = 15.3° for adenine, sum = 339.6°, $\varphi_e(N_1C_2N_2H_{2b})$ = 39.2° and $\varphi_e(N_3C_2N_2H_{2a})$ = 13.3° for guanine, and sum = 351.9°, $\varphi_e(N_3C_4N_4H_{4a})$ = 12.6° and $\varphi_e(C_5C_4N_4H_{4b})$ = 21.4° for cytosine from the 6-311G(2df,p) MP2 method;[28] $\varphi_e(N_1C_6N_6H_{6b})$ = 14° and $\varphi_e(C_5C_6N_6H_{6a})$ = 14° for adenine, $\varphi_e(N_1C_2N_2H_{2b})$ = 38° and $\varphi_e(N_3C_2N_2H_{2a})$ = 13° for guanine, $\varphi_e(N_3C_4N_4H_{4a})$ = 11° and $\varphi_e(C_5C_4N_4H_{4b})$ = 17° for cytosine with the augTZVPP MP2 method[30]], while the aug-cc-pVQZ predictions are slightly different from the previous theoretical research due to the addition of diffuse functions to the original cc-pVQZ basis set. Note that the aug-cc-pVXZ basis provides less variation for the valence bond angles and dihedral angles from DZ to QZ than the cc-pVXZ and cc-pCVXZ sets.

The aug-cc-pVQZ MP2 theoretical predictions show that adenine and cytosine have basically similar values for the sum of the three amino group valence bond angles and the amino group related dihedral angles, indicating the similar extent of nonplanarity for these two bases. Guanine possesses a value of the sum of the three amino group valence bond angles 13° smaller and a dihedral angle $N_1C_2N_2H_{2b}$ significantly larger than those of adenine and cytosine, demonstrating for guanine the strongest nonplanarity among the five common NA bases.

4.4.1.3 ENERGETICS

The MP2 total energies for the nonplanar C_1 structures of adenine, guanine, and cytosine are listed in Table 4.1-4.3. The MP2 planarization energies (i.e. the energy barriers for the nonplanar C_1 structures to reach the constrained planar C_s structures) of the three bases with various basis sets are summarized in Table 4.4 and Figure 4.5. Also included in Table 4.4 are the HF planarization energies. All the energy barriers are evaluated at the optimized HF or MP2 geometries. The energy barriers decrease as the size of the basis set increases, confirming the lessening nonplanarity of the amino groups for adenine, guanine, and cytosine. This reduction in the degree of nonplanarity of the amino group slows down when the QZ basis sets are used. Without electron correlation, the HF method predicts planar structures for adenine and cytosine due to the zero energy barriers with the large aug-cc-pVQZ basis set. At the optimized aug-cc-pVQZ HF geometries, the aug-cc-pV5Z single-point HF energy barriers show negligible changes relative to the barriers with the smaller aug-cc-pVQZ basis. The MP2 energy barriers are much higher than the HF predictions, implying the significant effect of electron correlation on the nonplanarity of NA base amino groups. At the MP2 level of theory, inclusion of core correlation effects (cc-pCVXZ basis sets) or diffuse functions (aug-cc-pVXZ basis sets) to the cc-pVXZ basis sets slightly decreases the energy barriers. Additionally, the aug-cc-pVXZ basis gives smaller energy barrier compared to the cc-pCVXZ basis, indicating the lower extent of the nonplanarity. Again, the aug-cc-pVXZ basis provides less variation for the energy barrier from DZ to QZ than the cc-pVXZ and cc-pCVXZ sets.

With the aug-cc-pVQZ MP2 method, the planarization energy of adenine is predicted to be 0.05 kcal mol^{-1}, which is smaller than the previous theoretical values of 0.13 kcal mol^{-1} (with the 6-311G(2df,p) MP2 method[28]) and 0.07 kcal mol^{-1} (with the augTZVPP RIMP2 method[30]). The energy barrier for guanine is predicted to be 0.83 kcal mol^{-1}, again below the previous theoretical values of 1.12 kcal mol^{-1} (with the 6-311G(2df,p) MP2 method[28]) and 0.92 kcal mol^{-1} (with the augTZVPP RIMP2 method[30]). Likewise, cytosine has an aug-cc-pVQZ planarization barrier of 0.06 kcal mol^{-1}, which is also lower than the previous theoretical predictions of 0.15 kcal mol^{-1} (with the 6-311G(2df,p) MP2 method[28]) and 0.07 kcal mol^{-1} (with the augTZVPP RIMP2 method[30]). The 0.83 kcal mol^{-1} energy barrier for guanine is seen to be much higher than those for adenine and cytosine, exhibiting the strongest degree of nonplanarity of guanine among five common NA bases.

We obtain MP2 basis set limit barriers by assuming the additivity of the effects of core correlation and augmentation of the basis set, relative to the cc-pVQZ MP2 predictions. The effects of core correlation lower the barriers by 0.030 (adenine), 0.090 (guanine), and 0.028 (cytosine) kcal mol^{-1}. Subtracting these increments from the aug-cc-pVQZ MP2 barriers yields our final results, 0.020 (adenine), 0.742 (guanine), and 0.032 (cytosine) kcal mol^{-1}.

The harmonic vibrational frequencies for the inversion mode of the NA base amino groups are estimated to be larger than 300 cm^{-1} (0.86 kcal mol^{-1}) for adenine and cytosine, and larger than 600 cm^{-1} (1.72 kcal mol^{-1}) for guanine at the cc-pVTZ MP2 level of theory. The zero-point vibrational energies associated with these normal modes (> 0.43 kcal mol^{-1} for adenine and cytosine, and > 0.86 kcal mol^{-1} for guanine) are higher than the MP2 basis set limits of the planarization energy barrier (0.02, 0.03, and 0.74 kcal mol^{-1} for adenine, cytosine, and guanine respectively). This helps explain why the nonplanar structures of NA base amino groups have been very difficult to directly obtain experimentally.

Additionally, the nonplanarity of the amino group for adenine, guanine, and cytosine is proven by the existence of a single imaginary harmonic vibrational frequency (283i, 448i, and 275i cm^{-1} at the cc-pVTZ MP2 level of theory for adenine, guanine, and cytosine, respectively) corresponding to the amino group out-of-plane bending mode of the constrained C_s structures. Incontestably, the imaginary harmonic vibrational frequency of guanine is significantly larger than that of adenine and cytosine. Again, it is seen that the amino group of guanine C_s structure has higher tendency toward nonplanarity than adenine and cytosine.

4.4.2 PLANARITY OF THYMINE AND URACIL

Without an amino group, thymine and uracil are predicted to be planar if the methyl group hydrogen atoms of thymine are not considered. The optimized C_s geometries of thymine and uracil using the MP2 method with various basis sets are shown in Figures 4.6 and 4.7, respectively. The DZ basis sets result in significantly longer bond distances compared to the other basis sets. The larger basis sets generally decrease the predicted bond lengths. Addition of core correction (cc-pCVXZ basis sets) in the cc-pVXZ basis sets shortens the bond distances, while inclusion of diffuse functions (aug-cc-pVXZ basis sets) only slightly changes the bond lengths for all structures. Again, the aug-cc-pVQZ predictions may be used as benchmark results for thymine and uracil.

In agreement with previous theoretical results, the planarization energies of thymine and uracil are predicted to be zero with all basis sets, indicating the planarity of the thymine and uracil bases, except for the methyl group of thymine. No imaginary vibrational frequency exists for the C_s structures of thymine and uracil, further evidence that thymine and uracil are planar.

4.5 CONCLUDING REMARKS

Second-order perturbation theory with various large basis sets shows that three out of the five common NA bases, namely adenine, guanine and cytosine, are intrinsically nonplanar due to the existence of pyramidal amino groups. Guanine is much more nonplanar than adenine and cytosine. Indeed, the planarization barriers for adenine and cytosine are very small, 0.05 and 0.06 kcal mol^{-1} with the aug-cc-pVQZ MP2 method, respectively. Larger basis sets decrease the degree of nonplanarity of the amino group, but the decrease attenuates when the QZ basis sets are used. Addition of core-core and core-valence correlation (cc-pCVXZ basis sets) or diffuse functions (aug-cc-pVXZ basis sets) diminishes the NA base nonplanarity compared to the cc-pVXZ basis sets. Moreover, the aug-cc-pVXZ basis sets give smaller degrees of NA base nonplanarity compared to the cc-pCVXZ basis sets. The aug-cc-pVXZ basis provides less variation for the amino group related bond angles and dihedral angles and planarization energies from DZ to QZ than do the cc-pVXZ and cc-pCVXZ sets. The final estimates of the MP2 planarization barriers are 0.020 (adenine), 0.742 (guanine), and 0.032 (cytosine) kcal mol^{-1}.

4.6 ACKNOWLEDGEMENTS

The authors would like to thank Dr. Yaoming Xie and Justin M. Turney for very helpful discussions. We thank Dr. Wesley D. Allen and Dr. Nathan J. DeYonker for useful suggestions on the paper. We are grateful to Professor Peter Pulay for communicating the results of the reference 26 prior to publication. This research was performed in part using the Molecular Science Computing Facility (MSCF) in the William R. Wiley Environmental Molecular Sciences Laboratory, a national scientific user facility sponsored by the U.S. Department of Energy's Office of Biological and Environmental Research and located at the Pacific Northwest National Laboratory (PNNL). PNNL is operated for the Department of Energy by Battelle. This research was supported by the National Science Foundation, Grant CHE-0451445.

4.7 REFERENCES

1. Hobza, P.; Sponer, J. *Chem. Rev.* **1999**, *99*, 3247.
2. Sponer, J.; Leszczynski, J.; Hobza, P. *Biopolymers (Nucleic Acid Sciences)* **2002**, *61*, 3.
3. Bludsky, O.; Sponer, J.; Leszczynski, J.; Spirko, V.; Hobza, P. *J. Chem. Phys.* **1996**, *105*, 11042.
4. Kydd, R. A.; Krueger, P. J. *J. Chem. Phys.* **1978**, *69*, 827.
5. Kydd, R. A.; Krueger, P. J. *Chem. Phys. Lett.* **1977**, *49*, 539.

6. Larsen, N. W.; Hansen, E. L.; Nicolaisen, F. M. *Chem. Phys. Lett.* **1976**, *43*, 584.

7. Sinclair, W. E.; Pratt, D. W. *J. Chem. Phys.* **1996**, *105*, 7942.

8. Lister, D. G.; Tyler, J. T.; Hog, J. H.; Larsen, N. W. *J. Mol. Struct.* **1974**, *23*, 253.

9. Quack, M.; Stockburgen, M. *J. Mol. Spectrosc.* **1972**, *43*, 87.

10. Nir, E.; Janzen, C.; Imhof, P.; Kleinermanns, K.; de Vires, M. S. *Phys. Chem. Chem. Phys.* **2002**, *4*, 740.

11. Hobza, P.; Spirko, V. *Phys. Chem. Chem. Phys.* **2003**, *5*, 1290.

12. Dong, F.; Miller, R. E. *Science* **2002**, *298*, 1227.

13. Sponer, J.; Hobza, P. *J. Am. Chem. Soc.* **1994**, *116*, 709.

14. Sponer, J.; Florian, J.; Leszczynski, J.; Hobza, P. *J. Biomol. Struct. Dyn.* **1996**, *13*, 827.

15. Luisi, B.; Orozco, M.; Sponer, J.; Luque, F. J.; Shakked, Z. *J. Mol. Biol.* **1998**, *279*, 1123.

16. Vlieghe, D.; Sponer, J.; van Meervelt, L. *Biochemistry* **1999**, *38*, 16443.

17. Prive, G. G.; Heinemann, U.; Chandrasegaran, S.; Kan, L.-S.; Kopka, M. L.; Dickerson, R. E. *Science* **1987**, *38*, 498.

18. Nelson, H. C. M.; Finch, J. T.; Luisi, B. F.; Klug, A. *Nature* **1987**, *330*, 221.

19. Heinemann, U.; Alings, C. *J. Mol. Biol.* **1989**, *210*, 369.

20. Sponer, J.; Leszczynski, J.; Hobza, P. *J. Mol. Struct.* **2001**, *573*, 43.

21. Juo, Z. S.; Chiu, T. K.; Leiberman, P. M.; Baikalov, I.; Berk, A. J.; Dickerson, R. E. *J. Mol. Biol.* **1996**, *261*, 239.

22. Gould, I. R.; Hillier, I. H. *Chem. Phys. Lett.* **1989**, *161*, 185.

23. Riggs, N. V. *Chem. Phys. Lett.* **1991**, *177*, 447.

24. Leszczynski, J. *Int. J. Quantum Chem.* **1992**, *19*, 43.

25. Sponer, J.; Burcl, R.; Hobza, P. *J. Biomol. Struct. Dyn.* **1994**, *11*, 1357.

26. Sponer, J.; Hobza, P. *J. Mol. Struct.* **1994**, *304*, 35.

27. Sponer, J.; Hobza, P. *J. Phys. Chem.* **1994**, *98*, 3161.

28. Sponer, J.; Leszczynski, J.; Hobza, P. *J. Biomol. Struct. Dyn.* **1996**, *14*, 117.

29. Podolyan, Y.; Rubin, Y. V.; Leszczynski, J. *J. Phys. Chem. A* **2000**, *104*, 9964.

30. Ryjacek, F.; Kubar, T.; Hobza, P. *J. Comput. Chem.* **2003**, *24*, 1891.

31. Pulay, P.; Saebo, S.; Malagoli, M.; Baker, J. *J. Comput. Chem.* **2005**, *26*, 599.

32. Mishra, S. K.; Shukla, M. K.; Mishra, P. C. *Spectrochim. Acta A* **2000**, *56*, 1355.

33. Sponer, J.; Hobza, P. *Int. J. Quantum Chem.* **1996**, *57*, 959.

34. Preuss, M.; Schmidt, W. G.; Seino, K.; Furthmuller, J.; Bechstedt, F. *J. Comput. Chem.* **2004**, *25*, 112.

35. Frisch, M. J.; Trucks, G. W.; Schlegel, H. B.; Gill, P. M. W.; Johnson, B. G.; Robb, M. A.; Cheeseman, J. R.; Keith, T.; Petersson, G. A.; Montgomery, J. A.; Raghavachari, K.; Al-Laham, M. A.; Zakrzewski, V. G.; Ortiz, J. V.; Foresman, J. B.; Cioslowski, J.; Stefanov, B. B.; Nanayakkara, A.; Challacombe, M.; Peng, C. Y.; Ayala, P. Y.; Chen, W.; Wong, M. W.; Andres, J. L.; Replogle, E. S.; Gomperts, R.; Martin, R. L.; Fox, D. J.; Binkley, J. S.; Defrees, D. J.; Baker, J.; Stewart, J. P.; Head-Gordon, M.; Gonzalez, C.; Pople, J. A. Gaussian 94, Revision C.3; Gaussian, Inc.: Pittsburg, PA, U.S.A., 1995.

36. Aprà, E.; Windus, T. L.; Straatsma, T. P.; Bylaska, E. J.; de Jong, W.; Hirata, S.; Valiev, M.; Hackler, M.; Pollack, L.; Kowalski, K.; Harrison, R.; Dupuis, M.; Smith, D. M. A.; Nieplocha, J.; Tipparaju, V.; Krishnan, M.; Auer, A. A.; Brown,

E.; Cisneros, G.; Fann, G.; Früchtl, H.; Garza, J.; Hirao, K.; Kendall, R.; Nichols, J.; Tsemekhman, K.; Wolinski, K.; Anchell, J.; Bernholdt, D.; Borowski, P.; Clark, T.; Clerc, D.; Dachsel, H.; Deegan, M.; Dyall, K.; Elwood, D.; Glendening, E.; Gutowski, M.; Hess, A.; Jaffe, J.; Johnson, B.; Ju, J.; Kobayashi, R.; Kutteh, R.; Lin, Z.; Littlefield, R.; Long, X.; Meng, B.; Nakajima, T.; Niu, S.; Rosing, M.; Sandrone, G.; Stave, M.; Taylor, H.; Thomas, G.; van Lenthe, J.; Wong, A.; Zhang, Z. NWChem, A Computational Chemistry Package for Parallel Computers, Version 4.7; Pacific Northwest National Laboratory: Richland, Washington 99352-0999, USA, 2005.

37. Dunning, T. H. *J. Chem. Phys.* **1989**, *90*, 1007.
38. Woon, D. E.; Dunning, T. H. *J. Chem. Phys.* **1995**, *103*, 4572.
39. Kendall, R. A.; Dunning, T. H.; Harrison, R. J. *J. Chem. Phys.* **1992**, *96*, 6796.
40. Kreglewski, M. *J. Mol. Spectrosc.* **1989**, *133*, 10.
41. Iijima, T.; Jimbo, H.; Taguchi, M. *J. Mol. Struct.* **1986**, *144*, 381.
42. Kuchitsu, K.; Guillory, J. P.; Bartell, L. S. *J. Chem. Phys.* **1968**, *49*, 2488.

Table 4.1: Adenine theoretical predictions of (a) the total energies in hartrees; (b) the three angles around the amino group nitrogen atom; (c) the sum of the three angles; and (d) the amino group related dihedral angles (only absolute values are reported). All angles are reported in degrees.

Level of Theory	Energy	C_6-N_6-H_{6a}	C_6-N_6-H_{6b}	H_{6a}-N_6-H_{6b}	Sum	N_1-C_6-N_6-H_{6b}	C_5-C_6-N_6-H_{6a}
cc-pVDZ MP2	-466.004404	115.20	114.38	115.72	345.30	21.63	23.42
cc-pCVDZ MP2	-466.382388	115.24	114.42	115.77	345.43	21.55	23.29
aug-cc-pVDZ MP2	-466.095803	117.74	116.80	118.22	352.76	15.64	16.76
cc-pVTZ MP2	-466.447497	117.08	116.24	117.87	351.19	17.12	18.03
cc-pCVTZ MP2	-466.954650	117.32	116.49	118.15	351.96	16.42	17.22
aug-cc-pVTZ MP2	-466.484961	117.97	117.15	118.62	353.74	14.73	15.22
cc-pVQZ MP2	-466.596568	117.77	116.92	118.52	353.21	15.23	15.80
cc-pCVQZ MP2	-467.143232	118.07	117.24	118.89	354.20	14.11	14.62
aug-cc-pVQZ MP2	-466.612877	118.43	117.62	119.17	355.22	12.92	13.30
Ref. 28: 6-311G(2df,p) MP2	...	...	...	...	352.9	16.5	15.3
Ref. 30: augTZVPP RIMP2	...	...	...	...	...	14	14

Table 4.2: Guanine theoretical predictions of (a) the total energies in hartrees; (b) the three angles around the amino group nitrogen atom; (c) the sum of the three angles; and (d) the amino group related dihedral angles (only absolute values are reported). All angles are reported in degrees.

Level of Theory	Energy	C_2-N_2-H_{2a}	C_2-N_2-H_{2b}	H_{2a}-N_2-H_{2b}	Sum	N_1-C_2-N_2-H_{2b}	N_3-C_2-N_2-H_{2a}
cc-pVDZ MP2	-541.066242	109.56	113.41	110.47	333.44	45.11	14.08
cc-pCVDZ MP2	-541.484232	109.59	113.45	110.51	333.55	45.07	14.01
aug-cc-pVDZ MP2	-541.176905	111.20	115.16	112.17	338.53	41.72	12.43
cc-pVTZ MP2	-541.583772	111.20	115.29	112.50	338.99	39.62	13.66
cc-pCVTZ MP2	-542.147339	111.41	115.54	112.73	339.68	38.94	13.53
aug-cc-pVTZ MP2	-541.627815	111.87	116.02	113.07	340.96	37.71	13.40
cc-pVQZ MP2	-541.757844	111.81	116.00	113.09	340.90	37.76	13.35
cc-pCVQZ MP2	-542.364436	112.08	116.32	113.39	341.79	36.85	13.14
aug-cc-pVQZ MP2	-541.776883	112.17	116.42	113.44	342.03	36.49	13.28
Ref. 28: 6-311G(2df,p) MP2	...	...	...	...	339.6	39.2	13.3
Ref. 30: augTZVPP RIMP2	...	...	...	...	...	38	13

Table 4.3: Cytosine theoretical predictions of (a) the total energies in hartrees; (b) the three angles around the amino group nitrogen atom; (c) the sum of the three angles; and (d) the amino group related dihedral angles (only absolute values are reported). All angles are reported in degrees.

Level of Theory	Energy	C_4-N_4-H_{4a}	C_4-N_4-H_{4b}	H_{4a}-N_4-H_{4b}	Sum	N_3-C_4-N_4-H_{4a}	C_5-C_4-N_4-H_{4b}
cc-pVDZ MP2	-393.826247	113.00	116.50	114.58	344.08	16.57	30.35
cc-pCVDZ MP2	-394.129954	113.04	116.55	114.63	344.22	16.50	30.22
aug-cc-pVDZ MP2	-393.911022	115.93	119.32	117.52	352.77	12.27	20.14
cc-pVTZ MP2	-394.211126	115.21	118.72	117.14	351.07	13.38	22.15
cc-pCVTZ MP2	-394.620687	115.44	118.98	117.39	351.81	12.85	21.23
aug-cc-pVTZ MP2	-394.243976	116.18	119.64	117.95	353.77	11.55	18.38
cc-pVQZ MP2	-394.339604	115.97	119.47	117.86	353.30	11.88	19.07
cc-pCVQZ MP2	-394.780478	116.26	119.80	118.20	354.26	11.04	17.65
aug-cc-pVQZ MP2	-394.353914	116.69	120.19	118.54	355.42	10.05	15.74
Ref. 28: 6-311G(2df,p) MP2	...	...	...	...	351.9	12.6	21.4
Ref. 30: augTZVPP RIMP2	...	...	...	...	...	11	17

Table 4.4: Planarization energies in kcal mol^{-1} for adenine, guanine, and cytosine using the HF and MP2 methods with various basis sets.

Level of Theory	Adenine	Guanine	Cytosine
cc-pVDZ HF	0.162	0.781	0.137
cc-pCVDZ HF	0.148	0.752	0.125
aug-cc-pVDZ HF	0.027	0.473	0.008
cc-pVTZ HF	0.020	0.419	0.005
cc-pCVTZ HF	0.021	0.426	0.006
aug-cc-pVTZ HF	0.005	0.336	0.000
cc-pVQZ HF	0.011	0.363	0.001
cc-pCVQZ HF	0.011	0.363	0.001
aug-cc-pVQZ HF	0.003	0.311	0.000
aug-cc-pV5Z HF[a]	0.003	0.310	0.000
cc-pVDZ MP2	0.511	1.957	0.585
cc-pCVDZ MP2	0.500	1.936	0.573
aug-cc-pVDZ MP2	0.103	1.085	0.097
cc-pVTZ MP2	0.183	1.202	0.180
cc-pCVTZ MP2	0.154	1.131	0.153
aug-cc-pVTZ MP2	0.093	1.010	0.089
cc-pVQZ MP2	0.114	0.992	0.106
cc-pCVQZ MP2	0.084	0.902	0.078
aug-cc-pVQZ MP2	0.050	0.832	0.060

[a] These energies were evaluated at the optimized aug-cc-pVQZ HF equilibrium geometries.

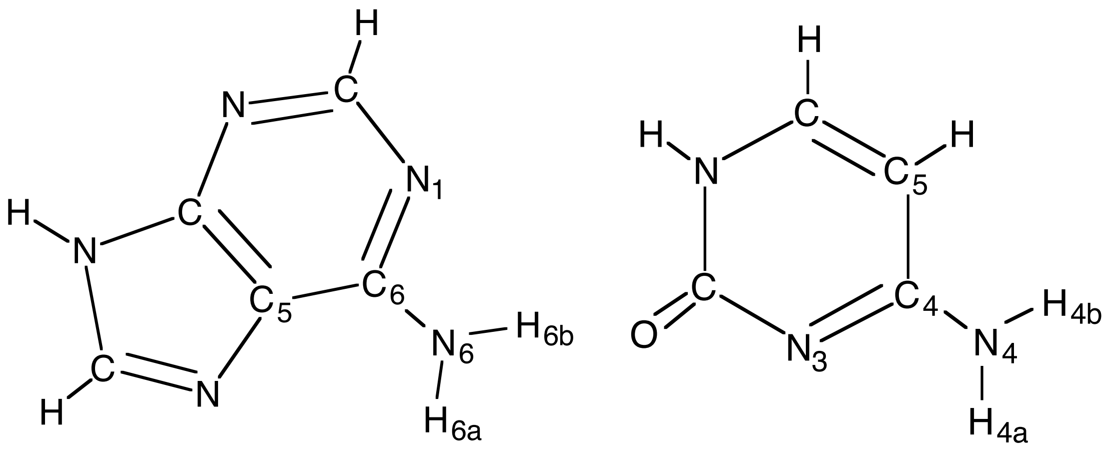

Adenine

Cytosine

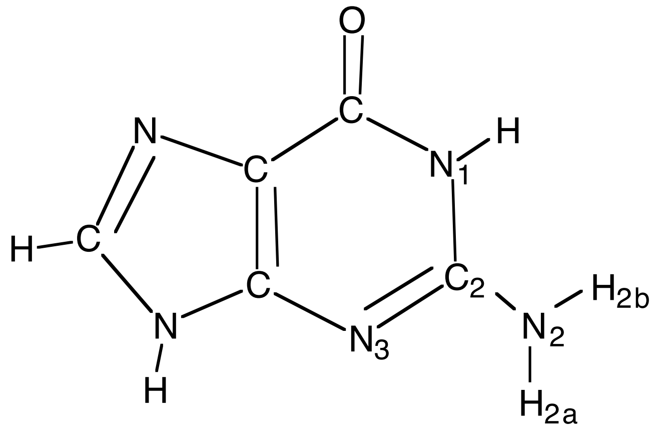

Guanine

Figure 4.1: Molecular structure and atom numbering for adenine, guanine, and cytosine.

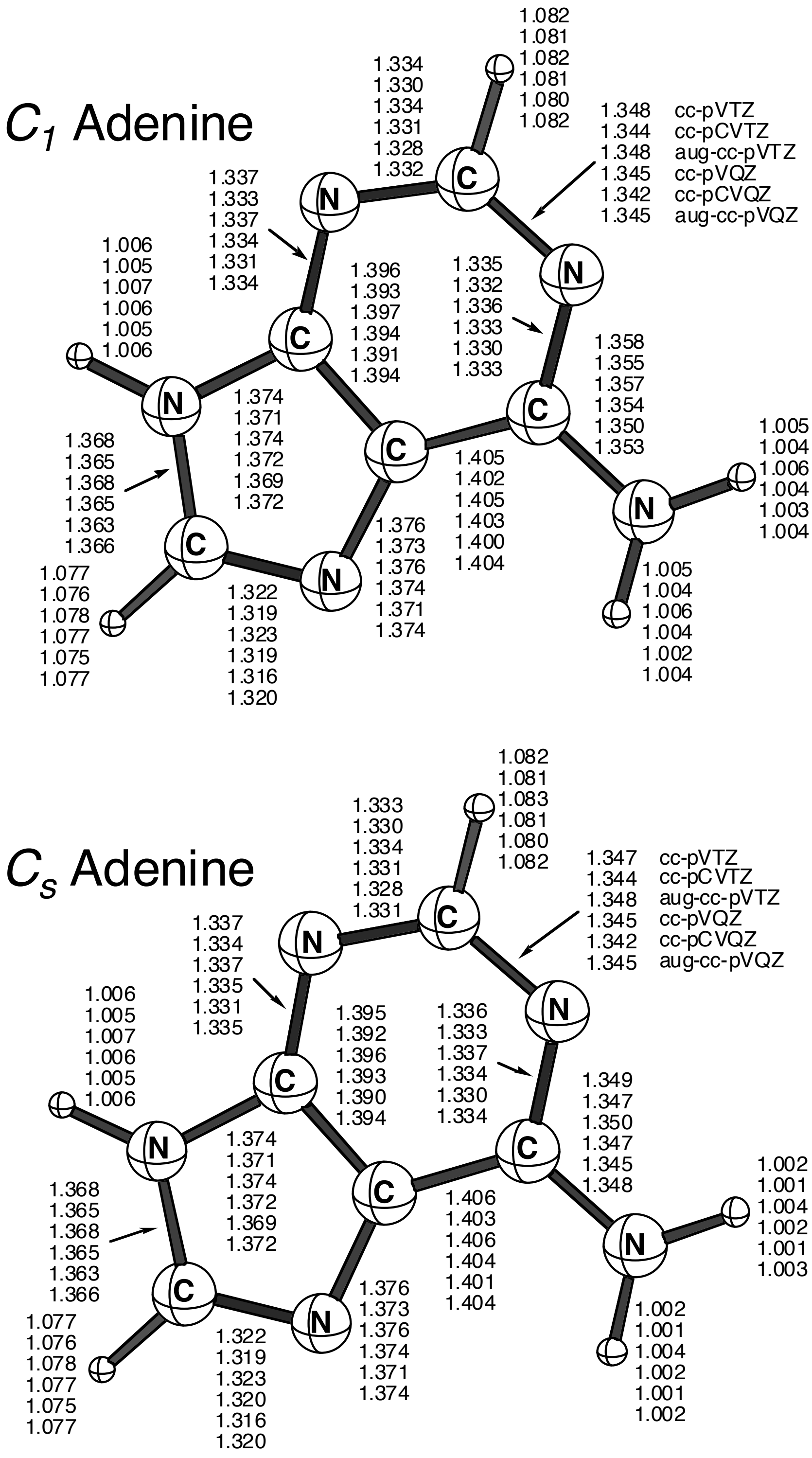

Figure 4.2: Optimized bond distances for nonplanar and planar structures of adenine (a. C_1 structure; b. C_s structure) using the MP2 method with various basis sets.

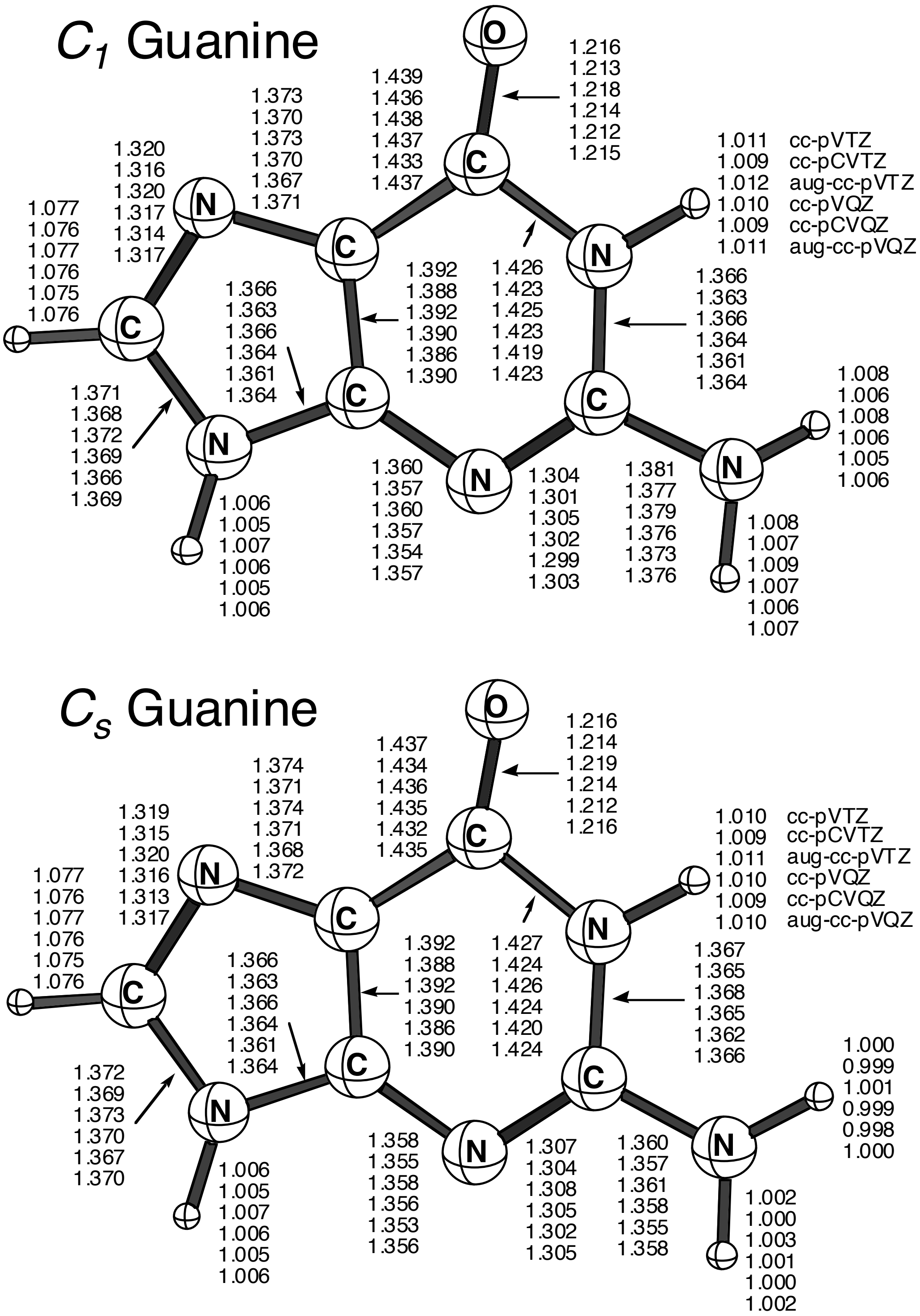

Figure 4.3: Optimized bond distances for nonplanar and planar structures of guanine (a. C_1 structure; b. C_s structure) using the MP2 method with various basis sets.

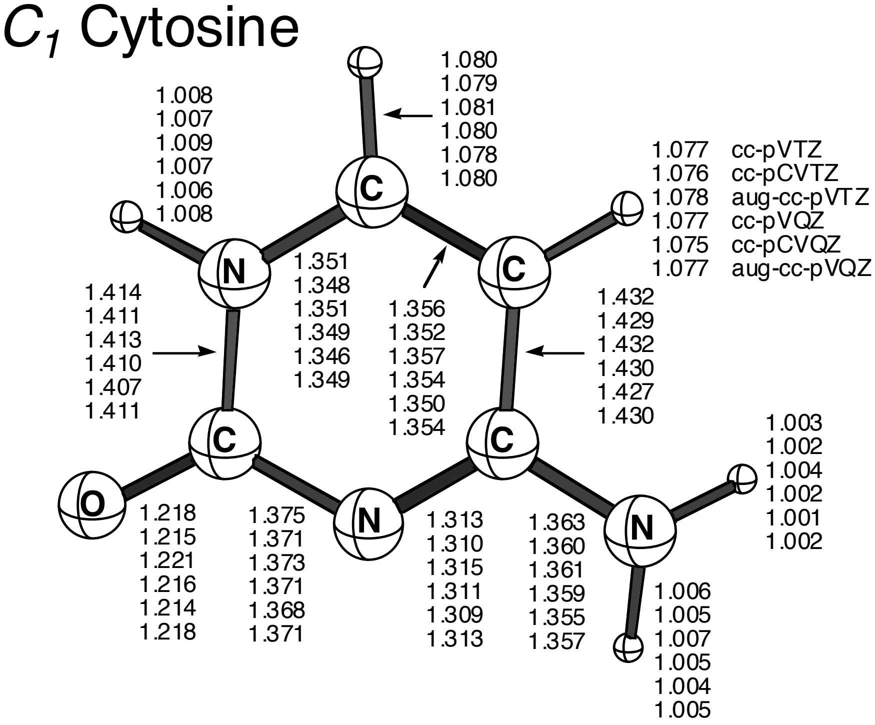

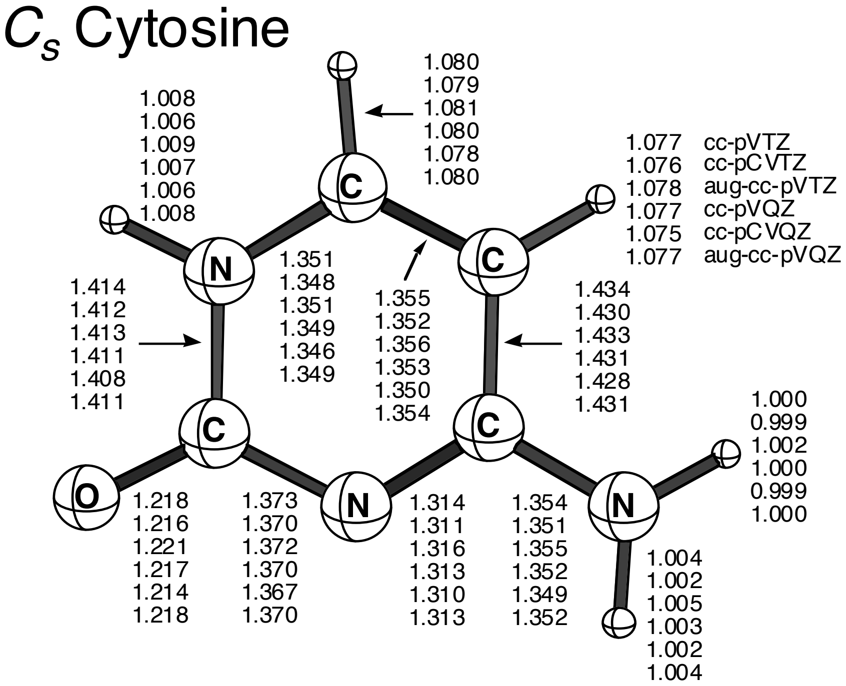

Figure 4.4: Optimized bond distances for nonplanar and planar structures of cytosine (a. C_1 structure; b. C_s structure) using the MP2 method with various basis sets.

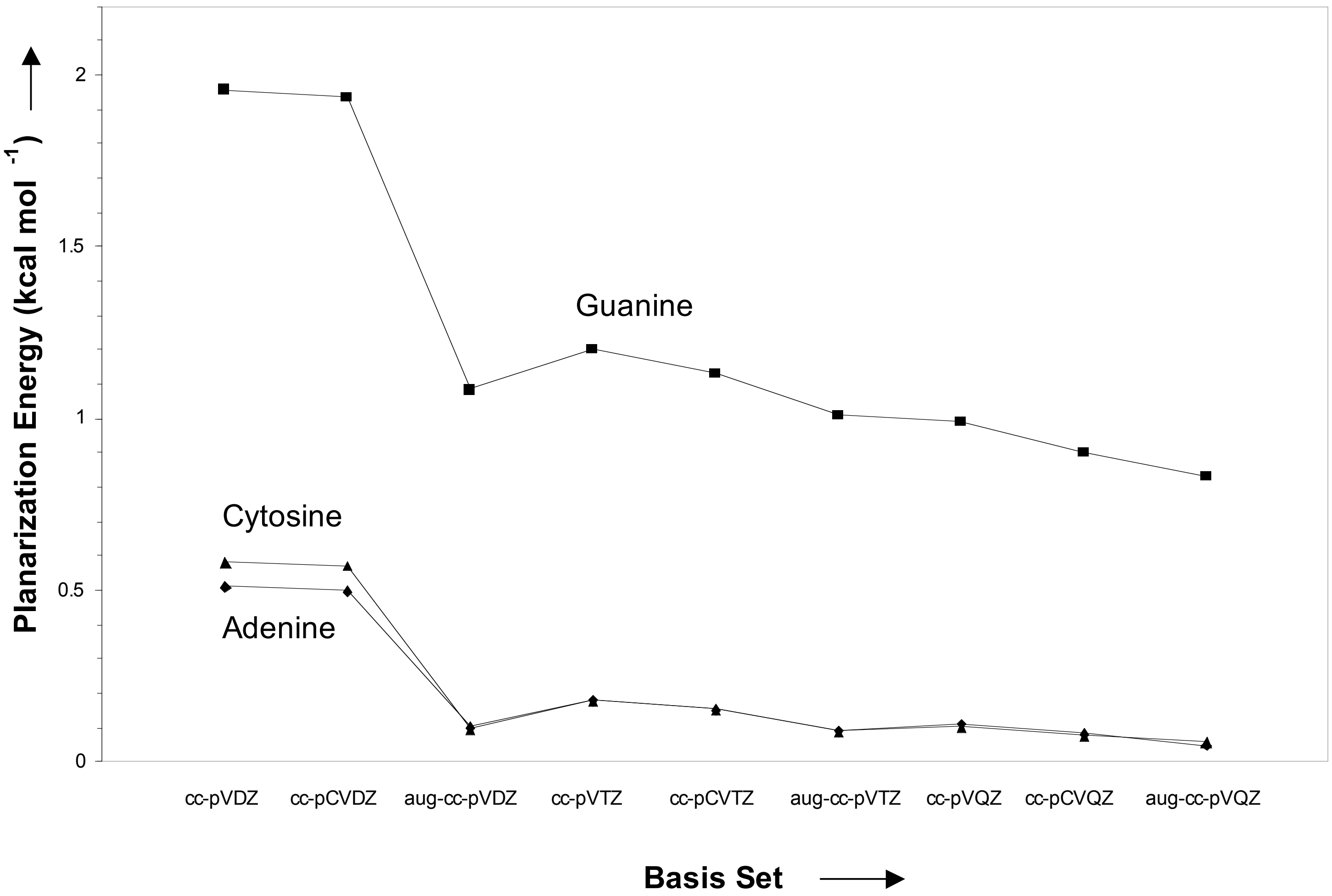

Figure 4.5: The planarization energies of adenine, guanine, and cytosine using the MP2 method with various basis sets.

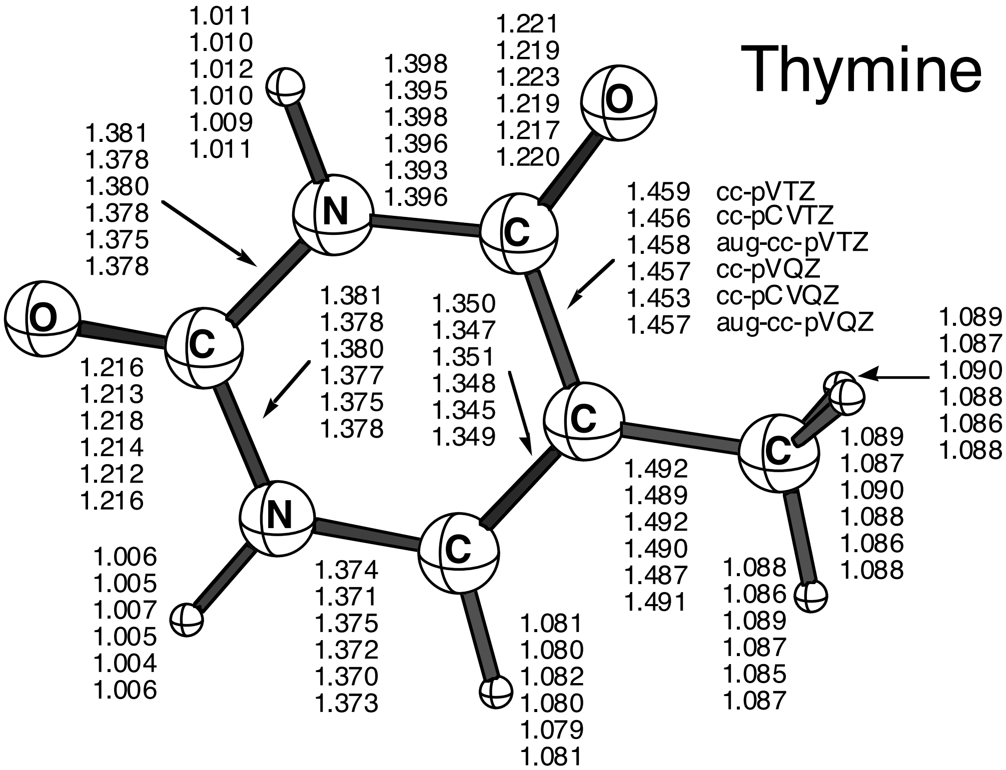

Figure 4.6: Optimized bond distances of thymine using the MP2 method with various basis sets.

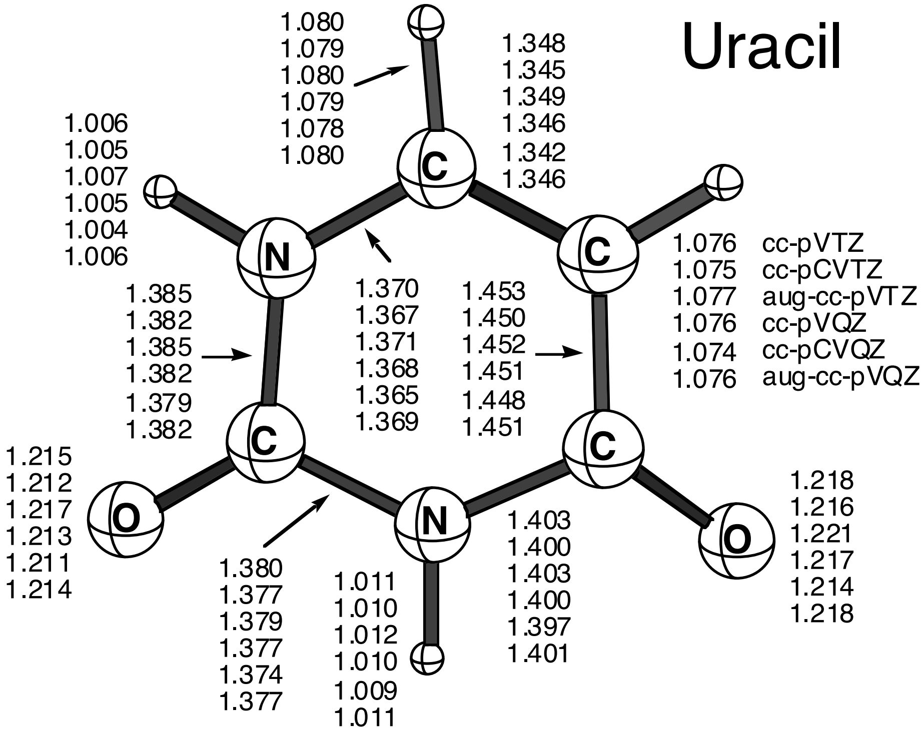

Figure 4.7: Optimized bond distances of uracil using the MP2 method with various basis sets.

CHAPTER 5

CONCLUDING REMARKS

The application of a*b initio* quantum mechanical techniques to various chemical systems is an important component in modern computational chemistry. These chemical systems of interests include atoms and molecules of small or medium size. The *ab initio* approaches have played a significant role in predicting, confirming, or even challenging experimental discoveries. The *ab initio* theoretical results range from the determination of optimal ground and excited state geometries, mapping of potential energy surfaces, to the assignment of vibrational frequencies and prediction of many other physical and chemical properties.

In order to carry out *ab initio* techniques on practical chemical problems, it is necessary to compromise accuracy and efficiency. For small-size systems, high-level *ab initio* methods can be applied to get more accurate predictions. However, computationally less expensive *ab initio* methods have to be used for medium-size systems.

In this dissertation, three molecular systems of different size have been successfully investigated by choosing appropriate *ab initio* approaches. The first two explorations involve questions of two small, yet fundamental systems: the lowest-lying electronic states of CuOH and the exothermic PNC → PCN reaction. Both systems are triatomics, thus enabling the relatively accurate computations with high-level *ab initio* mehods within a reasonable period of time. Such highly accurate computations employ the advanced coupled-cluster (CC) approaches and equation-of-motion CC (EOM-CC) techniques together with large basis sets up to quadruple zeta.

The third investigation addresses the small planarization barriers for the amino group in the nucleic acid (NA) bases. The five common NA bases (adenine, guanine, cytosine, thymine, and uracil) contain 12 – 16 atoms, in which most of them are non-hydrogen heavy atoms. For these medium-size systems, advanced CC computations will take tremendous amount of time to finish. Nevertheless, the second-order Møller-Plesset perturbation (MP2) procedure has a smaller computational scaling of N^5 than the CC method [e.g., N^6 for CC with single and double excitations (CCSD)], with N being the number of basis functions. Therefore, MP2 becomes a more appropriate correlated level of theory in this case, although MP2 may not provide predictions as accurate as the CC method.

Success in these three varied systems shows the flexibility of *ab initio* methods for different types of questions. With properly chosen theoretical techniques, detailed information can be accurately determined for the chemical systems of small or medium size. The further *ab initio* applications to large-size molecules will be possible with the development of new methodologies, more efficient algorithms and software coding, and more powerful computers in the future.